A New Type of Non-Mechanical Valves for Recirculation of Fine Particles

Azizaddini, Seyednezamaddin

Publication date:
2016

Document Version
Publisher's PDF, also known as Version of record

A New Type of Non-Mechanical Valves for Recirculation of Fine Particles

PhD Thesis

Seyednezamaddin Azizaddini

CHEC Research Center
Department of Chemical and Biochemical Engineering
Technical University of Denmark

Kongens Lyngby 2016

Technical University of Denmark
Department of Chemical and Biochemical Engineering
Søltofts Plads 229,
2800 Kongens Lyngby, Denmark
Phone +45 45 25 28 00
kt@kt.dtu.dk
www.kt.dtu.dk

Summary (English)

Gas-solid systems are applied in various industries such as pharmaceutical, food industry and chemical processes like catalytic cracking, combustion and gasification. One of the leading technologies to deal with such processes is the fluidized bed technology. Considering the increasing demands on production, process and application of solid particles, investigation, characterization and optimization of the whole or a part of a fluidized bed system is getting vital.

Nowadays, fine particles are utilized in lots of number of applications and due to present challenges in fluidization of these type of particles, assistive methods are applied to make it possible. One the major points where these challenges impacts is the loop seals. Conventional loop seals are operated around minimum fluidization condition and definitely fine particles have difficulties to be operated under this regime.

The goal of the project is to design a new type of a non-mechanical valve for transportation of the particles and closing the loop in circulating or interconnected fluidized bed systems. As the primary proposal, combination of three assistive methods (tapered fluidized bed, mixture of coarse and fine particles and high velocity gas stream) in a single device was examined to check feasibility of handling the fine particles.

A draft tube spouted bed is considered to be operated with coarse par-

ticles and the standpipe which is filled with fine particles represents the downcomer of a cyclone. This set-up was not properly capable of transporting the fine particles besides introducing the particles through an inclined tube was not possible.

After performing some supportive experiments, new version of the experimental set-up, namely four draft tubes pneumatic transport (4-DTPT), was design, constructed and examined. Successful introduction and transportation of fine particles are achieved for this device.

For the purpose of characterization of the 4-DTPT test rig, primary experiments were performed considering changes in operating conditions and geometric parameters as well as the particles size. Although, more investigations are needed to be carried out to thoroughly characterize and optimize the new device.

Further analysis, modifications, corrections and systematic investigation of the 4-DTPT will provide the knowledge about scale-up of this device to be utilized for industrial applications.

Summary (Danish)

Gas-faststof systemer anvendes i en lang række produktionsprocesser i den kemiske, bioteknologiske, farmaceutiske, fødevareteknologiske og energiteknologiske industri. Ofte anvendes fluid bed systemer til processering af de faste stoffer, og en stadig optimering af disse systemer er af stor betydning for procesøkonomien.

En af de væsentlige industrielle udfordringer er transport af især fine partikler imellem procesenheder, f.eks. mellem flere fluid bed reaktorer. Til regulering af denne transport anvendes ofte såkaldte "loop-seals", der består af ikke-mekaniske ventiler, der opereres nær partiklernes minimale fluidiseringsforhold. Disse ventiler fungerer ofte tilfredsstillende for større og tunge partikler (Geldart A og B partikler), mens små og lette partikler med en stor specifik overflade er vanskelige at transportere på grund af partiklernes høje specifikke overflade og væsentlige overfladekræfter.

Denne afhandling omhandler design af en ny type ikke-mekanisk ventil til håndtering af transport at små partikler, f.eks. rålmel i cementindustrien. Først blev et system bestående af en "draft-tube spouted bed" afprøvet med nogen succes. Imidlertid var der en række begrænsninger i systemets funktion, og en ny type bestående af flere indbyggede "draft-tubes" blev designet, opbygget og testet. Ved at operere dette system med større hjælpe-partikler, kunne systemet bringes til kontrolleret funktion med selv meget små og problematiske partikler. Afhandlingen dokumenterer

og karakteriserer det nye systems virkemåde under en række afprøvede driftsbetingelser.

Preface

The thesis has been conducted under the PhD program supported by the Technical University of Denmark (DTU). The dissertation is submitted as a partial requirement for acquiring a PhD degree at the department of Chemical and Biochemical Engineering (Kemiteknik). The PhD study was carried out in the period of December 2012 to November 2015 in CHEC research center at Kemiteknik, DTU. The project was supervised by Professor Kim Dam-Johansen and Associate Professor Weigang Lin.

The thesis deals with an industrial challenge which was observed in operation of the circulating and interconnected fluidized bed with fine particles. New type of a non-mechanical valve was investigated through this PhD project. It consists of a comprehensive literature review about different types of fluidized beds and difficulties in the processes which the fine particles are involved and are needed to be recirculated and transported with a controllable rate. So, the preliminary idea was established by design, construction and analyzing the first test rig and considering the limitations in operation, second version was proposed and examined which was successful to meet the demanded goals.

Handed-in: 30-11-2015
Defended: 28-04-2016
Seyednezamaddin Azizaddini

Acknowledgements

I wish to thank my supervisors for their invaluable support and guidance through the project and for continuously challenging my ideas in order to keep the project at the correct progress pace and to approach the project goals. I would also like to thank the technical and workshop staffs, especially Nikolaj V. Nissen, Søren V. Madsen, Jens H. Poulsen and Ivan H. Pedersen.

My former and present colleagues from Chemical and Biochemical Engineering Department at the Technical University of Denmark all deserve my gratitude. Specifically, my friends Asger Lindholdt and Mohammad Ahli-Gharamaleki for supporting my ideas and participating in the scientific discussions.

Contents

Chapter 1

Introduction

1.1 Background

Gas-solid systems are widely used in many industrial processes such as pneumatic transport, particulate pollution control, combustion of pulverized coal, drying of food products, sand blasting and gasification. Fluidized beds are considered as one of the well-developed technologies for these applications. In a fluidized bed, huge amount of the solids can be processed by the gas through the controlled residence time which results in an acceptable gas-solid contact efficiency. Different type of the fluidized beds based on the operational regimes and considering the inherent applications are identified.

Considering the gas-solid residence times, solids surface area and rate of the reaction between two phases, proper fluidization regime is suggested, such as circulating fluidized regime and bubbling regime. Another configuration is the interconnected fluidized bed which consists of two or more fluidized beds. The solid particles are circulated between the beds through different type of solid transportation devices. Mechanical valves

can be applied as solid transportation device, but their application is limited due to the material selection and resistance at high temperature.

Non-mechanical valves (such as J-, U-, L- valves, loop-seals or pot-seals) are the alternative to the mechanical valves. In addition to providing the solid circulation, these valves maintain the pressure balance of the system. These valves have been well-developed to be implemented in circulating and interconnected fluidized beds. Mostly the conventional non-mechanical valve are operated around minimum fluidization velocity of the particles.

Considering the significance of the fluidized bed as one of the promising technologies for processing a high amount of gas and solids per volume of the reactor, there is a rising demand on application of fine and ultrafine particles in various industries. However, fluidization of fine particles is difficult due to large interparticle forces.

Unlike coarse particles such as Group D, B and A particles which can be transported easily with non-mechanical valves, fine particles like Group C have difficulties being operated in these valves around minimum fluidization velocity. High interparticle force between the fine particles results in formation of the agglomerates and form the rat holes through the bed. It leads to not proper function of the valve. Besides, non-mechanical valve are supposed to act as a sealing device which means to prevent the flow of the gas in undesired direction through the valve as a short cut.

1.2 Objectives

The main objective of this project is to develop a new non-mechanical valve with the capability of:

- transportation of fine particles
- acting as a sealing device

Difficulties in operation of the fine particles in the conventional non-mechanical valves might be resolved inspiring the assistive methods for fluidization of fines. Application of mixture of coarse and fine particles, tapered bed and high velocity gas stream were considered as the solution which can be summed up in a single test rig, a draft tube spouted bed (DTSB). Regarding the observed issues in operation of the DTSB for this purpose, number of the auxiliary investigations such as modification of the test rig and characterization of the bulk solids were performed. It resulted in better interpretation of the DTSB for transportation of fine particles and led to introduction of a new configuration comprises of four draft tubes. In this concept, the feeding port of the fine particles is vertically introduced to the dense bed in the annular section. Because feeding through an inclined tube to the DTSB was learned as an obstacle for feeding of fine particles. The non-mechanical valve with this configuration is capable of transportation of fine particles and preventing the back flow of the gas stream.

1.3 Thesis structure

Extensive literature review on the fluidization phenomena was performed and included in Chapter 2. Rising demand on application of the interconnected fluidized bed and also utilization of the fine particles were conducted to focusing on a non-mechanical valve for recirculation of fine particles.

In Chapter 3, idea of utilization of a draft tube spouted bed (DTSB) which is operated with coarse particles is developed for transportation of fine particles. Rising difficulties were identified and in the mean while possible solutions were examined through number of different examinations and characterization steps. Then, regarding the founding from this studies, a new type of non-mechanical valves, namely four draft tube pneumatic transport (4-DTPT), was designed, constructed and examined.

Results from operation of the DTSB and the 4-DTPT test rig are presented in Chapter 4, besides, the influence of the geometric parameters,

operating conditions and particle size on the hydrodynamics parameters are studied.

In Chapter 5, a semi-empirical model is developed to investigate the DTSB hydrodynamics and one of the parameters was fitted to experimental results to having the equations closed. A model to describe the 4-DTPT results has studied the gas flow distribution in presence and absence of fine particles.

In the last chapter, results from the experimental studies on DTSB, supportive experiments and on 4-DTPT are concluded in section 6.1. And in section 6.2, suggestions for future investigations on the new non-mechanical valve (4-DTPT) are proposed.

Chapter 2

Literature review

2.1 Fluidization

2.1.1 Fluidization phenomena

2.1.1.1 Fluidization regimes

Fluid with an upward flow through a bed of particles penetrates into the voids of the particles and due to this restricted passage, a pressure difference is experineced between bottom and top of the bed. When the gas velocity is low, particles stay stationary as called fixed bed [1], under this regime, bed pressure drop increases linearly. For higher velocities, the drag force between solid particles and the gas flow overcomes the gravitational force and makes the particles suspended. For this condition, the pressure drop of each section equals to the weight of the particles and the gas [1,2]. Depending the particle size and type, increasing the gas velocity moves the particles further apart and resulted in an approximately uniform suspension which is called expanded bed [2].

Above this specific velocity, namely the minimum fluidization velocity (U_{mf}), pressure drop does not experience big changes due to balance of the suspended particles weight and the driving force (imposed drag of the gas on the particles which is represented as pressure difference). For higher gas velocities, different particle types show different behaviors.

Particles are classified based on the particle size and the difference between the density of the particles and the dentisy of the fluidization medium. Geldart has classified the particles into four groups, see Figure 2.1 where Archimedes number (Ar) includes both characteristics. In group A, the particles are expanded gradually and form a homogeneous solid-fluid suspension. This situation, smooth fluidization, takes place under special conditions in which the particles are fine enough and relatively dense fluid is fed at high pressure to the bottom of the bed. At higher velocities, the pores tend to get larger and bubbles are formed.

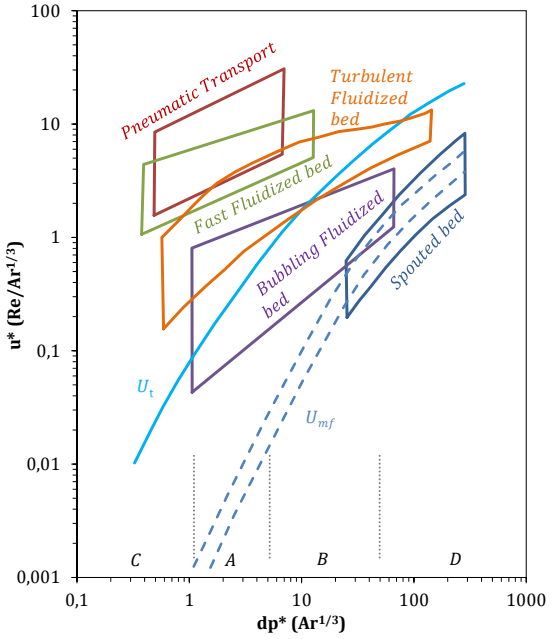

Figure 2.1: Grace diagram [3]

In Geldart's group B, the bed of material will change from a fixed bed to a bubbling bed by increasing the velocity. The bubbles rise upwards through the solid particles, particles which have entered and remained

inside the bubble wake can be transported up to the surface of the bed. While a bubble is rising due to decrease of the imposed weight of the solid particles, it grows and increases in size until it reaches the surface and erupts at the top of the bed.

In group C, particles are too much fine and due to the high interparticle force are so cohesive. In this case, the number of gas passages decreases, although their length increases and forms channels through the bed. In group D, with an increase in gas velocity above the minimum fluidization velocity, the bubbles become bigger and bigger and in special conditions bubbles in the size of the column diameter form (which is called slug flow).

Various fluidization regimes are defined based on the superficial gas velocity and particle characteristics: particulate fluidization, bubbling regime, slug flow, turbulent regime, fast fluidization and pneumatic transport [1, 3–5]. Dimensionless gas velocity and particle size are stated in Equations (2.1) and (2.2). dp^* range is illustrated in Figure 2.1 for Geldart's particle groups and also fluidization condition of each type of particle for dimensionless gas superficial velocity (characterized by u^*) is indicated [1].

$$u^* = \left(\frac{u^3\rho_g^2}{\mu(\rho_s - \rho_g)g}\right)^{\frac{1}{3}} = \frac{Re_p}{Ar^{1/3}} \tag{2.1}$$

$$d_p^* = \left(\frac{d_p^3\rho_g(\rho_s - \rho_g)g}{\mu^2}\right)^{\frac{1}{3}} = Ar^{1/3} \tag{2.2}$$

Considering a particle in size of d_p, density of ρ_s and sphericity of ψ that has fallen into a fluid (density of ρ_g), the free-falling velocity of the particle is called the terminal velocity which is shown on Figure 2.1 as U_t. The dimensionless terminal velocity (u_t^*) is calculated by Equation

(2.3) as an approximate for determination of the terminal velocity [1].

$$u_t^* = \left(\frac{18}{(d_p^*)^2} + \frac{2.335 - 1.774\psi}{(d_p^*)^{0.5}} \right)^{-1} \tag{2.3}$$

Increase in the gas velocity above the terminal velocity (U_t) for group A and C or even lower than U_t for group B and D, changes the fluidization regime to turbulent fluidization [1]. In a turbulent regime, as expected, the height of the dense phase is higher than in the bubbling regime and the void fraction (volume fraction of gas to total volume of gas and solid particles) increases definitely.

For higher gas velocities above the terminal velocity at which the particles are elutriated out of the system, two conditions are defined [1]:

- Pneumatic transport: The feeding rate of solids back to the system is small enough (usually mass of solid to gas less than 5%) for all the particles to be washed out. The particles are greatly scattered in the gas phase and the solid fraction under this condition is less than 2%.
- Fast fluidization: For a higher feeding rate of solid particles back to the fluidized bed, a dense region around (5-15)% solid fraction forms at the bottom. As well as higher solid feeding rate is provided, the greater height of the dense region is formed. Just on top of this region, the solid-gas fraction exponentially decreases. A fast fluidization regime can be distinguished by the core-annulus flow of the gas and the solids. The particles are transported upwards at the core of the flow in the dilute phase and the layer of the dense particles flows down attached to the wall.

A fluidized bed is designed considering appropriate gas-solid contact efficiency regarding operating conditions such as gas flow rate, solid inventory and fluidization regime, as well as the required residence time of the solids and the gas phase. Selection of a proper contact mode for a specific application should be performed under special considerations

like: the reaction rate of gas and solid phases, suitable solid particles size and the significance of heat distribution within the fluidized bed. Besides these items, the feasibility of operation of such systems should hydrodynamically be evaluated by a cold flow model study. But one big problem which has attracted researchers and process designers in this field is uncertainties in the scale-up procedure.

Fluidized beds have special characteristics which make them suitable for many gas-solid reactions in industrial applications, for example, quite effective and rapid mixing of solids, easy temperature control and flexibility for high-pressure and high-temperature applications. The mentioned items lead to an isothermal process and an approximately uniform product is yielded from a fluidized bed system.

However, fluidized bed systems have a number of disadvantages such as: reduction in gas–solid contact efficiency due to the by-pass of gas in bubbling beds, poor gas–solid contact in the annular section of fast fluidized beds, non-uniform products due to a large distribution of gas residence time in a bubbling regime, erosion of mechanical parts (riser, exit duct, cyclone and so on) due to the high momentum of the solids.

Modification of the mechanical parts and operational temperature considering, respectively, the hydrodynamics and the kinetics approaches are contributed to a high mass and heat transfer between the solid and gas phases. It increases the conversion efficiency and fluid dynamic performance of the system [6].

For specific processes for which regeneration of solids back to the original form, or transportation of heat and special species to/from a fluidized bed is required. Recirculation of solid particles between fluidized beds for the purpose of continuous operation of the system fulfills this demand. In next section, more details about this specific type of fluidized beds are given.

2.1.1.2 Interconnected fluidized beds

Interconnected fluidized bed (IFB) systems consist of more than one fluidized bed which are applied to process-associated reactions in an integrated structure which for continuous operation requires the regeneration of solid particles and heat/mass transportation. Heat transportation, mass transportation, regeneration of oxygen carriers, regeneration of sorbents and regeneration of catalysts are examples of applications of IFB systems.

In the primary fluidized bed, gas and solid phases are in contact with each other in order to accomplish the primary reaction. Solids are transported to the secondary fluidized bed for at least on of the following reasons: regeneration back to the original form, heating-up/cooling-down or capturing/releasing the reactant elements or oxidation/reduction of the bed inventory. Solid materials in IFB systems are transported via particular transportation devices between beds, in dense phase and in dilute phase. In a dense phase approach, particles are transported over a weir and recirculated via an orifice. And within a dilute phase approach, solids are transported by a riser (for instance by a fast fluidized bed) and captured by means of a cyclone.

Direct transportation of materials between two fluidized beds (internal recirculation) is achieved through an orifice (see Figure 2.2-(A)) next to the bottom of the partition plate between adjacent fluidized beds [7]. The different aeration velocity of each fluidized bed contributes to the unlike bulk density of each one, which leads to different pressure between the beds. The discrepancy between the operating pressure of two neighboring interconnected fluidized beds results in a driving force that pushes the materials from the dense bed to the lean bed through the orifice.

The fluidization velocity of the lean bed should be high enough to push up the particles to leave the bed surface, sufficiently high to be able to flow over the weir and accomplish the recirculation loop of the particles. This configuration is utilized mostly when the reactions in nearby compartments are taking place at around the same temperature.

Another type of transportation of materials between beds (external recir-

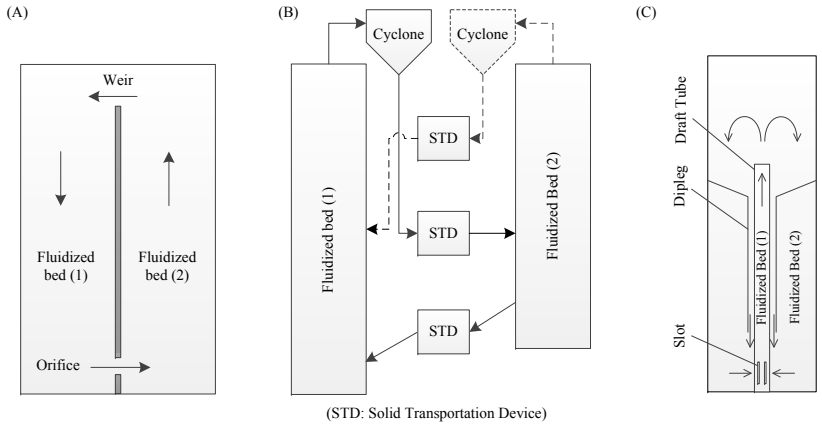

Figure 2.2: Examples of interconnected fluidized bed systems

culation) consists of two fluidized beds in which elutriated materials from the primary bed are captured by a cyclone and conveyed to the secondary bed. The recirculation loop of solid transportation is completed by conveying the materials back to the primary bed. This process is performed using various methods and solid transportation devices (STD) based on the configuration of the system which is dominantly defined by the inherent process of each fluidized bed. The rate of reaction and required residence time of solid particles in each bed define the fluidization regime of each bed.

If the secondary fluidized bed can act as a fast fluidized bed (riser), a secondary cyclone conveys the solid materials back to the primary reactor (see Figure 2.2-(B)). When a lower fluidization velocity and therefore a higher residence time of particles is required, solid materials are conveyed through solid transportation devices from the dense phase of the secondary fluidized bed.

Sealing devices are applied in each transportation line to prevent the mixing of gas products from different fluidized beds. Pot-seals and loop-seals are applied to minimize the leakage between beds, they can control the solid transportation rate in specific ranges. Pneumatic valves (e.g. L-valve, U-valve and J-valve) control the solid recirculation rate by implementing various aeration velocities [8–10]. When different operating temperature and minimum gas leakage between beds are needed for each

fluidized bed, non-mechanical valves are suggested.

In many processes, the recirculation of bed materials is mostly required for regeneration of the processed solid materials, as in oxidation/reduction cycles, an adsorption-desorption process and carbonation-calcination looping process. On the other hand, in some cases, transport of materials from one bed to another is applied for heat transportation from a fluidized bed with an exothermic reaction to another bed where heat demand exists. Distinct gaseous product streams from different processes in separate fluidized beds are achieved in an interconnected fluidized bed when continuous operation of all sequence processes is desired.

2.1.1.3 Classification of interconnected fluidized beds

Interconnected fluidized bed systems have been utilized in different applications and can be classified based on the various applications, configurations, fluidization regimes and solid transportation loops. But a desired process which is implemented by a specific particles group and solid transportation rate limits the design and fluidization regime.

The history of around 30 years of investigations and studies on various applications and configurations of IFB systems is shown in Table 2.1. Experimental and theoretical modelling of IFB systems by cold and hot models are indicated and followed by the application, configuration of the system, size of the main fluidized beds, group of particles, fluidization regime and solid circulation rate.

Processes with a low reaction rate, in which the solids require a long residence time in the fluidized bed for complete conversion, are performed in bubbling fluidized bed. A large amount of solid inventory is kept in the fluidized bed, and regarding the reaction rate, solid transportation out of the bed is adjusted and controlled. In a secondary fluidized bed, the desired corresponding process is implemented and solid particles are transported back to the primary fluidized bed. A solid circulation loop is performed in two phases, dense phase or dilute phase:

- Due to the difference in the bulk density of two adjacent fluidized beds, considering the driving force of variation in the operating pressure of each bed.

- Elutriation of particles by a fast fluidized bed and consequent device (e.g. cyclone) where gravity is the dominant force then the solid transportation device conveys the particles back to the primary fluidized bed.

Studies on different interconnected fluidized beds have been reported in the literature as shown in Table 2.1. Various combinations were suggested based on the inherent processes and required contact time of gas and solid phases. Examples of proposed configurations are two bubbling fluidized beds, one bubbling fluidized bed and one fast fluidized bed and two fast fluidized beds. Various possible methods for interconnection of the mentioned fluidized beds are applied to close the solid circulation loop.

Transportation through an orifice is the direct method of conveying solids from one bed to another, but gas will also be transported with the solids as an undesirable factor. Sealing devices, like J-valves, L-valves, U-valves, pot-seals and loop-seals, are applied to prevent or minimize the gas leakage, in addition to provide limited control of the solid circulation rate. For the second transportation procedure, two methods of sealing are utilized to prevent gas leakage from the secondary bed back to the cyclone: overwhelming the cyclone downcomer in the dense bed of the bubbling fluidized bed (in which this bed acts as a pot-seal) or an additional sealing device between the cyclone downcomer and the next fluidized bed.

A bubbling regime is preferred for fluidization of particles of groups B and D, however; fast fluidization of these particles is gained by introducing a large amount of gas due to high terminal velocity of particles in group B and D. Both bubbling and fast fluidization regimes are suggested for group A particles considering the solid and gas reaction rates. Particles in group C are difficult to be fluidized and especially in the bubbling regime, so fast fluidization is suggested, regarding methods for improvement of the fluidization quality which is explained later.

Table 2.1: History of at least three decades of interconnected fluidized bed systems

Modeling	Application	Configuration	Scale (m^3)	Particle Group	Regime	SCR ($\frac{kg}{m^2 s}$)	Institute	Year	Reference
CFM Thero.	Gasification	Two FB Orifice-Weir	0.2×0.2×0.2	B	BFB BFB	0-100	UB UK	1984	[7]
CFM Thero.	Desulfurization	Four FB Orifice-Weir	0.2×0.1×1	B	2(BFB) 2(BFB)	0-600	DUT Ntrlnd	1994-2001	[12, 13]
HFM Exp.	Adsorption Desorption	Two FB Orifice-Weir	0.4×0.2×0.6	B	BFB BFB	02-12	VUT Austria	1995	[14, 15]
HFM Exp.	HCl Dehydrogenation	Two FB J-tubes	Φ0.25×0.8	A-B	BFB BFB	0.1-0.5	USC USA	1996-1999	[9, 16]
CFM - HFM Exp. - Theo.	Gasification Combustion	Two FB Cyclone-LS	Φ0.175×2 Φ0.25&0.55×0.5	B	BFB FFB	0-200	VUT Austria	2003-2008	[17, 18]
HFM Exp. - Theo.	CL Combustion	Two FB Cyclone-LS	Φ0.150×4.1 Φ0.159×3.0	B	FFB FFB	0-100	VUT Austria	2008	[19]
CFM Exp.	CL Processes	Two FB Cyclone-LS	Φ0.050×1.6 Φ0.054×1.2	A	FFB FFB	0-120	VUT Austria	2009	[20]
HFM Exp.	CH_4 to Syngas	Two FB	Φ0.05×1.22	A-B	BFB BFB	-	RUB Germany	1997	[21]
HFM Exp.	Gasification	Four FB Orifice-Weir	0.095×0.095 ×0.25	A-D	2(BFB) 2(BFB)	-	UG, UCL Ntrlnd, UK	1998	[22]
HFM Exp. - Theo.	Pyrolysis and combustion	Two FB Orifice-Cyclone	Φ0.39×0.4-30° Φ0.02×0.55	B	BFB FFB	0-120	UT Ntrlnd	1999	[23]
HFM Thero.	Calcium looping CO_2 capture	Two FB	(Concept)	B	-	1500 (kg/s)	NU Japan	1999	[8]

Modeling	Application	Configuration	Scale $\left(\mathrm{m}^3\right)$	Particle Group	Regime	SCR $\left(\frac{\mathrm{kg}}{\mathrm{m}^2\mathrm{s}}\right)$	Institute	Year	Reference
HFM Thero.	CL Combustion	Two FB Cyclone-LS	2.5 m2 (Concept)	B	BFB FFB	50	ChUT Sweden	2001	[10]
HFM Exp.	CL Combustion	Two FB Cyclone-LS	Φ0.19×1.9 Φ0.19×0.5	B	BFB FFB	0-300	ChUT Sweden	2003	[24]
CFM - HFM Exp.	CL Combustion	Two FB Orifice-Weir	0.019×0.019×0.16 0.019×0.027×0.16	A	BFB FFB	0-2	ChUT Sweden	2004-2007	[25–27]
CFM - HFM Exp. - Theo.	Butane Dehydrogenation	Two FB Orifice-Weir	2/3(Φ0.08×2) 1/3(Φ0.08×2)	B	BFB FFB	0-12	CSIC Spain	2004	[28]
HFM Exp. - Theo.	Calcium looping CO_2 capture	Two FB Cyclone-LS	Φ0.1×6.0 Φ0.1×6.5	B	FFB FFB	0.8-2.3	CSIC Spain	2009-2011	[29–33]
HFM Exp.	CL combustion	Three FB Cyclone-LS	Φ0.108×1.5 Φ0.108×1.0	A-B	2(BFB) FFB	25-100	CSIC Spain	2006	[34]
CFM Exp.	Calcium looping CO_2 capture	Two FB Cyclone-LS	Φ0.17×4.0 Φ0.16×4.0	B	FFB FFB	0-5	CSIC Spain	2011	[35]
HFM Exp.	CL processes	Two FB Cyclone-LS	Φ0.05×0.2 Φ0.08×0.1	A-B	BFB FFB	0-2	CSIC Spain	2011-2012	[36, 37]
CFM Exp.	Gasification Of biomass	Two FB Orifice-Weir	0.067×0.023×0.25 0.133×0.023×0.25	B	BFB BFB	470	ULA Italy	2006	[38]
HFM Exp.	CL Hydrogen generation	Two FB Cyclone-LS	Φ0.15×0.8, Φ0.016 Φ0.15×0.8, Φ0.016	B	BFB-FFB BFB-FFB	0-20	KIER Korea	2007	[39, 40]
CFM Exp.	CL combustion	Two FB Cyclone-LS	Φ0.1×5.6 Φ0.3×1.9	A-B	BFB FFB	0-40	KIER, UBC Korea, Canada	2009	[41]
CFM Exp.	Gasification combustion	Two FB Cyclone-LS	Φ0.078×8.5 Φ0.2×2.1	B	BFB FFB	0-100	KAIST Korea	2010	[42]
CFM Exp. - Theo.	CL combustion	Two FB Cyclone-LS	0.040×0.11×4.50 0.285×0.11×2.13	B	BFB FFB	0-100	KAIST Korea	2011	[43]

Modeling	Application	Configuration	Scale (m^3)	Particle Group	Regime	SCR ($\frac{kg}{m^2 s}$)	Institute	Year	Reference
HFM Thero.	CL combustion	Two FB Cyclone-LS	(2D) 0.25×0.6	B	BFB FFB	-	NETL US	2008	[44]
HFM Exp.	CL Hydrogen generation	Two FB Cyclone-LS	0.1×0.1×0.15 Φ0.075×-	-	BFB FFB	-	DU Canada	2009	[45]
HFM Exp.	Calcium looping CO_2 capture	Two FB Cyclone-LS	Φ0.1×4.5 Φ0.1×2.0	B	BFB FFB	-	CANMET Canada	2009-2011	[46, 47]
CFM Exp.	CL combustion	Two FB Cyclone-LS	Φ0.1×1.5	B	FFB FFB	-	NCPU China	2009-2010	[48, 49]
CFM Thero.	CL combustion	Two FB Cyclone-LS	Φ0.19×1.9 Φ0.19×0.5	B	BFB FFB	90	HIT China	2011	[50]
CFM Exp. Theo.	Biomass Pyrolysor	Two FB Cyclone-orifice (Internally IFB)	Φ0.024×0.9 Φ0.039×0.6 Φ0.100×0.8	B	BFB FFB	70	SEU China	2009-2012	[49, 51–54]
HFM Exp.	CL processes	Two FB Cyclone-LS	0.034×0.030×0.370 0.050×0.030×1.000	B	BFB FFB	0-5	SEU China	2012	[55–57]
HFM Thero.	CL combustion	Two FB Cyclone-LS	(2D) 0.25×0.8 (2D) 0.15×4.0	A-B	BFB FFB	200-2000	ICL UK	2010	[58]
HFM Exp.	Calcium looping CO2 capture	Two FB Cyclone-LS	Φ0.071×12.4 Φ0.114×-	A-B	BFB FFB	-	IFK Germany	2010-2011	[47, 59]
HFM Exp.	CL combustion	Five FB Cyclone-LS	Φ0.13×1.0 2(Φ0.10×1.00) 2(Φ0.02×2.25)	B	3(BFB) 2(FFB)	400	IFP France	2011-2012	[60–62]
CFM Exp.	CL combustion	Two FB Cyclone-LS	Φ0.040×0.11 Φ0.035×0.17	B	BFB FFB	30-110	HUST China	2012	[63]
CFM Exp.	-	Two FB Cyclone-DLS	Φ0.230×5.0 Φ0.144×5.0	A-B-C	FFB FFB	40-220	NUST Norway	2013	[64]

Modeling	Application	Configuration	Scale $\left(\mathrm{m}^3\right)$	Particle Group	Regime	SCR $\left(\frac{\mathrm{kg}}{\mathrm{m}^2\mathrm{s}}\right)$	Institute	Year	Reference
CFM	-	Two FB	Φ0.17×4.0	-	FFB	0-2	CIRCE	2013	[65]
Exp. - Theo.		Cyclone-LS	Φ0.16×4.0		FFB		Spain		
CFM	CL combustion	Two FB	-	B	BFB	20-40	EPU	2014	[66]
Theo.		Cyclone-Pot-seal	-		FFB		China		
HFM	CL combustion	Two FB	-	B	FFB	20-40	HUST	2014	[67]
Theo.		Cyclone-cyclone	-		FFB		China		

CFM:	Cold flow mode	BFB:	Bubbling fluidized bed
HFM:	Hot flow mode	FFB:	Fast fluidized bed
Exp.:	Experimental	LS:	Loop-seal
Theo.:	Theoretical	DLS:	Divided loop-seal
CL:	Chemical looping	Ntrlnd:	The Netherlands

2.2 Applications of IFB systems

Generally, fluidized beds are applied in the following processes: (1) gas–catalytic reactions, (2) gas–solid reactions, (3) heat transportation and 4) particles processes [11]. The first group indicates a reaction occurring on a solid catalyst surface with the continuous gas phase, such as fluid catalytic cracking. The second group involves both gas and solids as reactants, like adsorption/desorption and oxidation/reduction processes. The third group utilizes solid materials to supply heat for a reaction or to transport heat out of a system by conveying the solid particles. And the fourth group explains particles processes, for example, particle drying, particle coating, or separation of specific particle sizes.

The fluidized bed reactor was introduced by the German engineer Fritz Winkler to gasify coal for industrial applications in the early 1920s [68]. Winkler patented this gasification technology in 1922 [69] and the first large-scale industrial unit was built in Lünen, Germany in 1926 [70]. The fluidization technology has not experienced great advances after the Winkler patent in 1922 until 1942 when the Fluidized Catalytic Cracking (FCC) process of kerosene was introduced by the Standard Oil Company.

The Standard Oil Company constructed the first industrial FCC unit in Baton Rouge, Louisiana, which was called for the first time an interconnected fluidized bed system [70, 71]. Their progress contributed to high demand for fluidized bed reactors because such a system could efficiently convert large amounts of heavy hydrocarbons into lighter components. The studies were mainly concentrated on the fluidization characteristics of the fine particles (Geldart's group A and C: particle density between 800 and 960 kg/m^3 and particle size between 10 and 150 μm) which is normally applied for the FCC processes [6].

Afterwards, other applications, such as the roasting of sulfide ore in 1947, the drying of dolomite particles in 1948 and the introduction of the Fischer-Tropsch plant in the 1950s for the conversion of natural gas to gasoline, were recognized [11]. Soon after, high demand for the production of light-weight hydrocarbons like gasoline by means of fluidized bed technology led to an increase in the utilization of fluidized beds in

industrial plants. Experimental and theoretical studies on fluidization phenomena were started for investigation of this technology and also the optimization of different items such as mechanical design, system configuration, particle size range and operating conditions.

The solid particles flow between two fluidized beds in an IFB system was first explained based on a process in the oil industry where the orifice connect a catalyst bed to a regenerator bed [72]. Two fluidized beds interconnected through an orifice were studied by Stanley et al. in 1984 [7], and the solid transportation from one bed to another was studied under various conditions of orifice opening size, superficial gas velocity and different particle sizes. Korbee et al. developed a mathematical model to investigate the flow of solid and gas through an orifice between two fluidized beds. An experimental test rig was examined to verify the fluidization phenomena and gas–solids flow, in addition to which the model was confirmed to be a promising tool for design [12].

An experimental and theoretical study on the capture of environmental contaminants in an interconnected fluidized bed was implemented by Snip et al. at Delft University of Technology [73]. A NOXSO capturing system was designed for a 150 MW_e power plant and the feasibility of a four interconnected fluidized bed system was examined for capturing SO_2 and NO_x. An adsorption–regeneration of calcium oxide process for CO_2 capturing was proposed by Shimizu et al., in which particles are recirculated between two fluidized beds in an interconnected fluidized bed [8].

Combustion of hydrocarbon fuels and in situ CO_2 separation was proposed as a chemical looping combustion (CLC) process at Chalmers University [10]. They developed a system comprising two fluidized beds (air reactor and fuel reactor) for the investigation and development of carbon dioxide capture in the combustion of gaseous fuels. The design [74] and operation of lab-scale [25, 26, 75] and pilot-scale CLC plants [76, 77] demonstrate that the combustion efficiency of syngas is around 99% for a wide range of operating temperatures around $1000°C$ and (70–94)% for natural gas considering similar operating temperatures, respectively.

A cold flow model of the CLC process in an IFB system was performed

to investigate the leakage between the fuel reactor, cyclone and sealing device in both directions. It was found that 6% of the gas leakage occurs from the pot-seal to the fuel reactor, which contributes to the dilution of the CO_2 stream out of the fuel reactor by 6% of air [24]. An exploration of various operating conditions (like temperature and gas velocity) and different oxygen carriers (iron-oxide, nickel-oxide, copper-oxide and so forth) was reported [78–83] and concluded that CLC is a promising method for CO_2 capture from the combustion of fuel gases without loss of energy for separation.

An IFB system was studied for CO_2 capture by a calcium looping process of biomass gasification and chemical looping combustion of gaseous fuels at Vienna University of Technology. A cold flow model of a two CFB interconnected system was studied, focusing on the solid circulation rate and pressure profiles regarding changes in the gas velocity, loop-seal fluidization and solid inventory [20]. They claimed that the solid circulation rate could be optimized by the primary fluidized bed and without any effect on the secondary fluidized bed, and the secondary bed could be independently optimized for fuel conversion [84]. Studies on operating conditions show that fuel conversion increases at higher temperatures.

Interconnected fluidized bed systems were established and studied at the Instituto Nacional del Carbon (INCAR), CSIC, Spain [28–37]. A calcium looping process was proposed for capturing carbon dioxide from combustion flue gases [29–31, 85], biomass combustion [33, 86] and chemical looping combustion of gaseous fuels [87]. These studies were mostly performed by directing the development and scale-up of interconnected fluidized bed technology for industrial applications. Experimental and theoretical studies on the CO_2 capturing process (Ca-looping or CLC) in an IFB system were performed [30, 32]. The result of the studies led to the construction and operation of a 1.7 MW Ca-looping pilot which is integrated into a 50 MW_e coal power plant.

During recent decades, a number of studies on various applications of interconnected fluidized beds have been carried out on the design, operation and optimization of IFB systems. Different combinations, configurations and operation of interconnected fluidized bed systems were studied for the purposes of heat transportation, catalyst regeneration and conversion

of special components. Some instances of applications of interconnected fluidized bed technology are:

- Fluid catalytic cracking in the oil industry
- Thermal cracking
- Adsorption–desorption process
- Chemical looping combustion for indirect oxy-combustion of fuels
- Carbonate looping for CO_2 capture by calcium carbonate
- Gasification, fast pyrolysis and combustion of hydrocarbon fuels
- Hydrogen production within a chemical looping reforming process

2.2.1 Fluid catalytic cracking

The first conventional interconnected fluidized bed system was established as a fluid catalytic cracking (FCC) system, which is shown in Figure 2.3. The system comprises one bed which acts as a cracker (the reactor) and another one as a regenerator of the catalyst [88]. FCC catalysts are mostly particles of group A with a density of (800–1500) kg/m^3 and a size of (60–100) μm. Catalysts with high reaction activity and a large pore size are selected for this purpose; additionally, particles should have a high resistance to attrition and low production of coke within the process.

Vaporized feedstock transports the catalyst particles from the standpipe of the regenerator to the cracker, then reacted and carbon-deposited particles due to the cracking process are conveyed back to the regenerator by hot feeding air for the purpose of combustion of the carbon deposited on the catalyst. General reactions of hydrocarbon fuels in the reactor and regenerator of the FCC are shown in Equations (2.4) and (2.5) , respectively. Heavy hydrocarbon molecules break down to lighter molecules in the presence of catalyst, to which the energy is supplied by high temperature solids. During the cracking process, carbon is deposited on the catalyst particles and combusted with high temperature air.

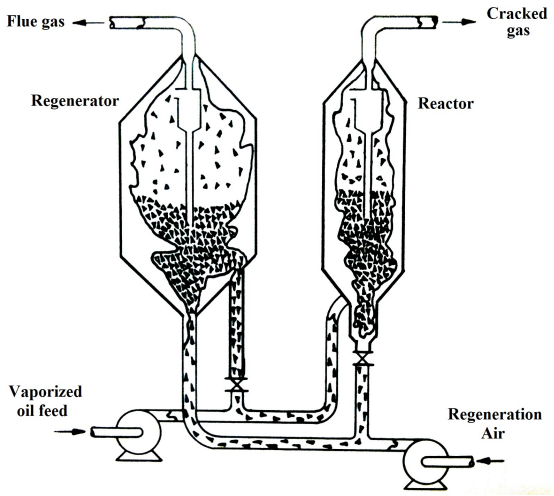

Figure 2.3: Early interconnected fluidized bed for FCC [88]

$$\alpha\, C_n H_m + (Catalyst) \longrightarrow \beta\, C_i H_j + (Catalyst + \gamma\, C) + \Delta H \qquad (\Delta H > 0)\,(2.4)$$

$$(Catalyst + \gamma\, C) + \gamma\,(N_2 + O_2) \longrightarrow (Catalyst) + \gamma\, CO_2 + \gamma\, N_2 + \Delta H \qquad (\Delta H < 0)\,(2.5)$$

After burning off the deposited carbon, hot catalyst particles return to the process loop via the regenerator standpipe. Considerable improvements and simplifications were applied on FCC systems, such as control of the catalytic circulation rate through the U bends by regulating the fluidization velocity of each line, single and self-supported column with one gravity transportation line and only one pneumatic transportation line, and a single column (Orthoflow design) similar to the configuration of an internally interconnected fluidized bed (see Figure 2.2-(C)).

Early FCC plants were constructed with two side-by-side fluidized beds, a reactor and a regenerator. Vaporized feedstock conveys hot catalyst particles from the bottom of the regenerator to the reactor. Afterwards, cracked products leave the reactor from the top and carbon deposited catalyst is transported back to the regenerator through a downcomer beneath the reactor. Combustion air carries the catalyst particles from the downcomer to the regenerator. Deposited carbon on the catalyst is burned by the high temperature combustion air and hot catalysts are applied in the next cycle for cracking the oil feed [4]. In the initial

designs, known as Exxon IV, the solid circulation rate was controlled by slide valves at the bottom of the fluidized beds [1].

Other configurations were developed later; the Universal Oil Products company (UOP) proposed a reactor–regenerator set-up in which a riser–cracker transported the catalyst from the regenerator to the reactor and solids were conveyed back to the regenerator by gravity via a downcomer initiated from the bottom of the reactor (see Figure 2.4-(A)) [1] . In each transportation line, a solid valve controls the solid flow rate from the regenerator to the reactor and vice versa. The column of solid on top of each valve prevents leakage between different parts.

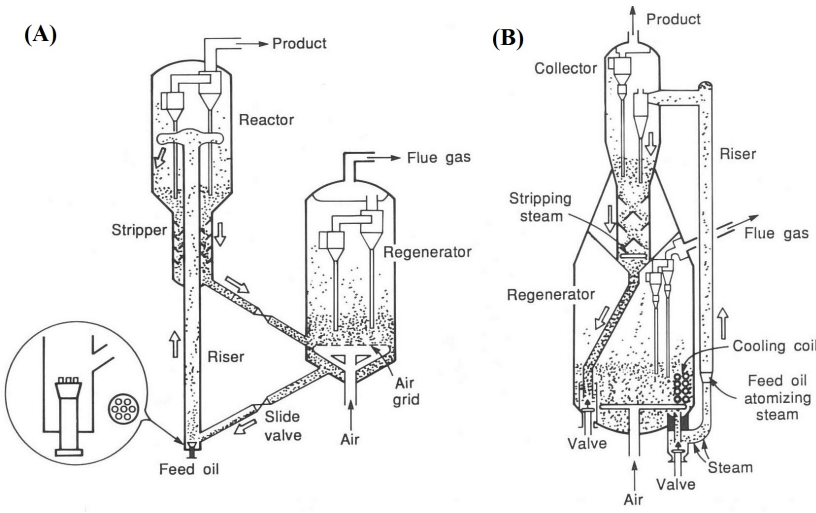

Figure 2.4: FCC plant: (A) UOP design, (B) Kellogg design [1]

During the upgrading process of heavy oil, rapid poisoning of catalyst particles, excessive carbon deposition on the catalyst and a need for further flue gas cleaning were experienced. Kellogg engineers designed a new FCC plant (Figure 2.4-(B), to overcome these problems, in which a riser–reactor transports catalyst from the bottom of the regenerator to another vessel where the gaseous products and catalyst particles are separated. Catalyst is transported back to the regenerator by gravity to accomplish the loop of solid circulation [89]. The solid flow rate into and out of the regenerator is controlled by two mechanical valves.

FCC plants have a significant function in the refinery and petrochemical industries. They are well-known as a gasoline machine, in which approximately 45% of gasoline production originates from FCC units directly or indirectly from downstream units. FCC plants reduce the residue of crude oil which in the distillation units increases the production of transportation fuel against the residue. FCC plants make refinery operations more flexible by adjusting the operating conditions to maximize the production of specific products.

2.2.2 Thermal cracking

A highly endothermic thermal cracking process is applied on hydrocarbon fuels for further organic synthesis and polymerization reactions. Fuel is cracked to hydrogen, methane and also other light hydrocarbon components. Bed materials – mostly sand – which act as the heat carrier is transported from the bottom of the reactor to a hot storage vessel. An intermediate riser conveys the materials, while during an exothermic combustion they receive enough heat to reach the temperature for further application in the reactor. The rate of solid transported from the reactor to the riser and from the hot storage vessel to the reactor is controlled by the sliding valves. Vaporized fuels are fed into the bed materials and elutriated materials are captured in a cyclone and then transported back to the solid circulation line.

The first thermal cracking plant was developed independently by Lurgi (see Figure 2.5-(A)), and Fujinagata in the 1950s to produce olefins from naphtha vapor. BASF introduced a process in which fluidized coke particles are used for olefins production from crude oil (see Figure 2.5-(B)). Their system was similarly two bubbling fluidized beds in which two solid transportation lines transport bed materials between the reactor and regenerator [1, 4].

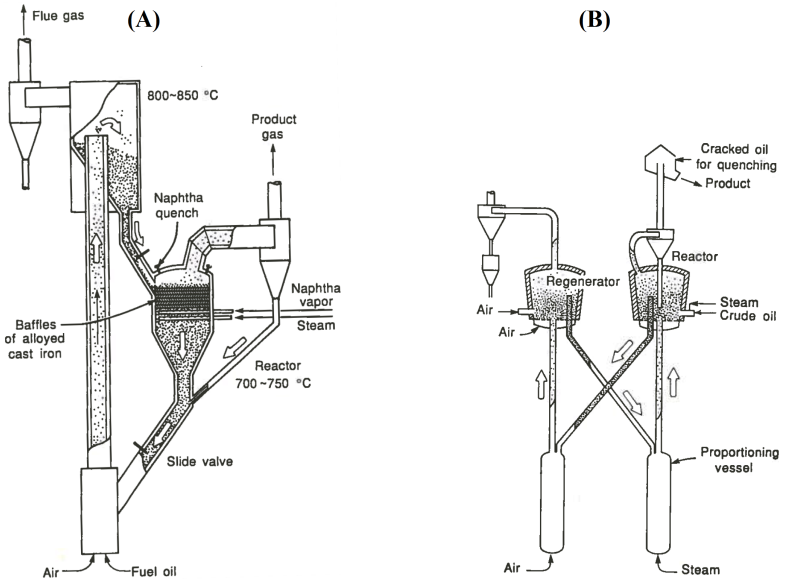

Figure 2.5: Thermal cracking (A) Lurgi unit, (B) BASF process [4]

2.2.3 Adsorption–desorption process

This process is applied for separation of gaseous pollutant and recovery of reusable compounds, which are very dilute components of a gas flow. In the primary fluidized bed, components are periodically absorbed on the active absorbent particles and in the secondary fluidized bed particles are stripped to the original form. To reduce the energy consumption for fluidization in the adsorber and also to achieve the adsorption process entirely, it mostly takes place in a multi-stage fluidized bed. Absorbent particles are transported to another fluidized bed for desorption of absorbed components on the absorbent, and finally a pneumatic transporter lifts the particles to the top of the multi-stage fluidized bed.

An interconnected fluidized bed system was proposed by Chinese engineers and reported by Wang et al. [63], to remove dichloroethane from foul gas, see Figure 2.6-(A). This plant had no mechanical devices to control the solid circulation rate, and a U-shape valve and a pneumatic pulsed feeder controled the rate of circulation.

Taiyo Chemical Laboratory (Japan) developed an internally circulating IFB system for adsorption of solvents and odorous materials of foul air. Figure 2.6-(B) shows the schematic of the process which was developed by Taiyo Chemical Laboratory. The Taiyo Chemical Laboratory unit removes odorous and soluble materials from foul gas up to 60,000 m^3/hr.

A multistage adsorber contributes to obtain stable continuous countercurrent gas–solid contact. Adsorbent materials are transported from the bottom of the adsorber to the desorber and conveyed back to the top of the adsorber by means of a riser.

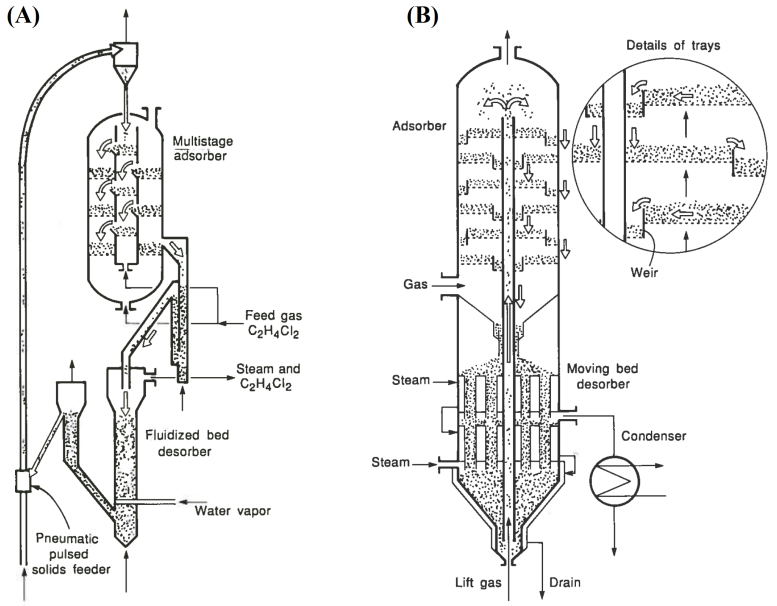

Figure 2.6: Adsorption-desorption process: (A) Wang et al., (B) Taiyo Chemical Laboratory [4]

Reichhold and Hofbauer [14] developed an internally circulating fluidized bed for continuous adsorption and desorption to separate gaseous compounds. Their configuration, which is shown in Figure 2.7, was more compact and could be operated with higher flow rates compared to traditional fixed bed separators. The IFB system comprises two compartments where the connecting wall of two fluidized beds has two openings on the top and bottom for solid material transportation. Circulation of solids between the two fluidized beds is required for a continuous ad-

sorption–desorption process. Polluted gas is utilized for fluidization of the adsorber in which unwanted components (carbon dioxide, sulphur dioxide or organic solvent vapors) are adsorbed by the adsorbent (e.g. activated carbon) and a hot air stream is applied for fluidization of the desorber. A higher flow rate of foul gas can be processed in this system, and in addition both reactors can be optimized individually.

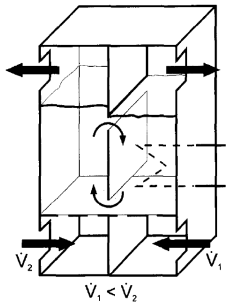

Figure 2.7: IFB system for adsorption of gaseous pollutants [14]

2.2.4 Chemical looping

2.2.4.1 Chemical looping combustion

Nowadays, regarding the utilization of hydrocarbon fuels, such as fossil fuels and coal, there is a high potential level of emission of environmental pollutants like CO_2, NO_x and SO_x. These gases which are contributed to the greenhouse effect and consequently global warming and reduction in emission of these compounds are necessary. The chemical looping combustion (CLC) which is implemented in IFB systems is proposed as one promising alternative for the separation of harmful gases.

In a CLC process, oxygen from the combustion gas is transported to oxygen carrier particles in the air reactor and then the particles are conveyed to the fuel reactor where they are in contact with fuel. So, direct contact of the fuel and combustion gas is avoided, which leads to the separate streams of combustion products and the rest of the flue gas.

Combustion products comprising carbon dioxide and water vapor are

separated after condensation of the water without any loss of energy for separation. No more or even less energy is consumed for CO_2 separation by this method compared to the oxy-combustion of fuels, for which an extra oxygen plant is also required. The separation process is implemented continuously in a CLC plant, due to the regeneration of solid inventory of the system. So, an IFB system is proposed as the potential technology to make the combustion of hydrocarbon fuels cleaner regarding the exchange of bed materials between air and fuel reactors in a CLC process.

Different superficial gas velocities in two adjacent interconnected fluidized beds lead to a driving force for solid circulation. Snip et al. [73] applied this technique to design the regenerative removal of NO_x and SO_2 for a full-scale power plant (see Figure 2.8). Two gas–solid reactions and two gas equilibria are applied for modelling of the system, as shown in Equations (2.6) to (2.9). Attrition of particles was minimized by the development of new pneumatic solid transportation procedures. Other researchers [31,34,79,90–92] also reported lower attrition of solids due to the elimination of conventional pneumatic transport systems.

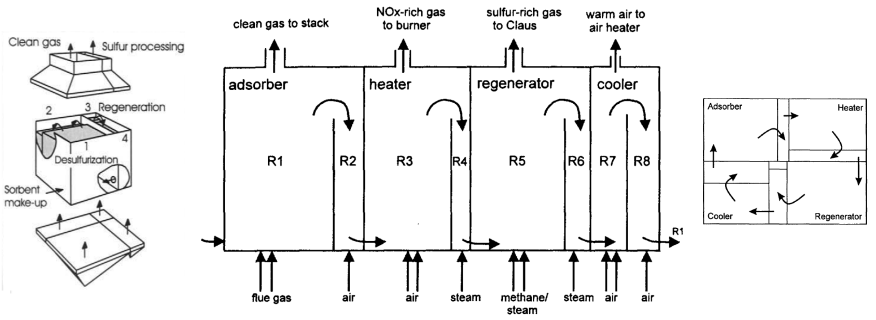

Figure 2.8: IFB system for regenerative removal of NOx and SO2 [15, 73]

$$CaSO_4 + H_2 \longrightarrow CaO + SO_2 + H_2O \tag{2.6}$$

$$SO_2 + 2H_2 \rightleftharpoons 0.5S_2 + 2H_2O \tag{2.7}$$

$$0.5S_2 + H_2 \rightleftharpoons H_2S \tag{2.8}$$

$$CaO + H_2S \longrightarrow CaS + H_2O \tag{2.9}$$

NO_x removal takes place by the application of various sorbent substances, such as: impregnated alumina with sodium carbonate [73], natural manganese ore [93] and a bed of sand with ammonia or urea injection [94]. Alumina sorbent is applied in an interconnected fluidized bed and regenerated by being in contact with natural gas or steam at around $700°C$.

Interconnected fluidized bed systems are applied for combustion of the fuels with oxygen which is provided by oxygen carrier particles, not from an isolated air separation plant for pure oxygen production [95]. In 1983, chemical looping combustion was presented as an alternative for regular combustion of gaseous fuels by Richter and Knoche [96]. Afterwards, Ishida and Jin [97] proposed a chemical looping combustion system which NiO has appropriate properties for this process with respect to oxidation rate, conversion, and physical strength. The new concept comprised two reactors, an air reactor and a fuel reactor, which were interconnected for circulation of the reactors inventory [98].

When the fuel in the fuel reactor is in contact with oxygen carrier particles, oxygen is transported to the fuel and, after complete reaction, water and carbon dioxide are the products. The reduced materials are conveyed to the air reactor (the next interconnected fluidized bed) and gets ready for the next oxidation process. Furthermore, the oxygen carrier particles receive heat during the reduction process which leads to simultaneous transportation of heat and oxygen for an endothermic fuels combustion reaction [25, 26, 34, 75, 99].

Comparing carbon dioxide separation in a convetional plant and a CLC plant shows that around (15–20)% reduction in overall efficiency of the power plants is observed due to less energy requirement for separation of CO_2. The chemical looping combustion process needs no additional energy for separation of carbon dioxide, where the rest of the combustion air in the air reactor (N_2 and rest of O_2) and the products of the fuel reactor (CO_2 and H_2O) have distinct streams. Carbon dioxide is separated easily by condensation of water vapour [78].

High reduction and oxidation reactivity, high resistance to attrition, fragmentation and agglomeration have been the most interesting characteristics of oxygen carriers, and for decads they were among the fascinating

issues in chemical looping combustion. Studies on the design and development of fluidized bed reactors for chemical looping combustion have been reviewed by Fang et al. [100]. In general, oxidation of the fuel and the regeneration of oxygen carriers can be represented by Equations (2.10) and (2.11) [74] . Particles with higher oxygen content are conveyed to the fuel reactor and particles with lower oxygen content are transported back to the air reactor.

$$C_nH_{2m} + (2n+m)\,Me_xO_y \longrightarrow nCO_2 + mH_2O + (2n+m)\,Me_xO_{(y-1)} \quad (\Delta H > 0) \tag{2.10}$$

$$Me_xO_{(y-1)} + \frac{1}{2}O_2 \longrightarrow Me_xO_y \quad (\Delta H < 0) \tag{2.11}$$

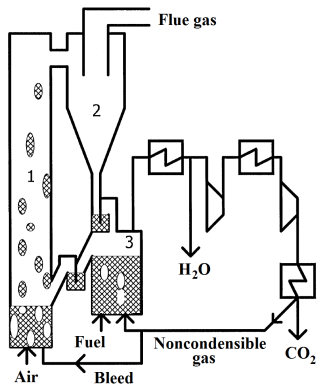

Figure 2.9: IFB system for CLC comprising an FFB and a BFB [10]

Lyngfelt et al. proposed an IFB system comprising a circulating fluidized bed (riser and cyclone) and a bubbling fluidized bed [10] for CLC of gaseous fuels. The schematic of their IFB system for CO_2 separation is shown in Figure 2.9, in which items 1, 2 and 3 are the air reactor, cyclone and fuel reactor, respectively. Construction and operation of a 10 kW CLC plant for natural gas as fuel and NiO as oxygen carrier was performed [101]. Analysis of the CLC plants shows that optimization of the following items makes it economically feasible [10]:

- sufficient reaction rate

- Appropriate conversion of gas flow
- High transfer capacity of oxygen carriers and realistic solid circulation rate

which are provided by enough solid inventory, appropriate design and reasonable pressure drops.

Kronberger et al. designed an IFB system for CLC based on (1) the solid inventory of the system, (2) the solid circulation rate and (3) gas leakage between reactors [102]. A 10 kW CLC plant for combustion of methane was developed by Adánez et al. [34] and full conversion of fuel and no deactivation of the oxygen carrier was reported at $800°C$. Son and Kim proposed a configuration of two annular fluidized beds with two additional risers for transportation of solid particles from one bed to another (see Figure 2.10) [103]. They reported full conversion of methane to CO_2 and H_2O, and a very low amount of CO and no H_2 emission in the exit gas were detected. Many studies on CLC with IFB systems have been done, the results of which are shown in the next chapters.

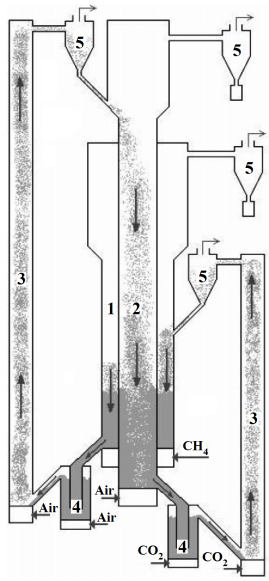

Figure 2.10: IFB system of KAIST for CLC of methane [103]

2.2.4.2 Carbonate looping for carbon dioxide capture

In 1999, Shimizu et al. proposed a novel process for continuous capture of the carbon dioxide from flue gas by means of a carbonation reaction of calcium oxide [8]. The concept of the process, shown in Figure 2.11-(A), consists of two interconnected fluidized bed reactors, an absorber and a regenerator, which are called the carbonator and calciner, respectively. CO_2 from the flue gas of a power plant is captured during the carbonation process in the carbonator, which is operated at around $650°C$, and practically the decomposition of carbon dioxide from $CaCO_3$ is achieved in a calciner which operates at around $950°C$ [29, 30, 85, 104–106].

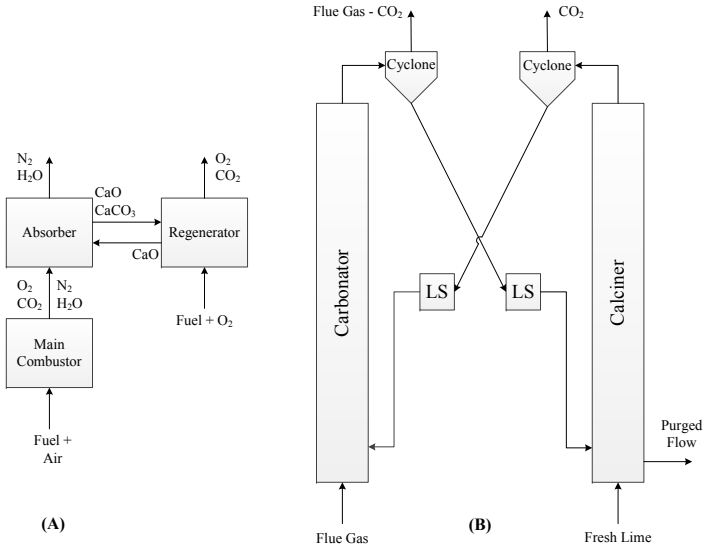

Figure 2.11: (A) Concept, (B) Schematic diagram of CO_2 capturing IFB (an example)

Oxy-combustion of coal in the calciner provides the energy required for the calcination process, and subsequently an almost pure CO_2 stream out of the calciner is purified and compressed to be ready for storage. Studies by Rodriguez et al. [107] on the energy demand of the endothermic calcination process show that this process employs (35–50)% of the total energy of the system. However, the high energy consumption of the calciner seems to be a point in need of optimization for the whole system [8, 106, 108].

A number of studies show that the high quality heat which leaves the calciner can be recycled in a highly efficient steam cycle, minimizing the heat loss of the system. Economic analysis of a carbonate looping process consists of a combustion plant, an oxy-fired calciner and a carbonator decreases around 30% in the operating cost of a standalone oxy-fired plant. In a carbonate looping process, there is no need for a gas pretreatment process and also the sorbent is cheap and easy to access. In addition, purged limestone has a great demand in cement production and the deactivated sorbent is a good absorber of SO_2 to apply in the desulphurization process of CFB combustion boilers [8, 29, 105].

The concept [8] and schematic diagram [30] of the interconnected fluidized bed system which was applied for CO_2 capture from flue gases are presented in Figure 2.11-(A) and (B). Flue gas from a power plant is utilized for fluidization of the carbonator, and the calciner is fluidized with oxygen plus recycled flue gas from the calciner itself. Calcium oxide is transferred to the carbonator and comes into contact with the flue gas, which contains high CO_2 concentration. Since the carbonation process is an exothermic reaction, the generated heat can be utilized for steam production and a subsequent power generator. When the CO_2 partial pressure is maintained at 0.15 *atm* in the carbonator, an efficiency of around 90% is expected for CO_2 capture [8].

The most prevalent configuration of the IFB systems which have been applied for chemical looping processes comprises a fast fluidized bed (riser), a cyclone, a bubbling fluidized bed and the solid transportation device (STD). In 2008, Pröll et al. [19] proposed the concept of two interconnected circulating fluidized beds comprising two circulating fluidized beds and loop-seals to prevent gas leakage between the two riser. Subsequently, Ryu et al. [109] and Abanades et al. [29] developed and constructed two interconnected circulating fluidized beds (a bubbling fluidized bed and fast fluidized bed, respectively) for CO_2 capture. Experimental and theoretical studies on the behaviour and operation of IFB systems for Ca-looping have been implemented, such as studies in CSIC (Spain), DoE (Italy), IFK (Germany) and VUT (Austria) [30, 59, 65, 110, 111].

2.2.4.3 Indirect gasification

The application of a four-compartment IFB system for combustion of biomass was proposed by Sniders et al. [112], the idea which was inspired by Kuramoto's study [113] on a two-compartment IFB system as a possible configuration for transportation of solid particles between two adjacent fluidized beds. The set-up (see Figure 2.12) consists of two vigorously fluidized beds (fast bed) and two slowly aerated beds (slow bed); gaseous products of each pair are prevented from being mixed with the other pair by extending the wall between them to the maximum height of the device. The gasification and combustion processes take place in their own pair of the beds and their products are not mixed. The solid circulation rate (SCR) was studied as a function of the fluidization velocity, bed inventory and orifice pressure drop, and the SCR was found to be higher when all these parameters became larger.

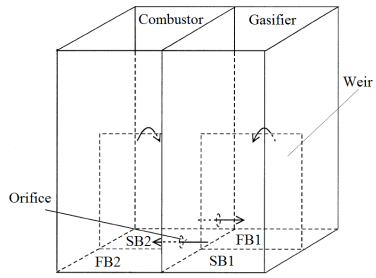

Figure 2.12: Four-compartment IFB system (FB: fast bed, SB: slow bed)

Two circulating fluidized beds as an IFB system were studied for the combustion of biomass and capture efficiency of CO_2 by the carbonation process [114, 115]. In the combustor – carbonator, biomass is burned under air-fired combustion conditions and CaO is supposed to capture CO_2 at specific operating temperatures around $650°C$. In the combustor–calciner, which is operated at around $950°C$, biomass is combusted to provide energy for calcination of $CaCO_3$ particles. The authors developed a simple model based on the carbonation – calcination process and validate it with their experimental results, which demonstrate that the overall process is controlled by the carbonation reaction rate [33], and the feasibility of this concept was assured technically [86].

Low-temperature gasification was proposed by the combination of a pyrolysis reactor and a char reactor in a circulating–bubbling IFB system [116] . The schematic of the low-temperature circulating fluidized bed (LT-CFB) gasifier is shown in Figure 2.13 [117, 118] . Biomass fuels are fed into the pyrolysis reactor to be in contact with hot sand and ash particles from the char reactor. The low pyrolysis temperature (around $650°C$) and retention time of particles result in the formation of only light tar compounds. The residual char and the pyrolysis gases are separated in the cyclone and solids are transported to a bubbling char gasifier which is operated at around $730°C$.

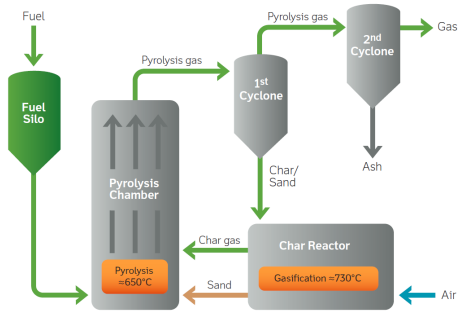

Figure 2.13: LT-CFB gasifier, Dong Energy (Pyroneer)

Gaseous products of the char gasification, as well as the hot sand and ash particles, are transported to the bottom of the pyrolysis reactor. The stream of sand and ash carries heat from the char reactor to the pyrolysis reactor, which supplies the heat required for low temperature gasification of the fuel. Hence, no additional heat transfer surfaces are necessary to provide heat for the pyrolysis. The secondary cyclone captures the fine particles, and deposited ash containing alkaline and phosphor components can be applied as a fertilizer product.

2.2.4.4 Carbonate-catalytic looping gasification

When hydrogen is utilized as a fuel it produces water, so hydrogen could be the most environmental - friendly fuel ever. In recent years, hydrogen has been applied in direct processes for energy production and also in indirect energy conversion processes. Most procedures for hydrogen

production need after-treatment for separation of carbon dioxide or additional strategies for enhancing the hydrogen yield.

Conversion of biomass to hydrogen is achieved by steam gasification, supercritical steam gasification, flash pyrolysis and biological pathways. Here, we discuss the steam gasification of biomass for the production of hydrogen. This process is developed in the presence of calcium oxide in interconnected fluidized beds, where one bed is a gasifier and another acts as a regenerator of calcium carbonate particles back to calcium oxide.

So, the presence of calcium oxide can basically affect both the production of hydrogen and the separation of CO_2. Absorption of carbon dioxide leads to pushing the water–gas shift reaction ($CO + H_2O \longrightarrow CO_2 + H_2$) towards the products; hence more absorption of CO_2 contributes to more production of hydrogen and a lower presence of carbon monoxide in the produced gas.

The utilization of biomass as a zero or negative factor of CO_2 emission (due to CO_2 adsorption by plants during cultivation), the production of hydrogen as one of the clean fuels, and the separation of CO_2 during the gasification of biomass are considered as significant advantages of this system.

However, two issues should be taken into account:

- Conventional steam gasification is endothermic and the required heat for this process should be prepared by combustion of a portion of biomass, produced gas or maybe another form of renewable energy. However, in a biomass steam gasification and in the presence of CaO, the carbonation process is exothermic, but the energy demand of the calcination process (regeneration of sorbent) should be considered when estimating overall process efficiency [119].

- From the view point of the carbonation process which takes place at around $(600–700)^\circ C$, the operating temperature of the gasification process cannot exceed this range [18]. So, due to the low operating temperature of the gasification process, heavy hydrocarbons cannot be broken down to lighter ones, so the production and presence

of tar is very probable. The application of nickel-based catalyst, dolomite and alkali metals eliminates tar formation. Additionally, the interaction of CaO and tar is observed to decrease the CO_2 capture efficiency due to sorbent deactivation by the formation of coke on the particles.

The operating temperature, operating pressure and steam/biomass ratio are the significant design parameters which can affect the H_2 production efficiency of an IFB system for biomass steam gasification with CO_2 absorption. Investigations on studies of these parameters are explained later.

Two options are proposed for the reforming of biomass to produce hydrogen and separate carbon dioxide [120], an IFB system comprising two fluidized beds (fuel reformer, sorbent regenerator) and a system of three fluidized beds (fuel reformer, sorbent regenerator and air reactor). In Figure 2.14, schematics of these processes are shown.

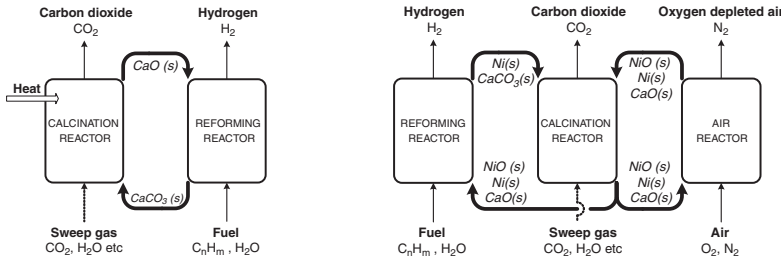

Figure 2.14: Schematic of steam gasification for hydrogen production [120]

2.2.5 Chemical looping hydrogen (water splitting)

The water splitting process involves two fluidized beds which are interconnected and act as an oxidizer and reducer [39, 121–123]. Syngas or pure methane as fuel is introduced to the reducer and the fuel is in contact with oxygen carrier particles to receive oxygen for reduction. Figure 2.15 reveals the concept of the water splitting process, where $Me_xO_{(y-1)}$

and Me_xO_y are metal particles and metal oxide particles (or metal oxide with lower and higher oxygen content), respectively.

The products of the reaction in the reducer are carbon dioxide and water, and after condensation of the water vapor, the pure carbon dioxide stream is utilized for further applications or sequestration. Oxygen carrier particles which have released oxygen are transported to the oxidizer to absorb oxygen again by being in contact with water. Then, regenerated oxygen carrier particles are conveyed back to the reducer for the next cycle and a stream of hydrogen and water vapor leaves the system. After condensation of the water, pure hydrogen flow is accessible.

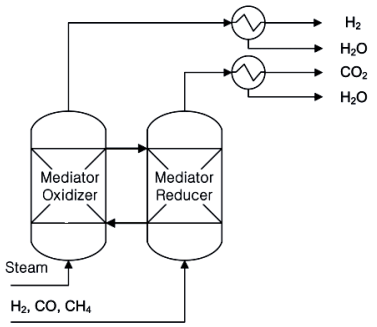

Figure 2.15: Theory of a water-splitting system

Ryu et al. proposed nickel as an appropriate oxygen carrier for maximum hydrogen generation by the water-splitting process and applied syngas from a gasifier of heavy residue oil as the reducing medium [39]. The effect on hydrogen production of nickel oxide, iron oxide and a compound of both was investigated and the compound of nickel and iron oxide was proposed for stable continuous operation of the process [121] . Studies on copper oxide supported on aluminium oxide showed better reactivity than when supported on silicon dioxide [122]. Murugan et al. also utilized iron oxide ($60wt\%$) and nickel oxide ($20wt\%$) supported on aluminium oxide to compare two perovskite-type oxides ($20wt\%$) [124]. Chiron et al. stated that a compound of iron oxide and copper oxide has a higher hydrogen yield than each individual one separately [123].

Various configurations of IFB systems for the operation of two simultaneous reactions in one process have been investigated, including:

- Two bubbling beds mode with gas switching: for processes with a low reaction rate in which higher contact time is favourable. The fluidization gas of the beds switches periodically. The different operating temperature and pressure of each fluidized bed makes this switching difficult.

- Bubbling-transport mode: in this system, a bubbling bed is used for reaction and a transport bed is used for both reaction and transportation. Maintaining the pressure balance between these two fluidized beds and loop-seals is difficult but feasible.

- Bubbling-bubbling-transport mode: Two bubbling beds are applied for reactions and a transport bed is used for conveying solids. The pressure balance is difficult to maintain and the problem of solid backflow generally exists.

A unique configuration for chemical looping processes, especially for water-splitting, was proposed by Rue et al. [40]. Each fluidized bed in this IFB system comprises a bubbling bed with solid injection nozzles in the bottom and a transport bed at the top (see Figure 2.16). Long-term operation, studies on the solid circulating rate and gas leakage and lower attrition and loss of bed materials indicate that this configuration is feasible for water-splitting applications by an IFB system [39, 109].

2.3 Fluidization of fine particles

Gas–solid flow in a fluidized bed is characterized by the mode of gas–solid fluidization and particle classification plays a significant role. This classification determines the fluidization regimes based on particle size and density, as explained in the introduction. Fine and ultrafine particles, regarding their density and size, are allocated to group C, which are very cohesive and difficult to be fluidized. The handling, dispersion and processing of the fine particles in industrial applications are increasing nowadays due to the large surface area to volume ratio despite of their small size, which satisfies the reaction rates per volume of the reactor in a gas–solid reaction [125].

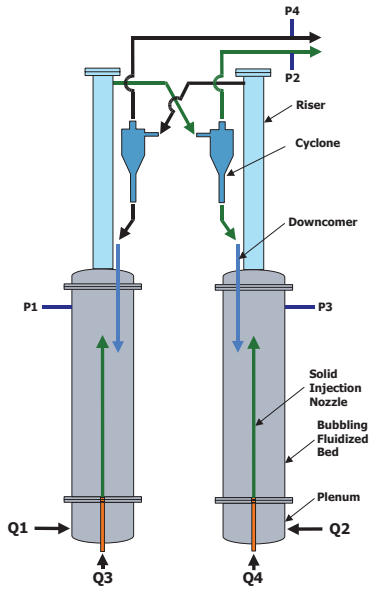

Figure 2.16: Two bubbling fluidized bed, Ryu et al.'s IFB system for water splitting [40]

Three types of force are considered which can affect and control the movement of particles in a gas–solid flow: (1) gas–solid interaction forces, (2) interparticle forces, (3) external field forces. The two latest items have no direct impact on the gas flow pattern, while gas–solid interaction forces affect it directly.

Mostly, group C particles are fluidized as very porous agglomerates due to their high interparticle forces, which increase the stickiness of the particles and the formation of agglomerates. Regarding the difficulties in fluidization of fine and ultrafine particles, a number of solutions and treatments have been applied on fluidized beds to improve fine particles fluidization. In following, the interparticle forces are briefly described and some solutions to the fluidization of fine particles are introduced as reviewed by Shabanian et. al [126].

2.3.1 Interparticle forces

A variety of forces cause the cohesion of particles in a gas–solid flow with fine particles, van der Waals force, electrostatic force and capillary force are considered the main forces which specifically have significant effect on fluidization of the fine particles.

van der Waals force

The van der Waals force is determined by the sum of the attractive or the repulsive forces between similar / neutral / charged molecules and also between microscopic solids. This force comprises the force between two permanent dipoles (Keesom force), a permanent dipole and an induced dipole (Debye force) and two instantaneously induced dipoles (London dispersion force) [126].

A quickly changing dipole of an atom generates an electric field which affects the polarizability of neighbouring atoms. An induced dipole to a neighboring atom tends to move in phase with the original dipole, which contributes to the generation of an attractive interaction known as the van der Waals force. The existence of this force can be explained not only on an atomic scale but also on microscopic particles scale.

The van der Waals force between two smooth spheres with radius R and distance Z is given by Equation (2.12), in which $h\varpi$ is the Lifshitz-van der Waals coefficient. This coefficient is a function of the nature of bodies in contact and the surrounding medium, and H_r is the hardness of the softer body. Values of Z and H_r are suggested as $4\mathring{A}$, where the van der Waals is the maximum for this distance, and $10^8 \frac{N}{m^2}$ for the hardness of undeformable solids, respectively [127]. If the spheres in contact are not the same size (R_1 and R_2), an equivalent R is stated as in Equation (2.13).

$$F_{vdw} = \frac{h\varpi}{8\pi Z^2} R \left(1 + \frac{h\varpi}{8\pi Z^3 H_r}\right) \quad (2.12)$$

$$R = \frac{R_1 R_2}{R_1 + R_2} \quad (2.13)$$

Most solid powders have many asperities on their surfaces; this consideration is implemented by Equation (2.13). Figure 2.17 represents the van der Waals force of 10 nm silica particles with a smooth surface and 0.5 nm asperities. The X-axis and Y-axis are the distance between the surfaces of particles and normalized van der Waals force, respectively. The force values are normalized by diving to the gravity force on a single particle. The effect of asperities on degradation of the van der Waals force is revealed at small distances between the surfaces.

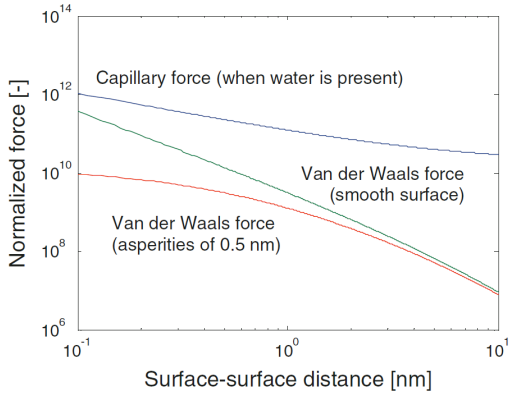

Figure 2.17: Comparison of van del Waals and capillary forces [128]

Electrostatic force

Sliding or contact of non-conducting particles with the surface of a dissimilar material, which is accompanied by an exchange of electrons on the surface of the two substances, contributes to the generation of electrostatic force. The motion of electrically charged particles in a gas–solid flow affects the nearby charged particles. According to Coulomb's law, the electrostatic force between two charged particles is expressed by the

product of the electrical charge of each and the inverse proportion of the square distance between their surfaces. Electrostatic force is shown in Equation (2.14), where q_1, q_2, s and ϵ are the electrostatic charge of the first and second particles, the distance between the two objects and the permittivity of the surrounding medium, respectively.

$$F_{esf} = \frac{1}{4\pi\epsilon}\frac{q_1 q_2}{s^2} \tag{2.14}$$

where s is the distance between the two objects. Electrostatic force, compared with other interparticle forces like van der Waals, is negligible, and this force disappears in a humid medium due to discharge of the objects.

Capillary force

Capillary force is generated due to condensation of moisture from the surrounding medium on the surface of the particles, which forms a liquid bridge in the gap between objects. Regarding pressure deficiencies in a bulk liquid and the surface tension of the liquid on both objects, an attractive force, namely capillary force, is produced. Figure 2.17 gives an impression of the quantity of the capillary force compared with van der Waals force.

Capillary force, in the case where the vapor pressure of the medium is close to saturation pressure, can overtake the gravitational force and van der Waals force. The capillary force is estimated by Equation (2.15), where γ, α, β and R are the liquid surface tension, half filling-angle, contact angle and radius of the objects (see Figure 2.18).

$$F_{cpl} = 2\pi\gamma R\, Sin\alpha\, Sin(\alpha+\beta) + \pi R^2\left[\gamma\left(\frac{1}{r_1}+\frac{1}{r_2}\right)\right] Sin^2\alpha \tag{2.15}$$

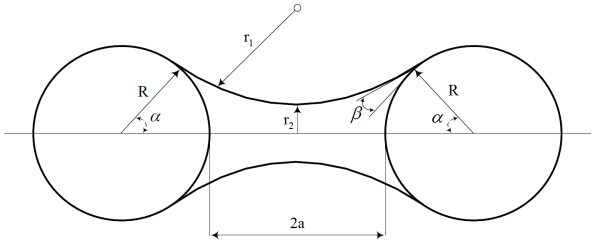

Figure 2.18: Liquid bridge between two spherical objects [126]

2.3.2 Assistive methods for fluidization of fine particles

During the fluidization process of coarse particles, group B and D in Geldart's classification, gravity force is the dominant force against the interparticle forces. Reducing the particle size down to group A, the ratio of interparticle force to gravity force increases and the interparticle force gets comparable with the gravity force. For lower size particles in group C, cohesion between particles overcomes the gravity force. In specific cases, for instance dry fine particles less than 30 μm, the adhesion exceeds the weight of particles by several orders of magnitude [126].

Considering the dominant interparticle forces of fine particles in group C, normal fluidization of this type of particle is difficult due to plugging, channeling and the formation of stable cake at the bottom of the bed. For superficial gas velocities far from the minimum fluidization of particles, such fine particles form dynamically stable agglomerates. Increase in the size of the agglomerated particle, even in the order of micrometer and millimeter, changes the fluidization behavior of these fine particles. However, this phenomenon does not take place for all sizes or types of group C particles.

In general, fine particles under fluidization are sub-classified to: (1) the particles which cannot be fluidized under any circumstances due to the lack of formation of agglomerated particles because there is no appreciable cohesion between particles. (2) the fine particles which form agglomerates and are fluidized under agglomerate particulate and bubbling fluidization. Various assisting methods have been developed to make appropriate fluidization of group C particles feasible. Following, these

methods are explained together with their limitations and advantages. A large number of studies on the fluidization of fine particles and assisting methods were reviewed by Shabanian et al. [126] and details of various operating conditions and particle properties are available in their study.

Sound-assisted

Various sound pressure levels and different frequencies were studied as an assisting method for fluidization of fine particles. In general, sound-assisting for fluidization eliminates the channeling and slugging, the size of agglomerate decreases and to some extent the fluidization quality of fine particles is improved. However, at the present time application of this method for large industrial plants is not proposed, given the high energy consumption and restriction on operation arising from the narrow boundary around optimal operating conditions.

High-intensity sound pressure levels: (1) reduce the entrainment of fine particles, (2) homogeneous fluidization take place under low frequencies and (3) degrade the minimum fluidization and minimum bubbling velocity. High frequency sound waves in the range of (200–600) Hz cause bubbling fluidization to take place.

Vibration-assisted

External vibration of a fluidized bed which is filled with solid particles involving fine/ultrafine particles improves the fluidization quality, increases the bed pressure drop, increases the bed expansion and decreases the elutriation of the particles. Mechanical vibration of a bed of fine particles makes the fluidization feasible, decreases the size of agglomerates up to a critical vibration intensity, postpones the formation of agglomerates, decreases the minimum fluidization velocity, and eliminates channels and cracks.

Magnetic field-assisted

An oscillating magnetic field applied on magnetic particles or a mixture of magnetic and non-magnetic particles is an effective assisting method to ease the fluidization of fine particles. Fine magnetic particles form chains which are moved by solid particles in the bed, mostly magnetic particles larger than the bed particles stay close to the gas distributor.

For a mixture of magnetic and non-magnetic particles, the bubble sizes are used as comparison criteria for the quality of fluidization, which is assisted by an oscillating magnetic field. Bubble size is strongly affected by magnetic field intensity and frequency, and the fraction of magnetic particles to bed particles. The frequency of the magnetic field and fraction of magnets in the bed have inverse effects on the size of bubble.

Electric field-assisted

Applying the electric field during fluidization of fine particles was investigated, although very few number of studies is available. A study of a fluidized bed of fine particles with horizontal electric field identifies an intense reduction in bed expansion, which is explained as the downward action of electric force in addition to the gravity force. So, at least this technique could be applied to decrease the elutriation rate of fine particles.

The electric charge of the bed of fine particles has no effect on the size and the structure of agglomerates. Instead, by pushing the agglomerates towards the wall of the bed, it results in a reduction of bed expansion and heterogeneous fluidization. Non-uniform distribution of electric field along the height of the bed of fine particles is considered as an effective way of implementing the electric field, in which: (1) at the surface of the bed fine particles and tiny agglomerates are prevented from elutriation by a weak electric field; (2) at the bottom of the bed, large agglomerates that have sunk are agitated close to the gas distributor and break the channels, which leads to an improved distribution of gas in the bed.

Centrifugal fluidized bed

In centrifugal fluidized beds, the following benefits are expected: (1) the initiation of an unstable bubbling regime is postponed, (2) elutriation of particles even at high fluidization velocities is prevented by controlling the rotational speed, (3) higher throughput per unit area of distributor is achieved, (4) greater gas and solid contact is resulted, (5) given the thin bed height, no bubbles or very tiny ones are formed, (6) the process time is shorter, and (7) the size of the fluidized bed is more compact. Such advantages can be applied to improve the fluidization of fine particles.

The application of a centrifugal fluidized bed could shift group C particles to group A or even group B at high rotational speeds. Highly agglomerated particles are fluidized under high rotational accelerations, which contribute to breaking down the agglomerates to smaller sizes close to the gas distributor. Increasing rotational acceleration has a direct linear effect on the minimum fluidization velocity, an inverse effect on bed expansion, an opposite effect on agglomerates size and a direct influence on the density of agglomerates.

Tapered fluidized bed

Fluidization of larger particle sizes and also larger agglomerates at the bottom of the bed, as well as fluidization of fine particles at the top of the bed, is feasible when the entrainment of particles and tiny agglomerates from the surface of the bed is prevented. The conical configuration of a fluidized bed leads to completely mixed fluidization of fine and coarse particles and agglomerates with no segregation, which cannot individually be fluidized in conventional cylindrical fluidized beds.

Binary particle-assisted

The addition of an appropriate amount of foreign particles to a bed of fine particles suppresses the agglomerates and a new mixture with free-flowing characteristics is achieved. The size and ratio of binary particles

to the bed of cohesive particles are selected in such a way that the cohesive interparticle force in the mixture between fine particles decreases and the cohesive particles collected on the foreign particles forms large enough hybrid particles to be characterized as group A. The Lifshitz–van der Waals coefficients of the binary and main particles should be close to each other to be assured of attraction and settling of fine particles on the foreign particles.

Micro jet-assisted

The fluidization quality of fine particles which form nanoparticle agglomerates is enhanced by the application of secondary flow into the bed. Downward flowing micro-nozzles toward the gas distributor result in significant bed expansion in the absence of bubbles. Micro-jets in a highly cohesive bed of fine particles break the agglomerates down to lower sizes, weaken the channelling, diminish bubble formation and promote particles flowability. Additionally, it reduces the minimum fluidization velocity and increase the bed pressure drop through the bed, which indeed represents better quality fluidization. Given the agglomerates–agglomerates collisions and reduction of their sizes, nanofluidization by micro-jets is enhanced and mixing of nanoparticle species occurs on the nanoscale.

The application of micro-jets has advantages compared with other assisting methods: (1) more efficient and simple to use, (2) no need for expensive equipment or additional particles, (3) lower energy consumption, (4) easy to scale-up, and (5) utilization for a wide range of fine particles and even nanoscale particles. The abovementioned items suggest the micro-jet assisting method as one of the future potential procedures for fluidization of fine particles even on an industrial scale.

2.4 Solid transportation devices

Two types of solid transportation device were applied for recirculation of solid particles in a circulating fluidized bed (CFB): mechanical and non-mechanical valves. In mechanical valves, the moving parts, such as the

rotary, screw, butterfly and slide valves, control the solid feeding rate. Due to sealing and mechanical problems, the mechanical valves cannot be used in processes which apply high temperature and pressure [129]. Thus, non-mechanical valves are proposed and are employed for high temperature and high pressure processes.

Initially, operation of the non-mechanical valves of the circulating fluidized bed (CFB) was one of the major challenges due to the importance of the solid recirculation rate. Non-mechanical valves are divided into two types: solid flow control devices and solid flow through devices. Examples of solid flow control devices are J-valves, L-valves and V-valves (Figure 2.19-(a), (b) and (c)). Solid flow through devices are pot-seals and loop-seals (Figure 2.19-(d) and (e)).

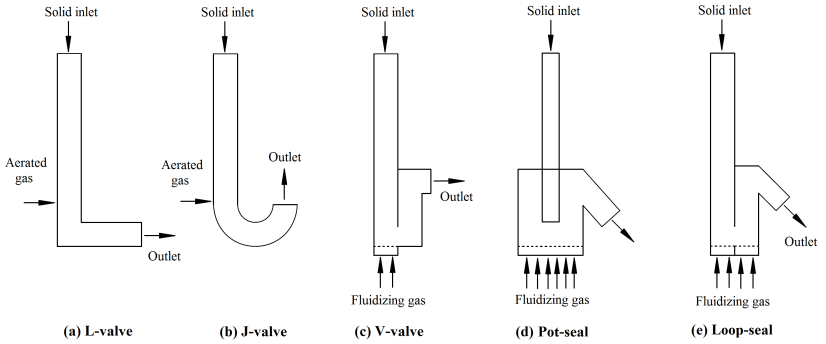

Figure 2.19: Non-mechanical solid transportation devices

Solid flow control devices are mostly employed for operation of the processes where Geldart's group B and D particles are applied. In addition to the mentioned particle types, solid flow through devices also can handle group A particles, but not group C. Group A particles are not defluidized just after shutting off the gas flow, but remain fluidized and flow like water through the L-, J- and V-valves (which makes the valve uncontrollable).

Geldart's group C particles are fine and ultrafine particles and the interparticle forces play a significant role in fluidization of this type of particles. solid transportation devices are regularly operated under a bubbling regime or around minimum fluidization velocity, but particles of group C are difficult to be operated under these conditions.

2.4.1 Solid flow control devices

L-, J- and V-valves control the flow of solids which pass through these devices by modifying the amount of aerated gas which is added to the valve. The major portion of the aerated gas flows to the outlet of the device and solids pass through the constricting bend considering the imposed gas drag on the particles.

Particles do not start moving through the valve unless after feeding air to the aerated ports. Up to a specific amount (minimum aeration rate), the solid transportation rate is zero and afterwards it increases sharply by increasing the aeration rate [130] (see Figure 2.20).

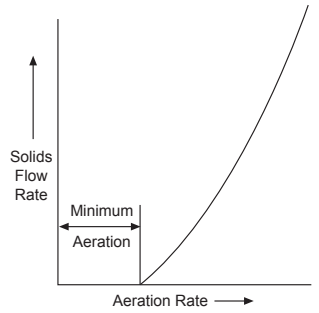

Figure 2.20: Aeration rate of the J-valves [130]

L-valves are mostly used for industrial applications and are generally employed for CFB reactors. The vertical leg of the valve is connected to the hopper of the cyclone, which is called the downcomer, and the outlet to the riser. Solids in the downcomer act as a moving dense bed in which a small amount of the aerated gas assists to transport them to the relatively dilute bed in the riser.

2.4.2 Solid flow through devices

Loop-seals are generally employed in CFB boilers and gasifiers. A typical loop-seal consists of two sections, the supply chamber and recycle chamber. The supply chamber is connected to the hopper of the cyclone,

namely the standpipe. The solids are transported within the loop-seal to the recycle chamber which is provided for the riser through the recycle pipe [130].

The solids are fluidized in the recycle chamber and flow to the recycle pipe like a fluid. A weir exists between the recycle chamber and the recycle pipe, where overflowing fluidized solids are transported to the recycle pipe and into the riser by gravity (see Figure 2.21). In a commercial size loop-seal, the bottom of the standpipe needs to be fluidized, mostly to help particles in Group B and lower sizes to move down to the device. Essentially, the standpipe is not aerated, but it can be applied in special cases to assist the transportation of the solids down to the loop-seal.

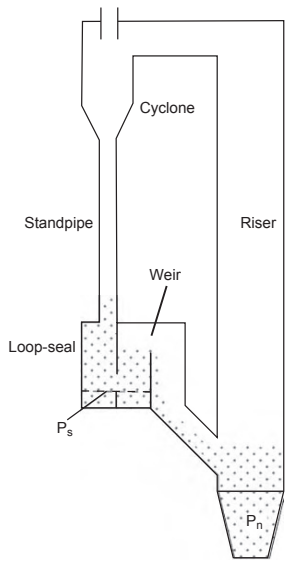

Figure 2.21: A CFB reactor with a loop-seal solid recirculating system [130]

2.4.3 Principles of solid transportation devices

When the fluidized particles are acting as a liquid, a simple test on a gas–liquid system can explain how a solid transportation device works. Consider two columns of water (AB and CD) which are connected to

each other from top and bottom, where there is an inlet at the bottom of the CD column and an outlet on the connection tube on top. WAir is introduced to the inlet, bubbles are formed and rise along the aerated column and flow toward the outlet (see Figure 2.22).

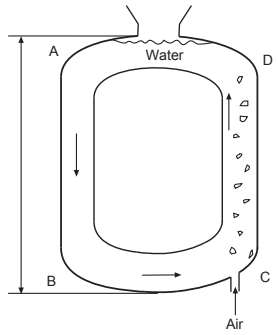

Figure 2.22: Simple test to demonstrate the principle of non-mechanical valves [130]

The bulk density of the water in column CD is less than the density of the water in column AB, which contributes to lower static pressure at the bottom of column CD. Therefore, the higher static pressure of the water in column AB pushes the water towards column CD. The flow of water between points B and C leads to continuous circulation of water in the vessel while the aeration is continued.

The same analogy is applied for the gas–solid contact flow in the solid transportation device of a CFB system. The particles collected by the cyclone accumulate in the standpipe and the function of the solid transportation device is to give fluid properties to the solid. Due to the presence of the static pressure difference of each side of the device, solids are transported from the standpipe to the riser.

Non-mechanical valves transport the solids from the high static pressure standpipe to the low pressure riser. So, the height of the solid in the standpipe limits the solid circulation rate in a fast CFB riser. This occurs when the height and static pressure of the solids in the standpipe are not enough to push an adequate amount of solid to the riser to compensate the solid carrying capacity of the gas in the riser.

And when the gas velocity in the CFB riser is not high, the high static pressure of the solid in the standpipe pushes more solids to the riser than the carrying capacity, which leads to the formation of a dense bed at the bottom of the riser [131].

The solids are captured in the cyclone and dropped to the standpipe and flow by the gravity to the supply chamber of the loop-seal. Aeration to the supply chamber should be low enough to keep the gas flow in the standpipe below the minimum fluidization velocity. For this case, the solids move downwards through the standpipe as a moving dense bed. If no gas is fed to the supply chamber, the solids move out of the standpipe to form a slope with the repose angle (α) of the particles.

The particles do not flow like liquid inside the supply chamber considering the presence of interparticle friction (f_{int}). The interparticle friction is a function of particle shape and size, and for fine particles other interparticle forces should also be taken into account. Therefore, different kinds of particles with various shapes and sizes flow differently within an individual system.

Aeration to the bottom of the supply chamber passes through the particles and acts as a lubricant which reduces the interparticle friction and the angle of repose ($f_{int} = tan(\alpha)$). The repose angle is reduced by increasing the amount of aeration up to the corresponding minimum fluidization velocity of the particles.

As an example, the repose angle of two types of silica sand (113 and 244) μm and glass beads of 262 μm were studied under different aeration gas velocities. A slight decrease of the repose angle against increasing the gas velocity is observed, while a sharp decrease takes place after reaching the minimum fluidization velocity (see Figure 2.23). At around the minimum fluidization velocity and higher values, the repose angle suddenly decreases due to the liquid-like behaviour of the fluidized solids. In this condition, the solids move like a liquid in a tube [130].

Solids flow from the standpipe and supply chamber to the recycle chamber by aerating the particles around the minimum fluidization condition. In the recycle chamber, the solids remain fluidized by feeding the gas to

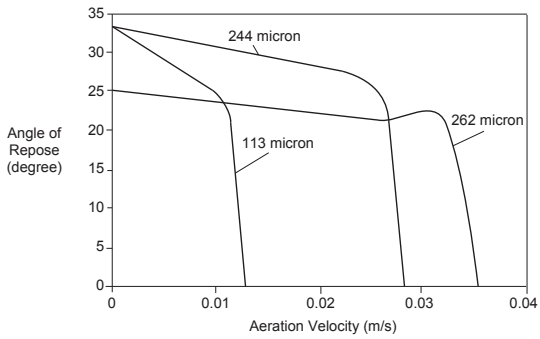

Figure 2.23: Repose angle versus aeration velocity [130]

the bottom of the chamber. Fluidized particles flow over a weir of the recycle chamber to the riser, as when the liquid level is higher than the weir and flows over. Figure 2.24 represents the schematic of a loop-seal with solids flowing over the weir.

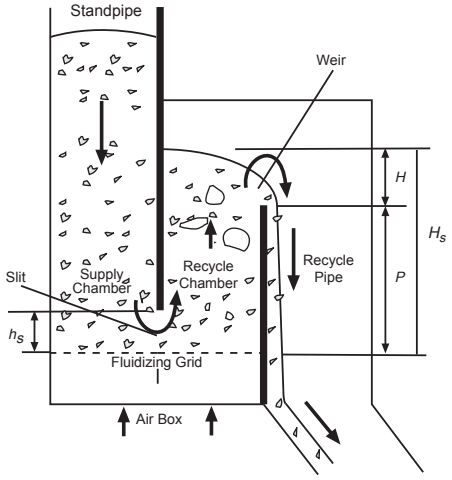

Figure 2.24: Supply chamber and recycle chamber of a loop-seal [130]

An empirical correlation defines the relationship between the design parameters and solid flow rate of a rectangular sharp-crested weir of the recycle chamber. Equation (2.16) represents the correlation to estimate the rate of solid transportation through the loop-seal for a specific range

of particle sizes [132].

$$W_s = \frac{2}{3}(1-\varepsilon)\,\rho_p\,C\,W\sqrt{2g}\,H^{1.5} \tag{2.16}$$

where W and H are the width of the weir and excess height of the fluidized solids above the weir, respectively. Coefficient C is between 0.065 and 0.08 for particles in the range of 150 μm to 250 μm.

Aeration of the recycle chamber produces a drag force on the particles which exceeds the interparticle friction force and the resistance of solid in the bends. On the other hand, aeration by keeping the particles fluidized and in the recycle chamber under a bubbling regime causes the particles to flow through the valve. Aeration is implemented in a way which is desirable for solid flow; this means the bulk density of the solids in the recycle chamber should be less than in the supply chamber, where the static pressure pushes the particles toward the recycle chamber and to the CFB riser.

The height of the fluidized solids in the recycle chamber (H_s) (see Figure 2.24) assures the sealing of the valve and prevents pressure fluctuation in the riser from interrupting the functionality of the loop-seal. It prevents the blow-up of solids in the loop-seal for the cases which a sudden pressure jump is experienced and it also avoids a by-pass of gas flow from the riser through the standpipe to the cyclone.

Therefore, a greater height of weir (P) assures better sealing performance of the loop-seal. On the other hand, a larger amount of aeration gas is required for a greater height of solids in the recycle chamber of the valve, which increases the cost of operation. Also, higher resistance of solid flow through the valve is experienced, which might cause an accumulation of solids in the standpipe and plug of the cyclone.

Later in Chapter 2.2, seven applications out of the numerous applications of the IFB systems are explained and investigated regarding chronological introductions and developments of IFB technology in petrochemical, bioenergy and environment-friendly issues. At the end in Chapter 2.5, we conducted to focus on a solid transportation device for fine particles,

regarding the difficulties in low fluidization regime of the fine particles in group C.

2.5 Summary

Fluidized beds have been applied to process large quantities of solid particles and a large amount of gas in various industries. In many processes the inventory of the fluidized beds are needed to be regenerated, evacuated or reduced for continuous operation of the process. Two fluidized bed systems are integrated which such system is called interconnected fluidized bed (IFB).

Various configurations of the IFBs have been designed and tested from laboratory scales to industrial scales based on the fluidization regime and demands of the process. Application of the fine particles in industrial processes has attracted extensive interest that nowadays is increasing still more due to the very small particle size and very large surface area of the fine particles per volume. Fine particles are extensively applied in catalytic processes, absorbing processes, pharmaceutical, food and cosmetic industries. Besides the industrial enthusiasm for fine particles, many studies in the academic sector show the growth of interest in the application of fine particles in the near future.

Within the processes in which such particles are mostly applied, solid particles should be well-dispersed to increase the gas-solid contact efficiency, so the fluidized beds are proposed as the best option. Operation of a fluidized bed of fine particles involves difficulties when operating at around minimum fluidization velocity of the particles which is the major problem in this project. Under a high fluidization regime, due to the formation of agglomerates, the properties of the agglomerated particles determine the characteristics of the fluidized bed not characteristics of an individual particle.

Regarding the strong interparticle forces between the fine particles, the operation under low fluidization regimes of such particles leads to cracks and channels where the major portion of the gas passes through the bed

within these shortcuts. This problem is especially significant in the non-mechanical valves of the circulating fluidized beds or the interconnected fluidized beds. Conventional non-mechanical valves are operated around minimum fluidization velocity at which the fine particles are operated with difficulties. Considering the rising demand on application of fine particles, new valve is going to be introduced to be more compatible with transportation of fine particles.

Chapter 3

Experimental apparatus

In this chapter, ideas for development of a non-mechanical valve for transportation of fine particles between two or more reactors are presented. Two experimental test rigs are designed, constructed and examined. During these investigations, a new method for characterization of the bulk solids was introduced and developed. The first test rig was a draft tube spouted bed (DTSB) which was expected to transport the file particles by means of application of the coarse particles. Based on the findings from the experiments on DTSB and the auxiliary test equipment, a four draft tubes pneumatic transport (4-DTPT) was conducted with the possibility of transportation of the fine particles through the device (non-mechanical valve).

3.1 DTPT test rig

3.1.1 Ideas

Idea of the new non-mechanical valve for transportation and flow rate control of fine particles was inspired from application of mixture of coarse and fine particles which is a method to assist the fluidization of fine particles. Moreover, the device should be capable of separation of fine particles from the coarse particles to keep the coarse particles in the system. The coarse particles in the valve act as a seal where the fine particles are fed below the surface of the coarse particles.

A draft tube spouted bed is an option where the coarse particles are operated under spouting regime which are internally circulated and fine particles under pneumatic transport regime which are elutriated out of the device. This apparatus is called draft tube pneumatic transport (DTPT) which is basically nominated for transportation of fine particles. A DTPT test rig was designed and constructed as shown in Figure 3.1.

Besides, internal circulation of coarse particles provide a moving dense bed in the annular section of the DTPT device which carries the fine particles from the feeding port to the bottom of the device. Fine and coarse particles at the bottom are entered the entrained zone where high gas velocity accelerates them through the draft tube.

Particles leave from the top of the draft tube where the coarse ones form a fountain on top of the tube and fell down on the dense bed. The fine particles are entrained by the gas flow and elutriated out of the system. This implies as fine particles transportation from the feeding port to the outlet section.

The test rig may act as non-mechanical valve for a circulating or an interconnected fluidized bed to circulate the particles captured in the cyclone back to the bottom of the riser. No flow of the gas from the riser to the cyclone through the non-mechanical valve in the undesired direction is expected.

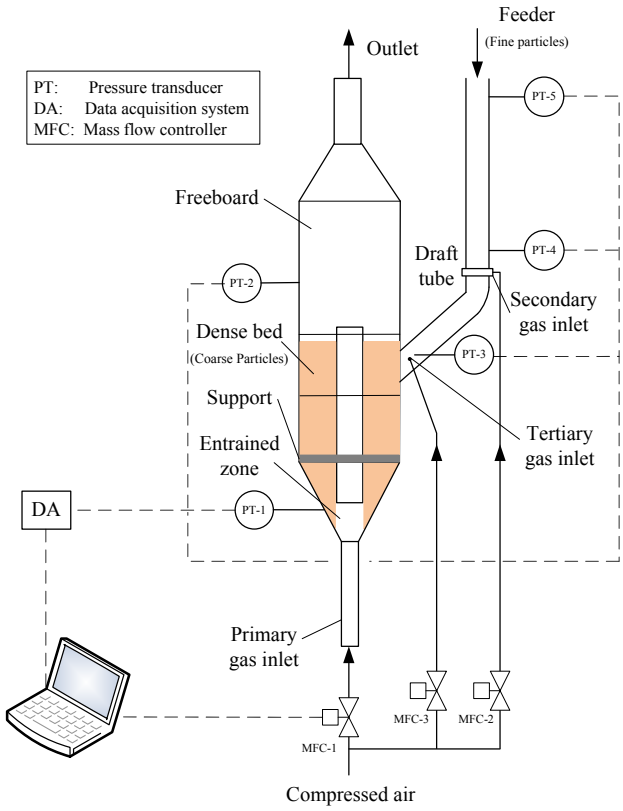

Figure 3.1: Schematic of draft tube pneumatic transport test rig

3.1.2 Set-up description

The DTPT set-up is capable of substituting the position of different parts to resemble various geometries. Height of the entrained zone is adjusted by sliding the draft tube up or down inside the support. Two different conical element for the lower section were constructed to study the influence of the cone inner angle on the parameters, such as pressure drop and internal solid circulation rate. Draft tubes with different diameters are mounted to study its effect on operation and hydrodynamics of the device. The range of geometric parameters of the DTPT test rig is presented as in Table 3.1.

Table 3.1: Geometric parameters of the DTPT device

Parameters		Unit	Values
Total height	H_{tot}	mm	350
Annulus diameter	D_{AN}	mm	60
Inner angle of the cone	α	degree	55, 80
Inner diameter of draft tube	D_{DT}	mm	14, 17
Height of draft tube	H_{DT}	mm	125
Height of entrained zone	H_{EZ}	mm	20, 30, 40

The main part of the set-up (DTSB) is made of transparent Plexiglass parts which provides visual observation of the particles flow pattern. Learning about particles movements and blockage of the moving bed are possible through the transparent walls. Beside, parts of the DTSB are made in a way that new configurations are made by relocation of the parts, for instance a change of the height of the freeboard or the depth of the moving bed (see Figure 3.1).

Tube for the feeding of fine particles is also transparent to provide the knowledge about how the particles are transported from the feeder to the DTSB. Another transparent tube is also considered for the outlet which assist the operator to prevent missing of the coarse particles, by controlling the gas flow rate.

A particle capturing unit is installed in the down stream to collect the elutriated particles. Additionally, a bag filter is considered for separation of fine particles from the gas stream before the gas was sent to the ventilation duct. All downstream piping is made by stainless steel tubes to prevent gas and fine particles leakage to the lab environment.

The pressure drop is measured by two pressure transducers (Honywell®) with a range of 0 to 70 *mbar* and a response time of 10^{-3} seconds. The data are logged to a computer by a data acquisition system (National Instruments LabView^{TM}). The height of the moving dense bed and solid velocity in annular section are measured manually by means of a ruler and stopwatch with accuracy of 0.001 m and 0.01 seconds.

3.2 Initial test of the DTPT test rig

3.2.1 Test of the relatively coarse particles

Initially coarse particles are fed into the device slowly. The gas flow should be high enough to prevent blockage of the gas inlet tube by the particles. After loading the particles, gas flow rate is further increased. In the initial series of tests, minimum gas feeding rate is identified at which the fountain forms and particles start recirculating. The maximum gas feeding rate is also determined, which is the critical value before elutriation of the coarse particles take place. During the operation within these boundaries, the fine particles are introduced to the device through the inclined tube where the feeding port is located as shown in Figure 3.1.

When the fine particles are fed into the moving bed of coarse particles, the coarse particles carry them downward to the entrained zone. Both fine and coarse particles which have reached the entrained zone are accelerated through the draft tube. The coarse particles fall down mostly to the dense bed. Fine particles are elutriated out of the DTPT device.

Initially, the influence of geometric parameters and operating conditions on hydrodynamics parameters of the DTPT is investigated where the set-up is operated with solely coarse particles. The experimental procedure is developed considering the modifications on the set-up as well as changing the operating conditions. Various geometric parameters, as stated in Table 3.1, are examined where some limitations are identified such as:

- For the large sizes of coarse particles, small height of the entrained zone leads to a limitation in particles flow from the annular section to the entrained zone.

- Large height of the entrained zone causes bubbling fluidization in the annular section while the small sizes of coarse particles are applied.

- Coarse particles are elutriated out of the device when the gas feeding rate is high or the particle size is small.

Based on the studies of Nagashima et al. [133,134], height of the entrained zone should be at least 10 times larger than maximum particle size. Besides, the observations show that for large height of entrained zone, high fraction of feeding gas flows to the annular section which causes formation of bubbles in the annular section. And considering low gas velocity in the draft tube, internal solid circulation does not take place. So, due to the mentioned limitations in the operation, those experiments are performed that the fountain forms and particles are internally circulated.

Results of the studies on operation of the DTSB set-up are illustrated in Chapter 4.1. Pressure drop, internal solid circulation rate and gas flow fraction to the annular section are investigated to be influenced by design parameters and operating conditions.

Internal solid circulation rate (ISCR) of the coarse particles with different sizes was studied as a parameter of the draft tube diameter, the height of entrained zone and the total gas flow rates. Expectedly, the ISCR of the coarse particles plays a significant role on transportation of the fine particles from the feeding port to the entrained zone.

Besides, the fraction of the gas which flows to the annular section is another parameter that is needed to be minimized. Because higher gas flow to the annular section is resulted in a higher pressure drop in the dense bed. Considering the minimal flow of the gas in undesired direction, the lower pressure drop and the lower gas flow to the annular section are demanded. Particle size, height of entrained zone and total gas flow rates are the parameters which affect the gas flow fraction. By looking into the pressure drop of the moving dense bed, portion of the gas to the annular section is calculated.

So, an optimum condition is needed to be defined which gives the maximum ISCR and minimum pressure drop. By operating under this situation, higher transportation of fine particles and lower back flow of the gas to the feeding tube are expected.

Within the experiments on the DTSB set-up, two different angles of the conical section at the bottom of the device were checked (as mentioned in Table 3.1, 55° and 80°). And a simple test unit which is explained later and shown in Figure 3.4, provided the opportunity to change the angle and the gap easily to check the particles flowability under different conditions.

Mostly, angle of the conical part at the bottom of the DTSB systems are considered as 60° where generally only one type coarse particles are applied [133, 135, 136]. New version of the transportation device was designed considering the facts which were observed from the experiments on the DTSB and supplementary studies. In the next section, developed idea of the next version of the set-up is explained.

3.2.2 Running with the fine particles

3.2.2.1 Difficulties in operation with fine particles

When fine particles were applied to the DTPT device, several problems were observed both with the feeding and transportaion within the device. Previously difficulties in fluidization of fine particles were explained in Section 2.3 which mostly are originated from large interparticle forces between fine particles. High cohesion tendency of the fine particles causes formation of large agglomerates, bridging in the low size tubes and blockage in elbows. Mostly fluidization and transportation of fine particles are not possible without applying any of the assistive methods.

In addition to mentioned issues for transportation of fine particles, inserting them to the moving bed of coarse particles at the feeding port interface did not take place properly. Even the secondary gas inlet on the feeding line (before the elbow) was not successful to assist the fine particles and push them into the device.

Considering the sealed feeder, difference between the pressures at PT-4 and PT-5 is zero then whole the secondary injected gas flows toward the inclined tube and the DTPT device. The secondary gas flow rate is ad-

justed in a way which the pressure drop between PT-3 and PT-4 is close to the theoretical pressure drop of the fine particles at minimum fluidization condition. Particles fluidization regime is expected to be around minimum fluidization velocity (U_{mf}) to provide smoother transportation through the tube.

While practically, it is observed that introduced gas mostly make a channel through the dense bed of fine particles in the feeding tube. And pressure between PT-3 and PT-4 is approximately cloes to zero which is definitely lower than the pressure drop of the particles at U_{mf}. So, the secondary gas injection does not keep the particles around minimum fluidization condition as it was expected and cannot assist feeding of fine particles to the DTPT device.

Tertiary gas injection, as shown on Figure 3.1, is close to the feeding port and the jet direction is adjusted toward the interface. High velocity gas jet helps for a short while it dilutes the particles in the surrounding region and push them to the dense bed. But, afterwards, fine particles form a bridge behind the jet and cannot further move toward the DTPT device.

A pneumatic vibrator was mounted on the feed line to check the effect of vibration force on transportation of fine particles. Even though, it was helpful but an effective steady feeding of fine particles was not experienced. After a while, particles in the inclined tube were fed into the device but the particles were compacted behind the elbow and due to bridging no more particles were transported to the inclined tube and the device.

Besides the mentioned issues in feeding of fine particles to the device, difficulties in transporting the fine particles within the moving dense bed were observed where some packages of fine particles were rarely fed into the device. Due to asymmetry of the feeding, the moving bed in the section close to the feeding port experiences lower velocities and in some cases blockage of the moving bed is observed. If the moving bed experiences lower velocities, transport capacity of the moving bed decreases and therefore no more fine particles cannot be fed into and transported by the DTPT device.

Accumulation of fine particles close to the outer surface of the annular section is another reason to increase the friction of the moving bed on the annulus outer wall. While normally the moving bed is in contact of the smooth surface of the annular cylinder, accumulated fine particles increases the friction and consequently decreases the moving bed velocity and leads to blockage of the coarse and fine particles in the annular section.

Moreover, performed experiments with low size particles (e.g. 300 to 500 μm) experienced missing of both fine and coarse particles. While in absence of fine particles, coarse particles are not individually elutriated out of the device. By increasing size of the coarse particles, elutriation of coarse particles and missing of bed inventory can be minimized or prevented.

3.2.2.2 Development ideas for the DTPT

A General solution which can simultaneously solve all the fine particles feeding issues was to introduce the feeding tube vertically to the middle of the annular section. For this purpose some modifications were applied on the DTPT set-up which the schematic is shown in Figure 3.2.

Fine particles are fed through a tube with inner diameter of 12 mm. Tube in this size was the maximum diameter which can be chosen, considering the limitations in horizontal distance of the draft tube, outlet tube, the outer wall of annular section and also the particle size.

After this modification, the problem with inserting of fine particles to the bed of coarse particles was not observed as an issue. But regarding the small diameter of the feeding tube, a pneumatic vibrator was required to be mounted on the feeding line. It was applied to break the bridges inside this tube and convey the fine particles down to the moving bed.

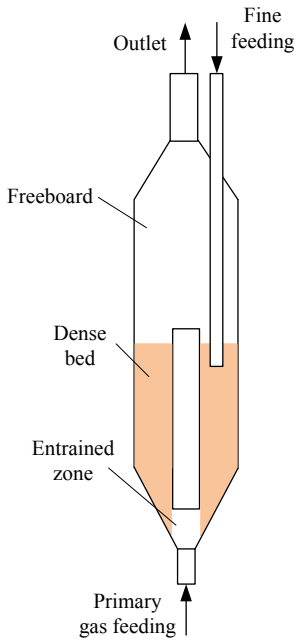

Figure 3.2: Schematic of the test rig with vertical feeding port

3.2.3 Conclusion

The findings from the investigations on the DTPT test rig reveal that this device experiences number of limitations for transportation of fine particles. Fine particles feeding on the lateral surface of the annular section through an inclined tube was not applicable. Besides, asymmetry of the feeding agitate the gas and specifically the solid flow pattern. Blockage of the moving bed or relatively lower velocity of the moving bed are resulted from the asymmetric pattern.

Fundamental modification of the set-up on the feeding port is expected where vertical feeding of fine particles was considered to presumably keep the symmetry of the particles and the gas flow pattern. It was crucial to modify structure of the first version completely to be able to satisfy the fine particles feeding and transportation.

3.3 Design of the new DTPT

3.3.1 Ideas

At first, four draft tubes which are located at each corner of a square body (as outer wall of annular section) was proposed, see Figure 3.3-(A). V-type bottom section was assumed for the bottom section where each two draft tube are located in each side of the V. Considering elimination of the dead triangular zone in each side, four compartment bottom was proposed, as in Figure 3.3-(B). In this version, each draft tube has separately its own entrained zone, moreover the dead zones are also eliminated.

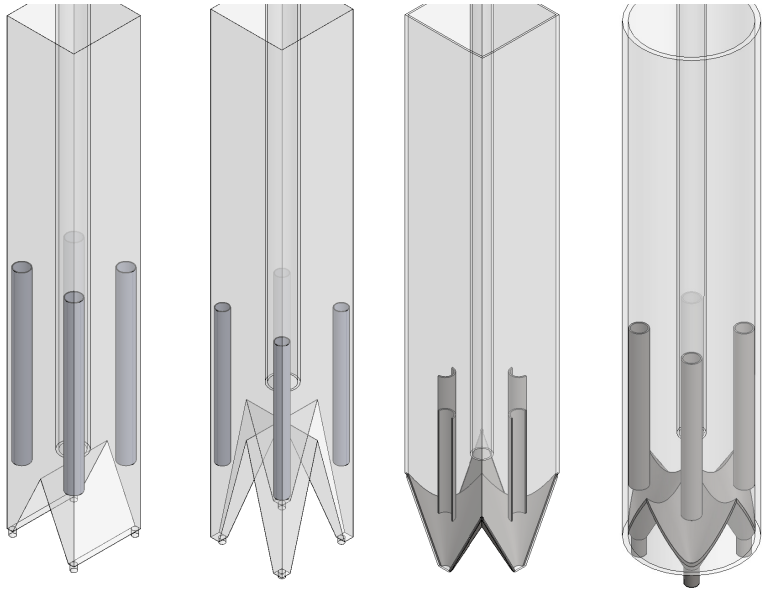

Figure 3.3: Developed procedure of 4-DTPT idea

To minimize the dead zone and considering the construction issues, two conical DTPTs are made and cut to two halves and then assembling them on a rectangular body, see Figure 3.3-(C). Then, four pieces are fixed together to provide the bottom section of the device.

But cutting the DTPTs to halves which means cutting the draft tube to half that leads to half cross section area of the draft tube while the cross section perimeter of two half-DTPTs mounted on a flat surface $((\pi D+2D)L)$ is much larger than each draft tube cross section perimeter (πDL). So instead of considering two DTPTs, four DTPTs are assumed to be applied and each one is cut in a radius beyond the draft tube.

Assuming the point which these four pieces meet as the center of the device, the material beyond a circle with this center is cut and eliminated. Besides, dead zone in the corner of the body is also eliminated by using a cylindrical tube instead of a rectangular one.

So, as it is observed in Figure 3.3 -(D), a cylindrical tube is applied as the main body of the device and four draft tube compartments fit each quarter. And finally it should be reminded that for all proposed versions, the feeding tube for fine particles is located at the center of the device. It is expected that fine particles are transported by means of the coarse particles moving bed down to the entrained zone.

3.3.2 Required knowledge

The primary experiments were performed on the DTSB to identify the effect of the operating conditions, geometric parameters and particles size on hydrodynamics of the device. Besides, number of additional methods and experiments were examined to check possibility of feeding and transportation of fine particles. Those experiments were generated out of the brainstorming and the experiences from the operation of the DTPT for transportation of the fine particles.

Following items were learned which may help operation with fine particles:

- Elimination of the inclined feeding tube
- Feeding to the middle of the moving bed instead of feeding on the wall

- Larger cross section of the annular section (considering the ratio of the particle size to gap size)
- Bigger draft tube diameter (increase the ISCR)
- Larger height of the freeboard

Characterization of the bulk solids and the mixture of coarse and fine particles are needed to conclude to a practical design of a new non-mechanical valve. Besides, a simple test rig was utilized for analyzing the angle of the conical section and its effect on particle flow pattern. In the next section details about the characterizing devices are given.

3.3.3 Devices for characterization

Supportive experiments are developed to investigated the particulate flowability. The analyzes are performed for investigation of the conical section of the device by means of a simple intermediate test rig. In addition, characterization of the particles is studied within a cylindrical transparent vessel to observe the sliding and resting angle of the samples. Findings from these studies are applied for design of the 4-DTPT set-up and also the results from the operation of the DTSB.

3.3.3.1 Study the angle of conical section

Angle-Gap test unit was constructed to simulate various angle of the bottom cone considering different gap size of the draft tube and inclined surface of the bottom cone. Figure 3.4 shows the test unit which the angle of the inclined plate is adjusted by the left screw and distance of the two vertical plates by right hand-side screws.

Particles are fed from top to the test unit and regarding the angle of the inclined surface and the gap, see Figure 3.5, are discharged with different flow rates. Increasing the normal distance between vertical and inclined plate increases the discharge rate. And decreasing the angle of

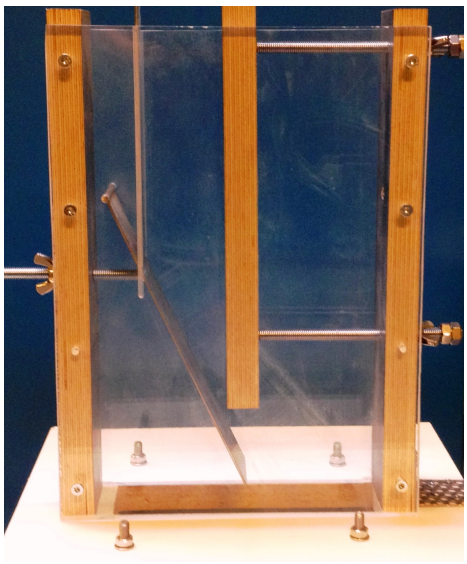

Figure 3.4: Angle-Gap test unit

the inclined plate increases the discharge rate which is the result of higher particle velocity close to the inclined plate. Velocity profiles along the cross section at different height of two examples are represented in Figure 3.6.

The test unit is capable of being modified and examined under different angles of the inclined plate, gap size between vertical and inclined plate, and also distance between two vertical plates, see Figure 3.5. The unit was adjusted for 50 mm distance of two vertical plates, 10 mm gap of vertical and inclined plate and four different angles of the inclined plate (20°, 25°, 30° and 40°). Particle velocity profiles along the height of the unit, for two conditions with 30° and 40°, are extracted from two captured sequential shots [137].

Figure 3.6 depicts the particle velocity profile along the cross section of the test unit at different heights. In the section with parallel plates, the particles velocity profiles have approximately similar trend. But for the lower sections within the inclined and the vertical plates, the velocity decreases close to the inclined plate while the decreasing rate for steeper plate is lower.

Figure 3.5: Angle-Gap test unit, Sand type SD-2023, angle of 30° and normal distance of 10 mm

Particles velocity in the unit with the inclined plate of 30° has a larger value, both close to the vertical plate and the inclined one. Consequently, the particles are discharged from the test unit with a higher rate and smoother than the unit with the inclined plate of 40°. So, it could be concluded that sharper angle of the inclined plate has lower restriction against the particle transportation. Especially for the particles close to the inclined plate which their low velocity or halt is contributed to an increase in the friction between the particles in that region.

3.3.3.2 Sliding angle and resting angle

Sliding angle and resting angle of the mixture of the sand type SD-0570 or SD-0710 with a sample of cement raw meal Type I (see Appendix A.2) were studied. Mixture of the sand-raw meal with the different mass fractions is prepared, mixed uniformly and filled into a cylindrical glass vessel upto around 50% of the volume of the vessel.

The vessel rests on 4 wheels where rotates smoothly around its axis. The test unit comprises of a glass vessel and 4-wheel support are shown in

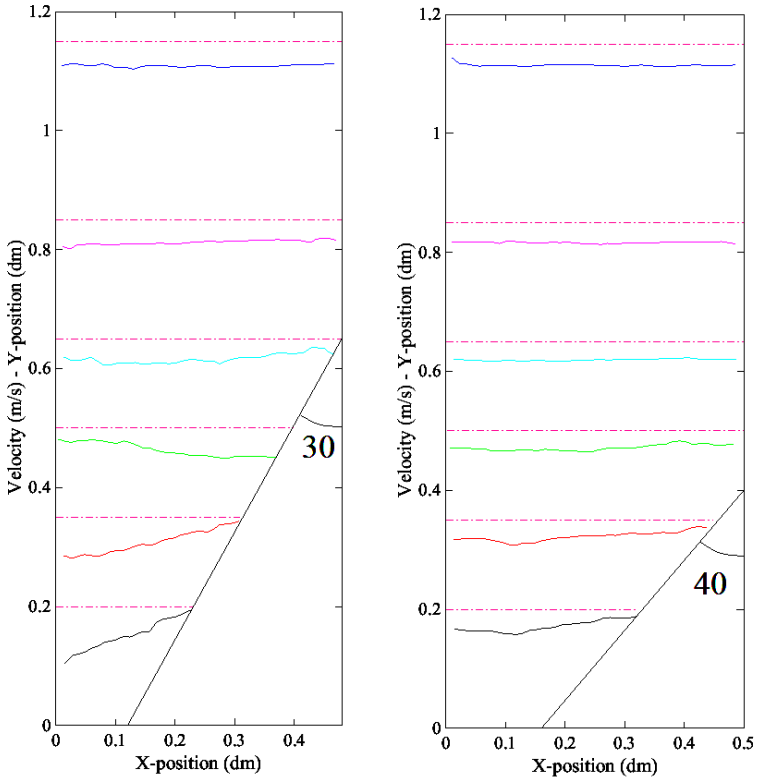

Figure 3.6: Instant particle velocity profiles for 30° and 40° angle of inclined plate

Figure 3.7. The maximum angle which the particles can stand and do not slither (or slide) down is called sliding angle (SA), and the angle where the particles form after smooth sliding is called resting angle (RA).

The cylindrical vessel containing the particles mixture is rotated around its axis very slowly to be able to distinct the sliding and resting angles. Cement raw meal type I is applied as an example containing large fraction of the fine particles. Particle size distribution of the raw meal type I is shown in Figure 3.8. Results of the characterization of the mixture of quartz sand and cement raw meal type I are presented in Figure 3.9.

Sliding angle increases slightly up to 20 $wt\%$ raw meal. Between 20 $wt\%$ and 50 $wt\%$ raw meal, sliding angle rises to its maximum, even higher

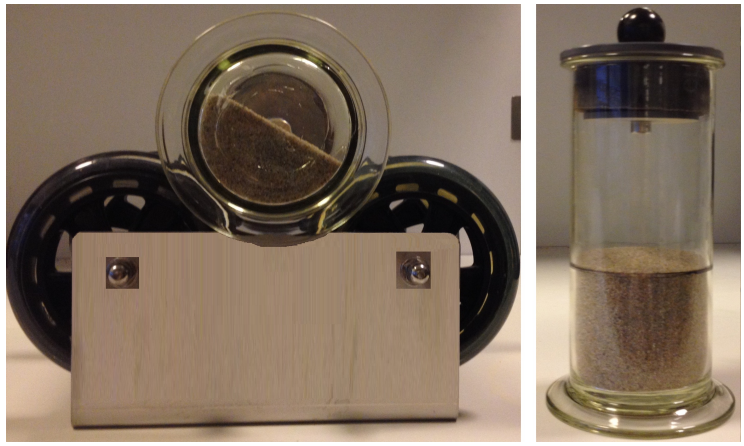

Figure 3.7: Set-up for measuring the Sliding angle and resting angle

than sliding angle of pure raw meal. And for fractions higher than 50 $wt\%$, sliding angle decreases from the peak to the sliding angle of 100 $wt\%$ raw meal.

Resting angle has the similar trend, slight increase for first 20 $wt\%$ raw meal and a sharp gradient upto 30 $wt\%$ raw meal, and for higher raw meal mass fractions, the sliding angle decreases to the sliding angle of 100 $wt\%$ raw meal.

Trend of changes for sliding angle of the mixture of sand type SD-0507 and SD-0710 with raw meal is similar and mostly the angles are very close. Even though, similar behavior is also observed for resting angle (RA) but maximum resting angle of the mixture of sand type SD-0507 is lower than the mixture of the sand type SD-0710. And generally, the rest corresponding angles are close to each other.

The discrepancy between the maximum resting angle of the sand type SD-0507 and type SD-0710 could take place due to one of the following reasons:

- The resting angle of the sand type SD-0507 and type SD-0710 which can influence the behavior of the sand in the mixture.

- Volume of the void between larger sand particles is larger which can contain larger amount of raw meal between sand particles. It probably leads to higher friction between the mixture components and consequently larger resting angle.

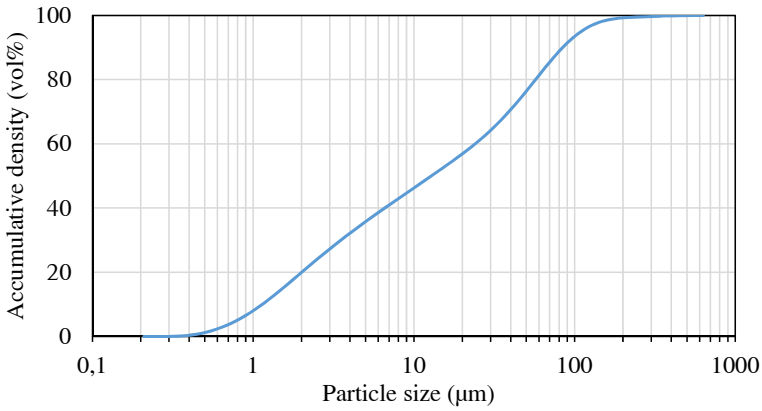

Figure 3.8: Accumulative distribution of raw meal type I

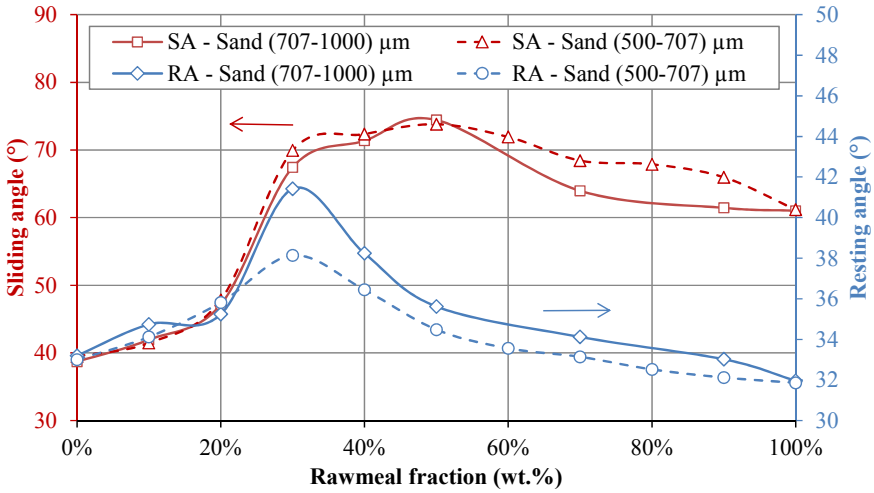

Figure 3.9: Sliding angle (SA) and resting angle (RA) of the mixture of sand and raw meal type I

3.3.3.3 Loose and tapped Bulk densities

Bulk density of the mixture of sand and raw meal was measured to find possible explanation for the similarly bell-shape behavior of the sliding and resting angle. Due to similarity of the trends between the mixture of sand type SD-0507 and type SD-0710 and the cement raw meal, bulk densities were measured for just type SD-0710.

Two type bulk densities were investigated for this investigation, loose bulk density (LBD) and tapped bulk density (TBD). For performing the measurements, a 250 ml graduated cylinder is filled with the samples after it was mixed uniformly.

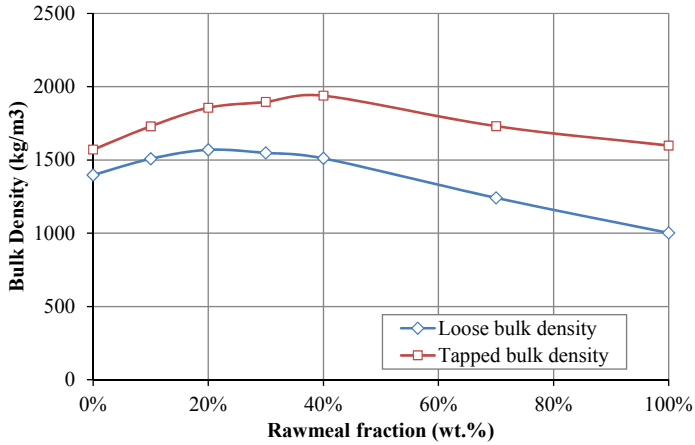

Figure 3.10: Loose bulk density (LBD) and tapped bulk density (TBD). Quartz sand (707-1000)μm

The loose bulk density corresponds to the mass of the particles which are filled in the cylinder very gently. In the other words, minimum possible mass of the sample which is filled in to a 250 ml cylinder. In this condition particle sample rest in the cylinder with the maximum void, and minimum loose bulk density is measured.

The cylinder containing the sample is tapped to decrease the volume of the mixture to the lowest possible amount, corresponding bulk density is called tapped bulk density. Measurement of both loose and tapped bulk

densities are repeated at least five times to check the reproducibility and the average values are reported.

Bulk density measurements are plotted as in figure 3.10 which shows that there is a maximum for loose and tapped bulk densities at around 20 $wt\%$ and 40 $wt\%$ of raw meal, respectively.

Considering the void of the coarse sand particles which is filled-in by fine raw meal particles, loose bulk density increases by adding more fine particles to the coarse particles. It means that volume of the sand and raw meal mixture does not change significantly while the mass of the mixture increases, by adding extra fine particles. Increase in loose bulk density is experienced up to a specific fraction of raw meal (20 $wt\%$) and for higher percentages the loose bulk density decreases regarding increase of the volume of the mixture.

Similar theory can be explained for tapped bulk density but regarding the compacting process of coarse and fine particles, larger amount of fine particles can be compacted in the void of coarse particles. And due to this reason maximum of the tapped bulk density curve shifts to the larger mass fraction of raw meal. From the tapped bulk density and the maximum at around 40 $wt\%$ of the fine particles, it implies that fine particles are filled in the void of coarse particles (approximately around 40%).

3.3.3.4 Summary of the bulk solid characterization

Experimental studies on the DTPT set-up for transportation of fine particles, on DTSB for operation with solely coarse particles and also supportive experiments for investigation of the angle of conical section and characterization of the bulk solids were concluded to new design parameters and configuration of the device for pneumatic transportation of fine particles.

Following items were applied for the design of the new device for fine particles transportation:

- Assumed that higher ISCR of coarse particles will transport more fine particles within and increases the fine particles transportation. By looking into the results from operation of the DTSB with coarse particles, refer to Section 4.1.3.2, bigger draft tube diameter, smaller inner angle of the conical section and higher gas feeding rates lead to higher ISCR of coarse particles.
- Investigation on angle of the conical section demonstrates that particles flow more easily down through the device while smaller angle of the inclined plate is implemented. Considering presence of the fine particles within the coarse particles and due to higher sliding angle of the mixture (which implies as higher internal friction), even sharper angle is required for the bottom cone (inner angle of 40° versus the angle of 60° for normal DTSBs).
- Larger height of the freeboard is taken into account to prevent missing of coarse particles where high gas feeding rates are applied.
- Considering the vertical port for feeding of fine particles and also keeping the symmetry of the solids flow pattern, new configuration should be designed to fulfill this demand.
- Besides these design parameters and regarding the functionality of the new device, location of the support for the draft tubes is adjusted in a way which no dismounting is needed.

These facts are considered for the design of the new set-up (4-DTPT) while the progressive steps of the design were explained in Section 3.4.

3.4 4-DTPT test rig

3.4.1 Final selection

Based on the latest idea (Figure 3.3 -(D)) and feasible construction of the new test rig, four draft tube pneumatic transport (4-DTPT) is proposed as in Figure 3.11.

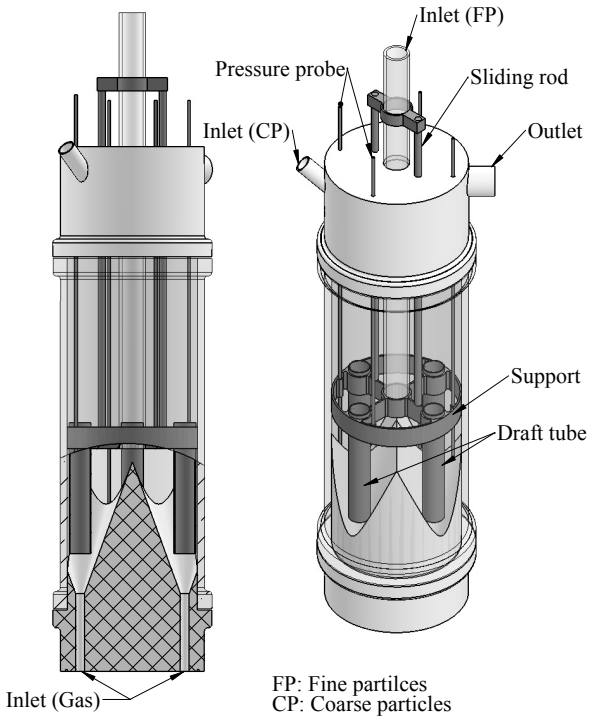

Figure 3.11: Four draft tubes pneumatic transport (4-DTPT) set-up

The 4-DTPT device is designed considering the maximum ISCR which supposedly higher ISCR leads to higher internal transportation rate of fine particles. Four pressure probes are considered for pressure measurements and pressure balance. Two pressure transducers measure the differential pressure through the dense bed, another pressure probe represents the pressure on top of the device close to the outlet section. And the last probe from top of the device is connected to a port on the feeder to balance the pressure between these two levels.

3.4.2 4-DTPT set-up

Three following items were taken into account and conducted to the design and construction of the 4-DTPT device:

- Findings from the performed experiments on the primary version of the set-up
- Desired operational conditions (lower pressure drop, higher fraction of gas flow to the draft tube and higher internal solid circulation rate)
- Appropriate schematic of the new device (4-DTPT) to fulfill the demands (feeding and transportation of fine particles)

Results of the previous study on first version of the DTPT shows that larger diameter of the draft tube, higher gas flow rate and larger distance from top of draft tube to the outlet (provides a condition which the set-up can be run under higher gas flow rates) increases the internal solid circulation rate (ISCR).

Experimental results on the DTSB show that sharper angle of the conical section, larger fraction of the draft tube diameter to the diameter of annular section and higher gas feeding rate are contributed to higher internal solid circulation rate and lower pressure drop (lower flow fraction of the gas to the annular section). Moreover, vertical feeding of fine particles provide a condition which makes feeding of fine particles possible.

Based on the mentioned items, alternative geometric parameters are listed in Table 3.2.

Table 3.2: Geometric parameters of the 4-DTPT test rig

Parameters		Unit	Values
Total height	H_{tot}	mm	600 - 1400
Height of freeboard	H_{FB}	mm	400 - 1200
Annular diameter	D_{AN}	mm	150
Inner angle of the cone	α	degree	40
Inner diameter of draft tube	D_{DT}	mm	22
Height of draft tube	H_{DT}	mm	150 - 200
Diameter of feeding port	D_{FD}	mm	24
Height of entrained zone	H_{EZ}	mm	27 - 37
Height of the dense bed	H_{bed}	mm	170 - 220

The main body of the 4-DTPT device is made by a cylindrical glass which provides the visual observation. Even though, after some minutes running with fine particles, inner wall is covered by fine particles and difficult to see clearly through it. But making it out of glass was definitely helpful for operation and commissioning.

Pressure measuring instruments are Huba Control differential pressure transmitters Type 699 with the response time of less than 20 ms and accuracy of less than 0.7% of the full scale.

3.4.3 Operation of the 4-DTPT

Support of the draft tubes and pressure probes are grounded to release the electro-static charges and reduce agglomeration of particles. On the gas feeding lines of each compartment, a needle valve is mounted to be able to adjust the flow to each compartment and make a stable internal circulation of particles when the particles are loaded into the device. Usually, the adjustment of needle valves are required at the beginning while initially the particles are fed into the device to increase or decrease the flow of each draft tube and distribute the coarse particles equally in the compartments.

While the level of solid particles are equal in four compartments, needle valves are opened fully. After feeding of coarse particles as internally circulating inventory, total gas flow increases to form a fountain on top of each draft tube where the particles recirculation get started. For different gas feeding rates, pressure drops and internal solid circulation rates are measured. Various particle sizes are also examined to characterize the device hydrodynamics. Results of the operation of the 4-DTPT set-up are presented in Chapter 4.2.

After successful feeding of fine particles, it was observed that for some chaotic frequent times the coarse particles reach the outlet and elutriated out. Height of the device freeboard was increased to eliminate this issue. So, the new version has a total height of 1400 mm and height of the freeboard is around 1200 mm.

3.5 Conclusion

Fluidized beds are introduces as one of the promising technologies for process of solid particulates. For the processes which comprise of more than two fludized beds, particles transportation between the fluidized bed is mostly controlled and achieved by non-mechanical valves (NMV). There is rising demand on production and application of fine particles in different industries. But the conventional non-mechanical valves are not capable of dealing with the fine particles or the particles containing large fraction of fine particles. The conventional NMVs are operated just above the minimum fluidization condition where fine particles have difficulties to be handled.

Here, a draft tube spouted bed (DTSB) was introduced for transportation of fine particles (named draft tube pneumatic transport - DTPT) which presumably presence of coarse particles and high velocity gas stream may assist the transportation of fine particles. The new designed solid transportation and sealing device for fine particles was inspired from (1) application of the mixture of coarse and fine particles which eases the difficulties in fluidization of fine particles and (2) high velocity gas stream to break down the fine particles agglomerates, (3) fast fluidization regime which transport the fine particles but not the coarse particles. These ideas were combined and conducted to a draft tube spouted bed (DTSB) where (1) coarse particles are internally recirculated inside the DTSB which transport the fine particles from the feeding point to transportation point (entrance of the draft tube), (2) fine particles are entrained through the draft tube and elutriated out of the DTSB.

Proper gas flow rate results in transportation of the fine particles out of the device and recirculation of the coarse particles inside the DTSB. Functionality of the DTSB was changed to a transportation device which we called it draft tube pneumatic transport (DTPT). DTPT test rig was designed, constructed and examined for transportation of fine particles. Feeding of fine particles arises some difficulties both in the feeding of the particles and also conveying the particles inside the DTSB.

Considering the feeding of the fine particles to the device and limitations

in operation, number of supplementary experiments were performed to support the idea for design and construction of a new non-mechanical valve. Based on the findings from the hydrodynamic investigation of the DTSB and the challenges with the operation, a configuration with four draft tubes was proposed.

In this configuration which can locate the fine particles feeding tube at the center may resolve the issue with asymmetry of the gas and solid flow pattern in the DTPT. The design parameters of the new non-mechanical valve (four draft tube pneumatic transport, 4-DTPT) was comprehended from hydrodynamic investigations of the DTSB and characterization studies of the sole and the mixture of the particles.

The valve was examined and proved capability of transportation of the fine particles. Moreover, it also can act as a sealing device, while the coarse particles are recirculated and stay in the system and the feeding port is submerged to the coarse particles.

Chapter 4

Results and discussion

The experimental investigations were carried out in two steps. The influence of the geometric parameters and particle sizes are presented in this chapter. The results of the hydrodynamic study of the DTSB is presented first. Some difficulties raised with the operation of the DTSB as a DTPT for fine particles are addressed. The results from the improved 4-DTPT are presented for the coarse particles and also after feeding of the fine particles.

4.1 Hydrodynamics of the DTSB

4.1.1 Operational boundaries of the DTSB

The experimental studies were first focused on determination of the operational boundaries of the different size groups of sand particles.

Within the preliminary experiments of the DTSB, it was found that a

minimum and a maximum gas flow rate exists for operation of this set-up. The minimum gas flow rate is defined as the flow rate at which the fountain starts to form. Above the minimum flow rate, particles start to be transported up through the draft tube and circulated through the annular section, or in an other word, the internal solid circulation is initiated. On the other hand, the maximum gas flow rate is corresponded to the flow rate which the particles reach the outlet section but are not elutriated out.

Based on the experimental results, the minimum and the maximum gas flow rates are correlated by groups of dimensionless numbers, representing the gas flow, particle size and geometric parameters of the set-up. The minimum gas flow rate can be estimated by Equation (4.1), which applies Re and Ar numbers as dimensionless numbers containing the gas and solid characteristics and gas velocity. Other parameters were normalized by particle diameter to apply all influential parameters into the correlation. Similar approach was applied by Altzibar et al. [138] where correlations are fitted to the experimental results of a draft tube conical spouted bed.

$$Re_{min} = A\,(Ar)^{B}\left(\frac{D_{DT}}{d_P}\right)^{C}\left(\frac{H_{EZ}}{d_P}\right)^{D}\left(tan\,\frac{\alpha}{2}\right)^{E} \tag{4.1}$$

where the coefficients are demonstrated in Table 4.1.

Table 4.1: Coefficients of the Equations (4.1) and (4.2)

Parameters	A	B	C	D	E	F
Min. feeding rate	0.1166	0.7144	0.0896	0.1679	-0.2276	–
Max. feeding rate	29.6934	0.5488	0.6148	0.0395	-0.0107	-0.8079

The maximum gas flow rate is correlated by Equation (4.2). Last term represents height of the freeboard ($H_{FB} = H_{Tot} - H_{EZ} - H_{DT}$) which is normalized by the particle size, too. Comparison of the experimental and calculated gas flow rates are shown in Figure 4.1, minimum gas flow rates by the triangle symbols and maximum gas flow rates by the circle

symbols.

$$Re_{max} = A\,(Ar)^{B} \left(\frac{D_{DT}}{d_P}\right)^{C} \left(\frac{H_{EZ}}{d_P}\right)^{D} \left(tan\,\frac{\alpha}{2}\right)^{E} \left(\frac{H_{FB}}{d_P}\right)^{F} \tag{4.2}$$

where the coefficients are demonstrated in Table 4.1.

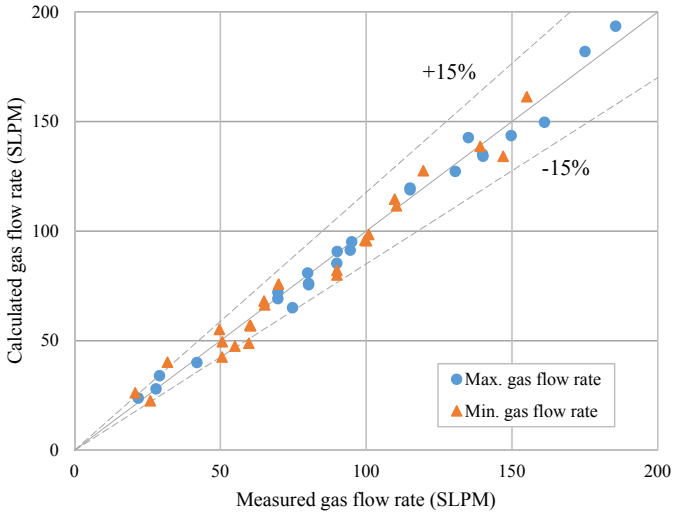

Figure 4.1: Comparison of experimental and calculated gas flow rates

Correlations to calculate the minimum gas flow rate (Equation (4.1)) and maximum gas flow rate (Equation (4.2)) are extracted based on the geometric parameters in Table 3.1. These correlations are applied to determine the boundaries for operation of the DTSB, which are implanted on Grace's diagram as illustrated in Figure 4.2.

4.1.2 Flow regime of the DTSB

Generally, operation of a draft tube spouted bed experiences three conditions with an increase of gas flow rate: dense bed regime (low gas flow rates with no formation of the fountain), pulsive spouting region, and

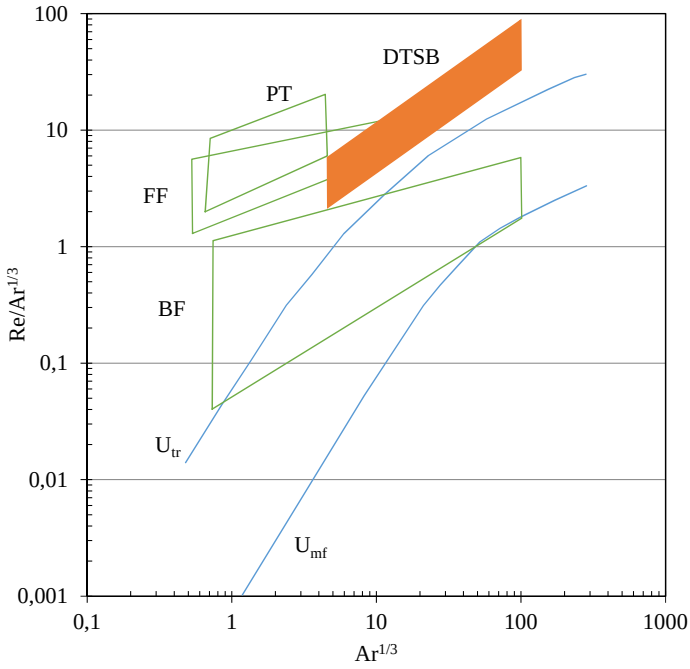

Figure 4.2: Boundaries for operation of the present DTSB on Grace's diagram [3]. (BFB: Bubbling fluidized bed, FFB: Fast fluidized bed, PT: Pneumatic transport)

stable spouting. Two operating gas velocities are definedin trasition between each neighboring regime, minimum spouting velocity (U_{ms}) and minimum stable spouting velocity (U_{mss}) [133–135, 139–141].

The pressure drop curve can be divided to three regimes based on the gas flow rate: (1) upto minimum spouting flow (U_{ms}), (2) between U_{ms} and minimum stable spouting (U_{mss}) and (3) higher than U_{mss} upto the maximum gas flow rate, as illustrated in Figure 4.3. In regime (1), pressure drop increases linearly with increase of the gas flow, similar to the trend of pressure drop in a dense bed [133, 140]. The pressure drop reaches a maximum at minimum spouting condition at which the recirculation starts. In regime (2), pressure drop decreases within these conditions, due to flow of lower fraction of the gas to the annular section. Additionally, increasing the gas flow rate leads to decrease of the solid

concentration in the draft tube which results in lower pressure drop. In regime (3), internal solid circulation rate through the draft tube is more stable [142] (smoother and more uniform fountain is observed) and pressure drop slightly increases with an increase of gas flow rates [133, 134, 140] because at high gas flow rates, slightly higher amount of gas passes through the dense bed.

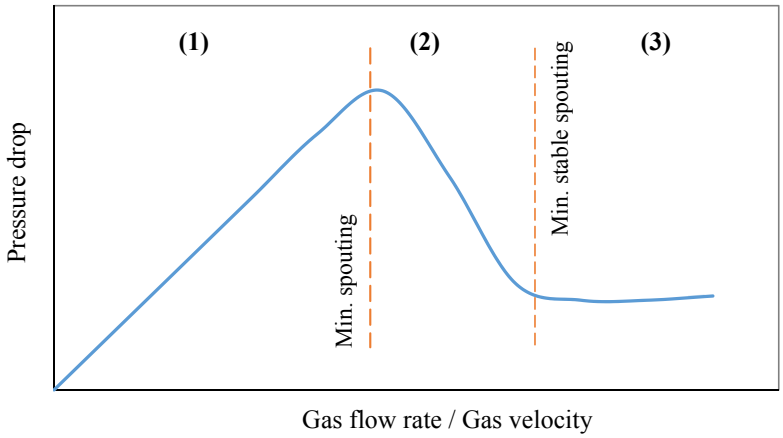

Figure 4.3: Pressure drop versus total gas flow rate, operating regime definitions

The draft tube and the annular section are operated like two interconnected parallel system which the pressure drop of these two sections are in balance with each other. While the DTSB is operated close to higher boundary of the regime (3), the draft tube acts like a pneumatic transport fluidized bed. Particles are transported through the draft tube with low solid concentration resulting in a low pressure drop over the draft tube. Consequently, lower pressure drop of the annular section is observed because of the lower gas flow to this section.

4.1.3 Experimental results

Considering the draft tube as a fast fluidized bed, lower gas flow rates increase the chance of formation of a dense zone in the draft tube. Higher solid concentration in the dense zone of the draft tube leads to higher

pressure drop. For lower gas flow rates, it is observed that maximum of the pressure drop curve is corresponded to the minimum spouting condition and by increasing the gas flow rate, higher fraction of the gas passes through the draft tube and void of the draft tube dense zone gets more dilute therefore pressure drop descends.

4.1.3.1 Pressure drop variations

Sand particles with narrow size ranges, see Table 4.2, are applied to perform the experiments on DTSB test rig. Primarily, the experiments are carried out for quite coarse particle in Group D and B and afterwards with Group A (Geldart's classification). And then, the set-up was tested for operation of the fairly fine particles (samples containing large fraction of Group C particles), but considering impossible operation of the DTSB, nothing can be reported here.

Table 4.2: Size range of sand particles as the coarse bed inventory of DTPT

Particles size	Unit	Type
125-250	μm	SD-0102
250-355	μm	SD-0203
355-500	μm	SD-0305
500-707	μm	SD-0507
707-1000	μm	SD-0710
1000-2000	μm	SD-1020
2000-2360	μm	SD-2023

The operating conditions are referred to the case studies which are represented in Table 4.3.

Figure 4.4 shows the effect of particle size on pressure drop within the operational boundaries which was illustrated in Figure 4.2. Vertical axis represents the pressure drop per unit height of the dense bed ($\Delta P/H_{DB}$) and horizontal axis is the gas flow rate in standard liter per minute ($SLPM$). Hollow and solid symbols correspond to the height of the entrained zone of 20 mm and 30 mm, respectively. Draft tube inner

Table 4.3: Experimental case studies on DTSB

Parameters			Particle type					
D_{DT}	H_{EZ}	α	SD-0203	SD-0305	SD-0507	SD-0710	SD-1020	SD-2023
	20	55	01	03	06	09	17	25
	30	55	02	04	07	10	18	26
17	40	55		05	08	11	19	
	20	80				12	20	
	30	80				13	21	
	20	55				14	22	
14	30	55				15	23	
	20	80				16	24	

diameter and inner angle of the conical section are 17 mm and 55°, respectively.

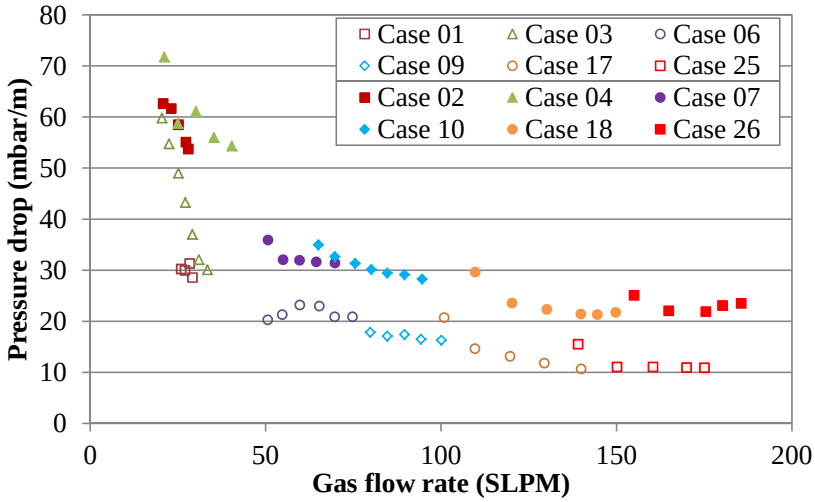

Figure 4.4: Pressure drop through the DTSB for different sets of particle sizes and height of entrained zone (H)

Figure 4.4 shows that the large particles will result in a pressure drop. It may be explained by the Ergun's equation [143] (Equation (4.3)). The dense bed pressure drop correlation has $\frac{V_g}{{d_p}^2}$ and $\frac{{V_g}^2}{d_p}$ in first and second parts, respectively. Considering the constant gas flow to the annular section, larger particles results in lower pressure drops. For the same particle size, higher gas flow to the DTSB does not give a higher pressure drop which implies as lower gas flow fraction to the annular section.

Increasing the height of the entrained zone leads to expansion of the gas stream and higher flow fraction of the gas through the annular section and consequently higher pressure drop. Entrained zone in a DTSB acts as a conical CSB [140] which large fraction of feeding gas flow through the dense bed due to expansion of the gas stream close to the inlet section. So, lager height of the entrained zone leads to higher pressure drop.

$$\frac{dp}{dh} = 150\frac{(1-\varepsilon)^2}{\varepsilon^3}\frac{\mu V_g}{{d_p}^2} + 1.75\frac{(1-\varepsilon)}{\varepsilon^3}\rho_g\frac{{V_g}^2}{d_p} \tag{4.3}$$

When the height of the entrained zone increases, the pressure drop will increase. A High gas flow to the annular section is contributed to a higher the pressure drop as indicated by Equation (4.3) [143]. Higher expansion of the gas stream close to the inlet causes of higher fraction of the gas flow to the annular section and resulted in higher pressure drop. This can be experienced when higher height of the entrained zone is set or smaller draft tube diameter is selected.

Influence of the two important geometric parameters, height of the entrained zone and inner angle of the conical section, are shown in Figure 4.5. Pressure drop of the annular section increases significantly for larger height of entrained zone. And wider angle of the conical section pushes the operating regimes of the DTSB to lower gas flow rates. For the cases 20 and 21, regime (3) and for the cases 17, 18 and 19 regime (2) and (3) are observed. Larger height of entrained zone leads to even higher pressure drop for the wider angle of the conical section, cases 20 and 21 versus cases 17 and 18. This takes place due to expansion of the inlet gas stream to the annular section bed which results in a higher pressure drop.

Operation of the DTSB is investigated for the same height of the entrained zone, and variation in inner angle of the conical section and draft tube diameter. The results are shown in Figure 4.6. Pressure drop of the cone with larger inner angle is higher considering. But this time, it is observed that draft tube with smaller diameter pushes the operational regimes toward the lower gas flow rates, even though; higher pressure drops are experienced.

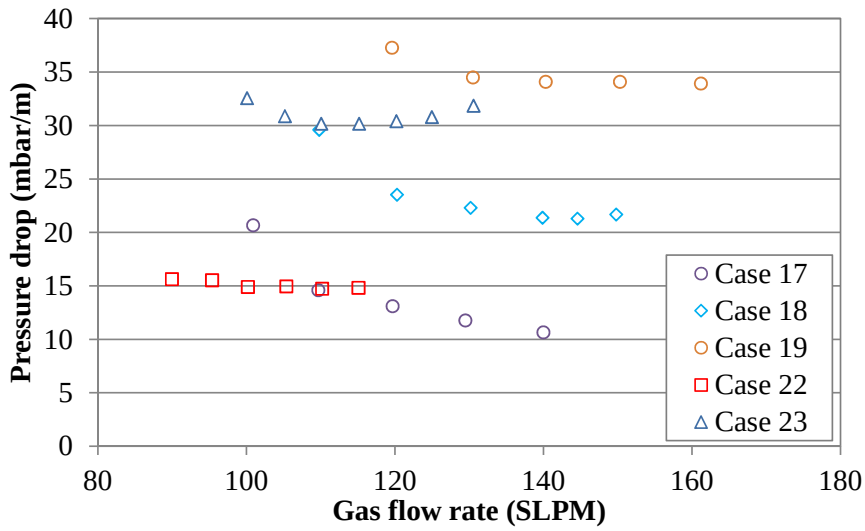

Figure 4.5: Pressure drop through the DTSB for different height of entrained zone and inner angle of the bottom cone for sand type SD-1020

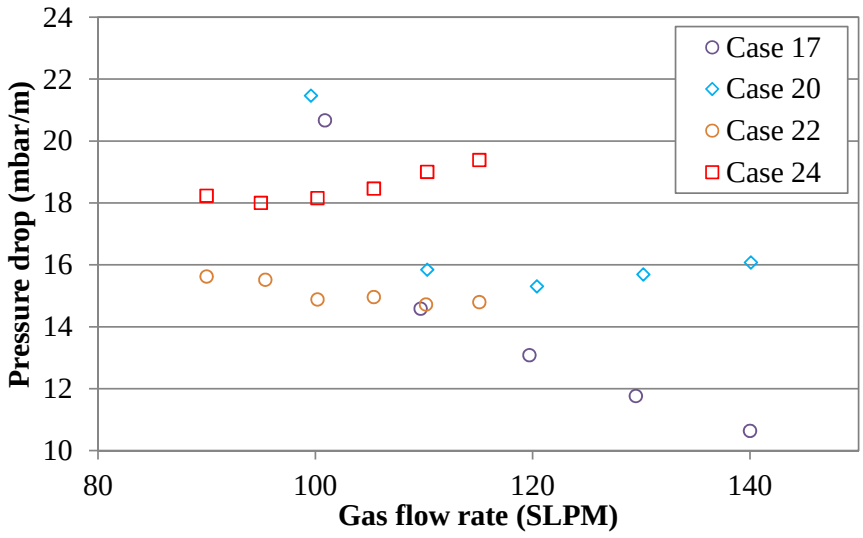

Figure 4.6: Pressure drop through the DTSB for different draft tube diameter and inner angle of the bottom cone for sand type SD-1020

4.1.3.2 Variation of the internal solid circulation rate

In general, internal solid circulation rate (ISCR) increases with increasing the total gas flow rate at the beginning. This trend continues up to the point where the minimum stable spouting is reached. Comparing the operating conditions of the results in Figure 4.4 and Figure 4.7, it is shown that maximum ISCR takes place at the gas flow rate, at which the pressure drop is minimum. As stated before, minimum pressure drop occurs at minimum stable spouting flow meaning that the maximum ISCR is at the same point.

The ISCR results as a function of gas flow rate are shown in Figure 4.7 with the height of entrained zone of 20 mm and 30 mm and different particle types. Higher ISCR is observed for the larger height of the entrained zone [144]. Higher height of the entrained zone results in lower restriction against the particles flow from the annual section to the entrained zone, therefore higher ISCR can be expected.

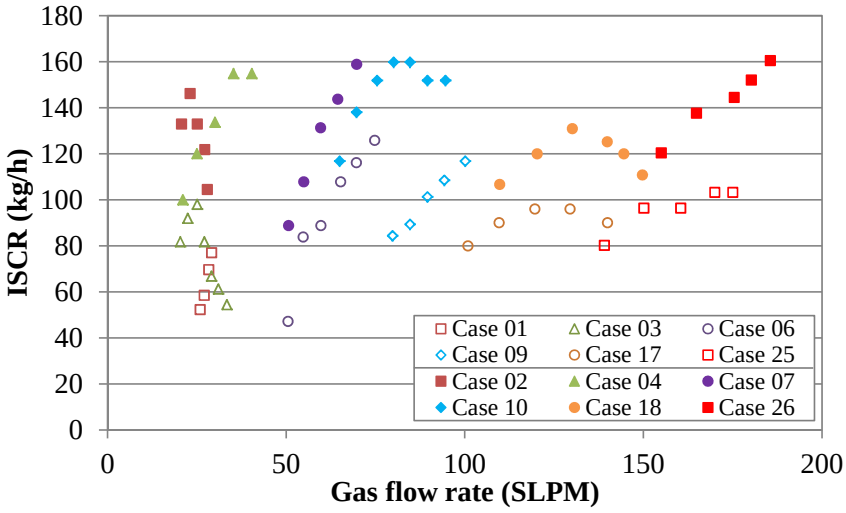

Figure 4.7: Internal solid circulation rate for different sets of particle sizes, height of entrained zone 20 mm (hollow symbols) and 30 mm (solid symbols)

Results of the sand type SD-1020 for different height of the entrained zone with two sizes of draft tube are demonstrated in Figure 4.8. ISCR

increases with an increase of the entrained zone. The degree of the increase become large for the draft tube with bigger diameter. Maximum of the ISCR curve is shifted to the higher gas flow rate, when the height of the entrained zone increases. This means that minimum stable spouting takes place at higher gas flow rate where the height of the entrained zone is larger.

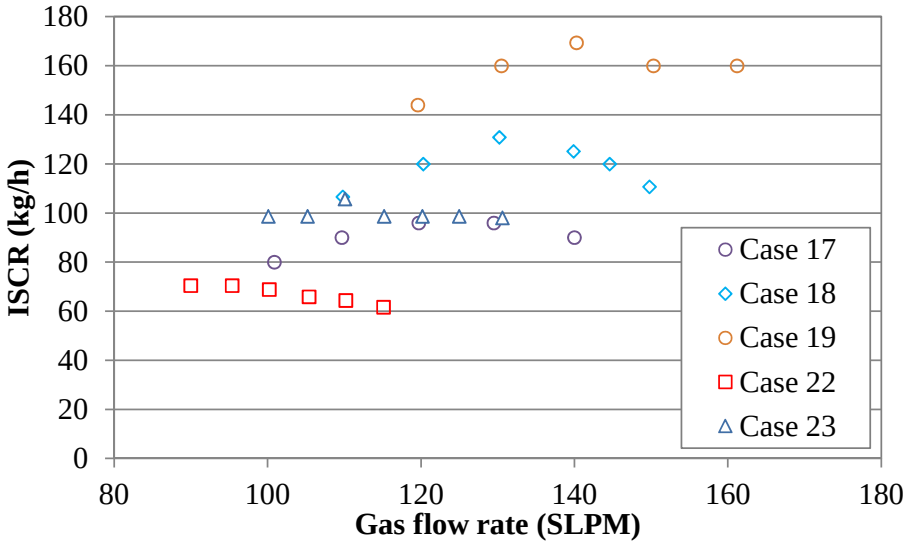

Figure 4.8: ISCR for draft tube of ϕ17 and ϕ14 mm and different height of the entrained zone (20, 30 and 40 mm). Sand type SD-1020

The results with two inner angles of the bottom cone and two sizes of the draft tube with the sand type of SD-1020 are shown in Figure 4.9. Higher ISCR is observed when the inner angle of the cone is smaller (55°). This may be due to the smooth flow of the particles over the surface of the cone with the smaller angle and the lower restriction to the downward flow of the particles from the annular section to the entrained zone.

Results in Figure 4.9 reveals that ISCR is larger at the lower gas flow rates with the sharper bottom cone. Despite that maximum of the ISCR for the cone with smaller angle is bigger and takes place at lower gas flow rates. It maybe concluded that a DTSB with larger draft tube and sharper angle of the bottom cone results in a higher ISCR.

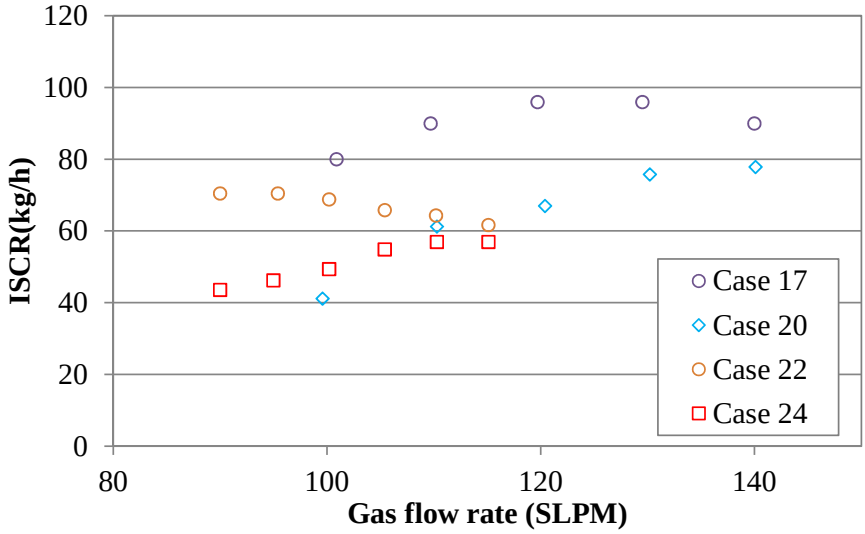

Figure 4.9: ISCR for draft tube of ϕ17 and ϕ14 mm and different inner angle of the bottom cone (55° and 80°). Sand type SD-1020

4.1.3.3 Variation of the gas flow distribution

The experimental results show that fraction of the gas flow rate to the annular section decreases with an increase of the total gas flow rate as shown in Figure 4.10. Higher gas flow rate has a higher velocity and higher kinetic energy in axial direction, so possibility of flow of higher fraction of the gas through the draft tube is larger than the annular section. So, it may support the fact of lower gas flow fraction to the annular section at high gas flow rates. Results in Figure 4.10 show that fraction of the gas flow to the annular section is high for the large particles. Moreover, increasing the height of the entrained zone leads to the higher gas flow fraction to the annular section. The larger surface area of the gas-solid interface in the entrained zone increases the possibility of higher flow of the gas to the dense bed in annular section.

Results of the experiments on the sand type SD-1020 with the draft tube of 14 mm and 17 mm, and with three different heights of the entrained zone are shown in Figure 4.11. For the cases with 17 mm draft tube, smaller difference between gas flow fraction is observed with respect to

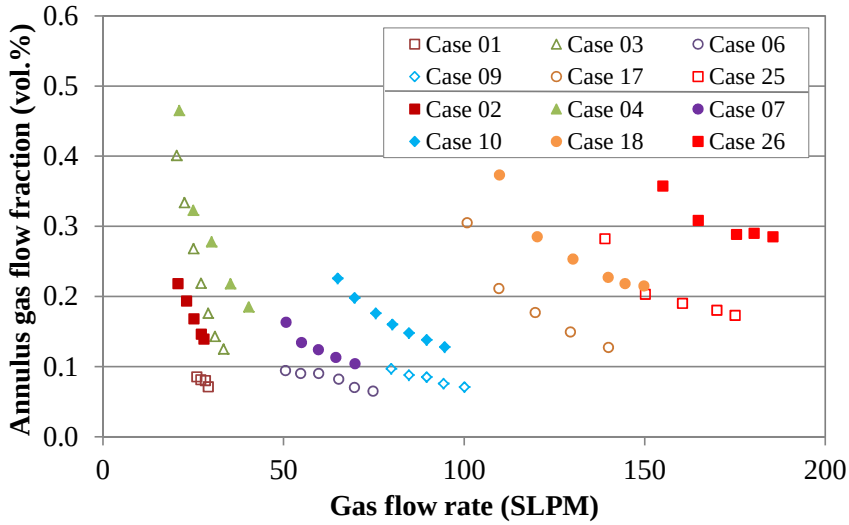

Figure 4.10: annular gas flow fraction for different sets of particle sizes, height of entrained zone 20 mm (hollow symbols) and 30 mm (solid symbols)

increase of the height of entrained zone than the cases with a draft tube diameter of 14 mm. It may be explained by larger ratio of the annular cross section area to the draft tube cross section area, which provides higher possibility of gas flow to the annular section.

The results of the influence of the bottom cone angle and draft tube size on the annular gas flow fractions are shown in Figure 4.12. With an increase of the gas flow rate, the difference of the gas flow fraction between the bottom cones is increased. Higher gas flow fraction is observed for a wider angle, which may be explained by higher possibility of expansion of the inlet jet which leads to higher gas flow rate to the annular section.

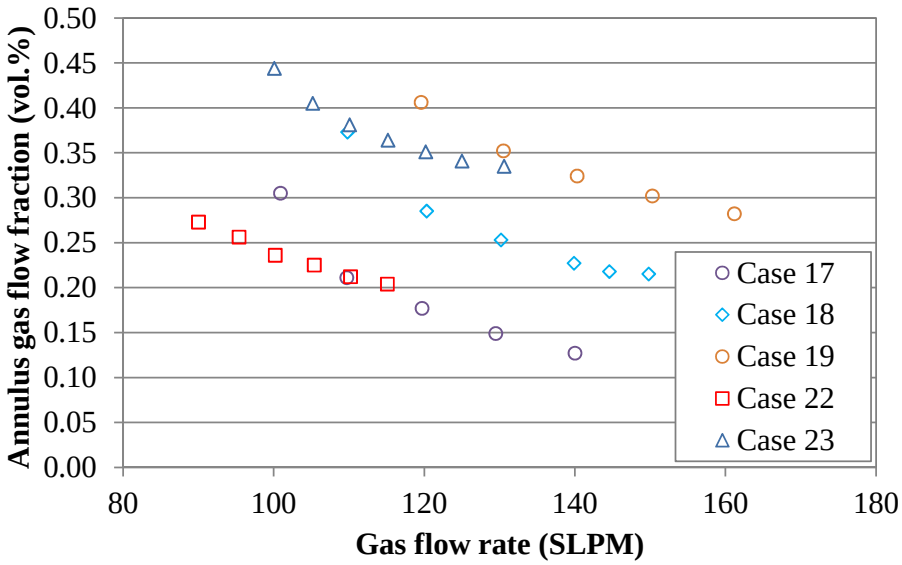

Figure 4.11: annular gas flow fraction for draft tube of ϕ17 and ϕ14 mm and different height of the entrained zone (20, 30 and 40 mm). Sand type SD-1020

4.1.4 Summary of the influential parameters on DTSB results

The results are summarized in Table 4.4. It shows how larger: diameter of the annular section (D_{AN}), height of the entrained zone (H_{EZ}), diameter of the draft tube (D_{DT}), inner angle of the conical section (α) and total gas flow rate (Q_{tot}) effect the pressure drop (ΔP), internal solid circulation rate (ISCR) and annular flow fraction (X_{AN}). Bigger H_{EZ} and α increase the pressure drop and the rest parameters decrease it. The D_{AN}, H_{EZ}, D_{DT} and Q_{tot} has a direct influence on ISCR where the α inversely affects the ISCR.

The trend obtained in this study is in a good agreement with the result reported in the literature [134, 141], but more parameters are systematically covered in this study.

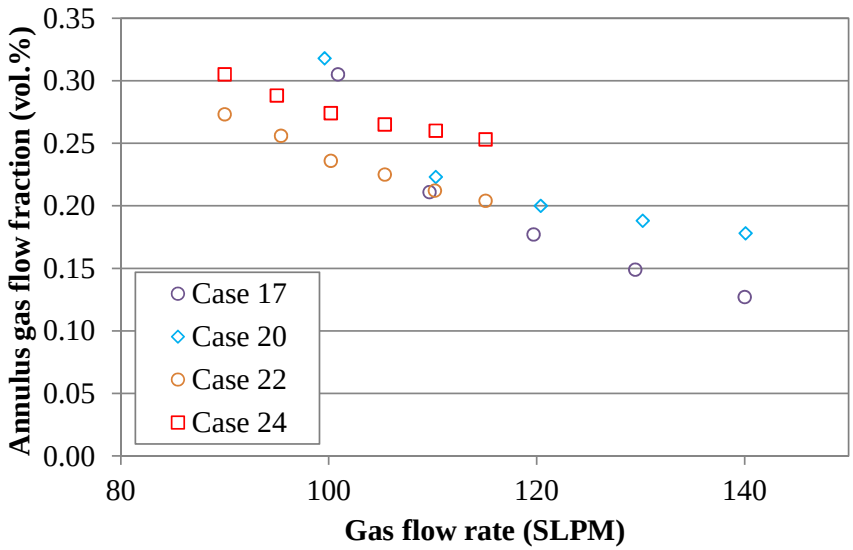

Figure 4.12: annular gas flow fraction for draft tube of ϕ17 and ϕ14 mm and different inner angle of the bottom cone (55° and 80°). Sand type SD-1020

4.2 The 4-DTPT results

New designed four draft tubes pneumatic transport (4-DTPT) is characterized and studied for identification of the optimized operating conditions for various geometric parameters. The test rig is investigated for two cases: (1) only coarse particles and (2) mixture of coarse and fine particles.

Sand particles with narrow size ranges (see Table 4.5) are applied to perform the experiments on 4-DTPT test rig.

Experiments are performed on 6 groups of the particles listed in Table 4.5 by varying the geometric parameters, such as height of the entrained zone (H_{EZ}), height of the draft tube (H_{DT}) and height of the solids in the dense bed (H_{Bed}) with step increase of the total gas flow rate. Hereafter, all results are referred to the cases as defined by Table 4.6. It should be

Table 4.4: Effect of geometric parameters and operating conditions on hydrodynamics.

Parameters	ΔP	ISCR	X_{AN}
H_{EZ}	↗	↗	↗
D_{DT}	↘	↗	↘
α	↗	↘	↗
Q_{tot}	↘*	↗**	↘
d_P	↘	–	↗

* reaches a minimum

** reaches a maximum

Table 4.5: Size range of sand particles as the coarse bed inventory of 4-DTPT

Size range	Unit	Type
500-707	μm	SD-0507
707-1000	μm	SD-0710
1000-1400	μm	SD-1014
1400-1700	μm	SD-1417
1700-2000	μm	SD-1720
2000-3000	μm	SD-2030

mentioned that the parameter H_{Bed} is measured from the level of the gas inlet port.

For the cases of mixture of the coarse and fine particles, experiments were performed for transportation of the fine particles. It was observed that the two types of sand SD-0507 and SD-0710 are not suitable for transportation of fine particles. Due to this, sand type SD-0507 and SD-0710 are not listed on the Table 4.6.

4.2.1 Results of the operation with coarse particles

The test rig runs solely with coarse particles to investigate effects of the operating conditions on particles flow behavior and to be able to compare with the results of the DTSB. Pressure drop of the dense bed of coarse particles in the annular section was measured by two pressure

Table 4.6: Case number for the performed experiments on 4-DTPT set-up

Parameters			Particle type			
H_{EZ}	H_{DT}	H_{Bed}	SD-1014	SD-1417	SD-1720	SD-2030
27	150	170	1	5	11	14
	200	170	2	6		
	200	220	3	7		
37	150	180	4	8	12	15
	200	180		9		
	200	230		10	13	

transducers.

For all the experimental cases the probes for the pressure transducers which measure the annular section pressure drop are fixed with the distance of 135 *mm*. First probe is in the level close to the gas inlet and the next one is close to the dense bed surface in the annular section. Besides, standard deviation of the pressure measurements are also presented on the data points to indicate the intensity of the spouting in the draft tube. Large deviations of the dense bed differential pressure present a more frequent fountain formation and in some cases bubble formation in the annular section.

Pressure drop of a DTSB follows the trend which is schematically shown in Figure 4.3. Results from 4-DTPT indicate that the pressure drop trend of the 4-DTPT test rig is similar to those of the DTSB.

The time series of the pressure drop and the gas flow rate in the 4.DTPT test rig are shown in Figure 4.13, which confirm that pressure drop has small deviations in regime (1) and (3) but large deviations in regime (2). In regime (1), below the minimum spouting condition, the test rig acts as a fixed bed. The pressure drop increases with an increase of the gas flow rate with a constant level for each flow rate.

In regime (3), higher than the minimum stable spouting condition, particles are steadily recirculated inside the system and stable fountain is observed. Thus, the pressure drop has a low deviation at a fixed flow

rate. But in regime (2), internal recirculation of particles starts with an fluctuation where formation of the fountain is observed by frequent intervals. This instability in formation of the fountain which results in a large fluctuation of the pressure drop in the system, causing a large deviation of the pressure drop.

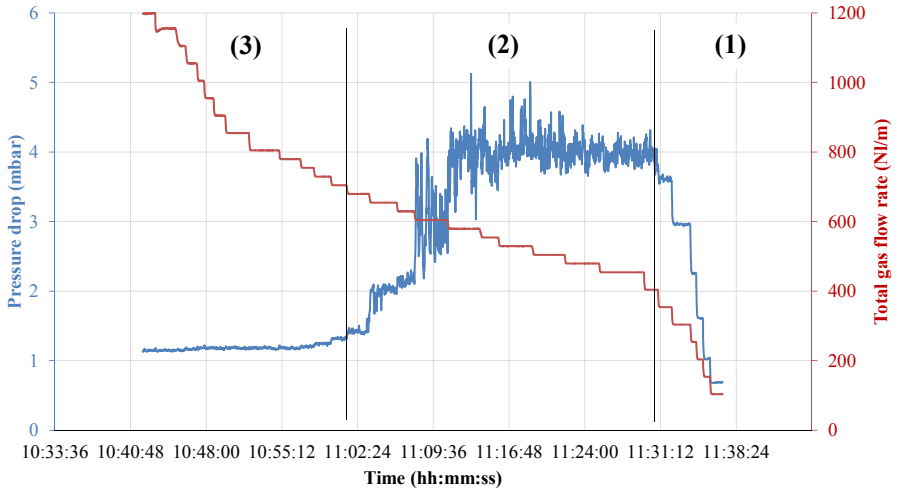

Figure 4.13: Time series of the pressure drop and the gas flow rate

4.2.1.1 Operational boundaries

In the same way as the case of the DTSB, the operational boundaries are determined. But for this series of the experiments, the gas flow rates are covering a wider range, so the gas flow rates at the minimum spouting and minimum stable spouting conditions are considered as inputs for the correlation, as shown by Equation (4.4).

$$Re = A\,(Ar)^{B}\left(\frac{d_P}{H_{EZ}}\right)^{C}\left(\frac{D_{DT}}{H_{EZ}}\right)^{D}\left(\frac{H_{Bed}}{H_{EZ}}\right)^{E} \tag{4.4}$$

Parameters A, B, C, D and E for minimum spouting and minimum stable spouting conditions are obtained by fitting the experimental results, which are listed in Table 4.7.

Table 4.7: Coefficients of the Equation (4.4)

Parameters	A	B	C	D	E
Min. spouting	14.51	0.8934	-0.4947	-0.4563	0.3324
Min. stable spouting	330.1	0.6572	-0.4672	0.0658	0.0314

The comparison of the experimental data and the calculated resutls are shown in Figure 4.14. It is shown that the calculated data and the experimental results are within the accuracy of less than 10%. The results indicate that similar correlation for DTSB in Chapter 4.1 can also be applied to the 4-DTPT results.

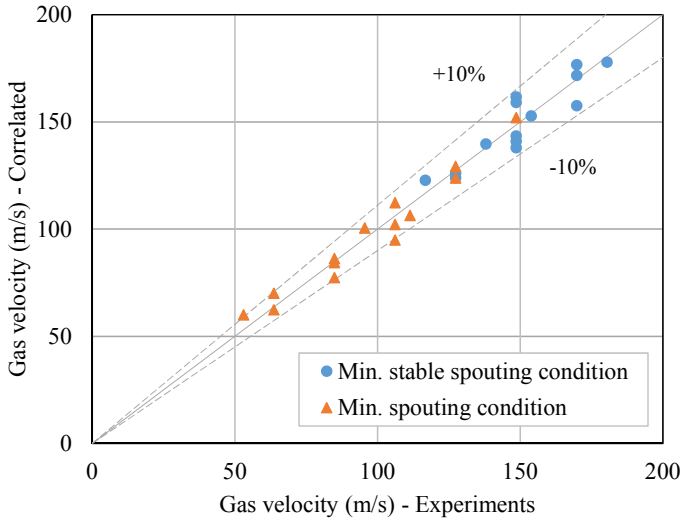

Figure 4.14: Comparison of experimental and predicted inlet gas velocity for minimum spouting and minimum stable spouting conditions

4.2.1.2 Pressure drop - Influence of geometric parameter

Pressure drop over the dense bed in the annular section is measured when the test rig is operated from low gas flow rates to the maximum. Pressure drop curves for different cases are shown in Figures 4.15 to 4.17, where the same trend is observed.

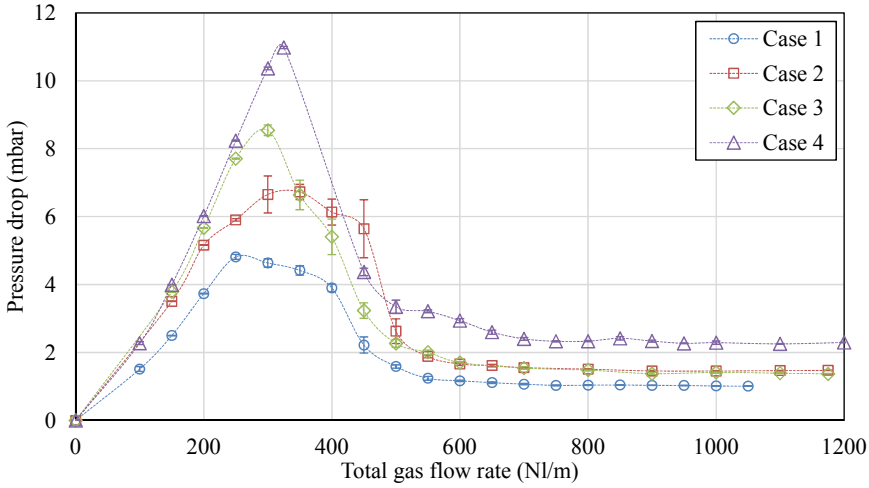

Figure 4.15: Pressure drop versus total gas flow rate for sand type SD-1014

In Figure 4.15, pressure drop curves for cases 1 to 4 are illustrated. From the results of the cases 1 and 2, it is concluded that the pressure drop increases with increasing the height of the draft tube when the other geometric parameters are kept constant. Higher pressure drop of the case 2 than 1 may be explained by the fact that higher length of the draft tube increases the pressure drop over the draft tube which is equal to pressure drop of the dense bed. In addition, a high deviation of the pressure drop is observed for regime (2) of the case 2.

For cases 2 and 3, height of the dense bed is varied and the other geometric parameters are kept constant. This variation results in a higher pressure drop in regime (1), lower one in regime (2) and approximately the same for regime (3) for case 3. Even though, pressure drop has a direct linear relationship with the bed height and it is measured over 135 mm of the bed, but this fact cannot be applied for a dense bed with a draft tube.

In regime (2) of the case 3, the pressure drop is low with small deviations in comparison with the case 2. Deeper dense bed might be the reason for reducing the pressure fluctuations in the annular section, leading to the lower pressure drop deviations.

Pressure drop of the cases 2 and 3 in regime (3) are almost identical and independent of height of the bed in the annular section. This indicates that the effective parameter is height of the draft tube instead of the height of the bed, when the gas flow rate is higher than the minimum stable spouting condition.

For the case 4, all parameters are same as the case 1 except for the height of the entrained zone. Increasing the height of the entrained zone results in a higher pressure drop because of a higher flow of the gas passing through the dense bed of the annular sections. Larger height of the entrained zone increases the surface area of the interface of the entrained zone with the particles and the dense zone. It causes higher flow of the gas from the inlet gas stream to the annular section.

The curves in Figure 4.15 indicate approximately similar operational boundaries for the four cases though the geometric parameters are different. It may be concluded that particle size is the limiting parameter for the boundaries of operational regimes.

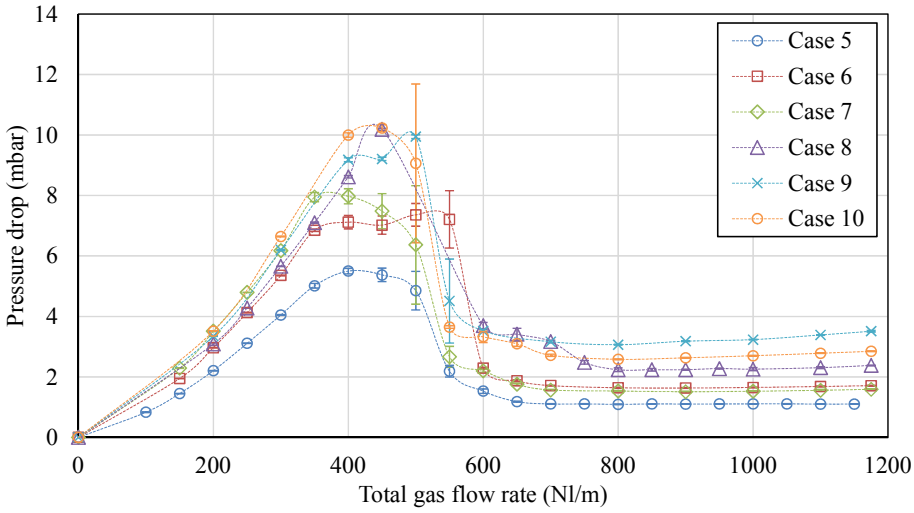

Figure 4.16: Pressure drop versus total gas flow rate for sand type SD-1417

Similar trend as the one in Figure 4.15 is observed. In a same way, Figure 4.16 presents the results of another particle size with varied geometric

parameters. Pressure drop of the case 9 is higher than the case 8, for all three operational zones. Comparing the results of the cases 8-9 with 5-6, where the only difference between these cases is height of the entrained zone, shows similarities in pressure drop behaviors

Comparing the results of case 10 with 9, where the only difference is the height of the bed in the annular section, it is shown that the pressure drop is slightly higher that case 9 in regime (1) and (2). However, in regime (3), the value of the pressure drop is reverse.

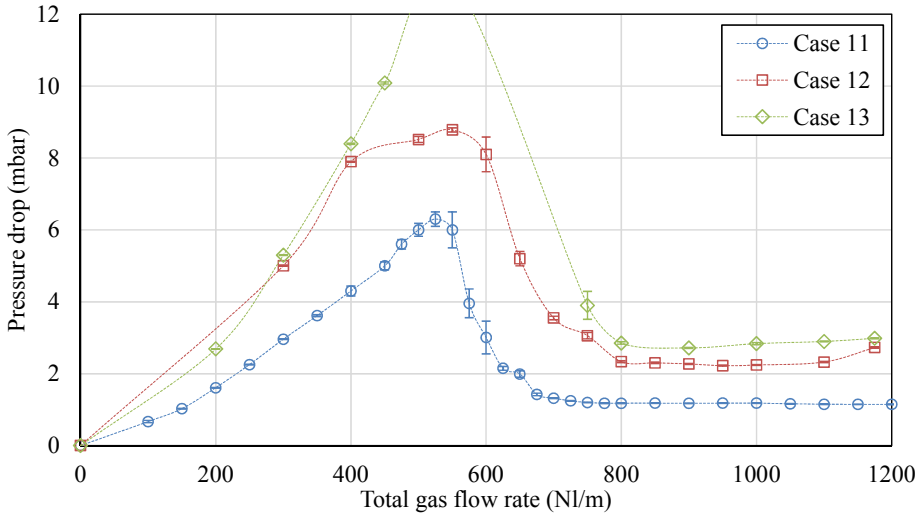

Figure 4.17: Pressure drop versus total gas flow rate for sand type SD-1720

Figure 4.17 shows the results with the sand type SD-1720 for three different cases: height of the entrained zone (27 mm and 37 mm) and height of the draft tube (150 mm and 200 mm). A large difference between pressure drop of the case 12 and 11 is due to the increase of the height of the entrained zone. The reason is same as what was explained for cases 1 and 4. It is noticed that larger particles size produces larger pressure drop difference. It is also shown that increasing the length of the draft tube and height of the bed (case 13 against case 12) leads to higher pressure drop.

4.2.1.3 Pressure drop - Influence of particle size

Results of the experiments with different size groups of sand are presented in Figure 4.18 for the cases where height of the draft tube and entrained zone are 150 mm and 27 mm, respectively. From Figure 4.18, following phenomena can be observed:

- Minimum spouting flow rate (upper boundary of regime (1)) is shifted to a higher value when the particles size increases.
- The minimum stable spouting flow rate (upper boundary of regime (2)) is shifted to higher values accordingly.
- In regime (1), pressure drop gradient with respect to the gas flow is low for the large particles.
- The pressure drop experiences has a sharp decrease in regime (2).
- In regime (3), approximately constant pressure drop is observed for all type of particles with the same geometric parameters.

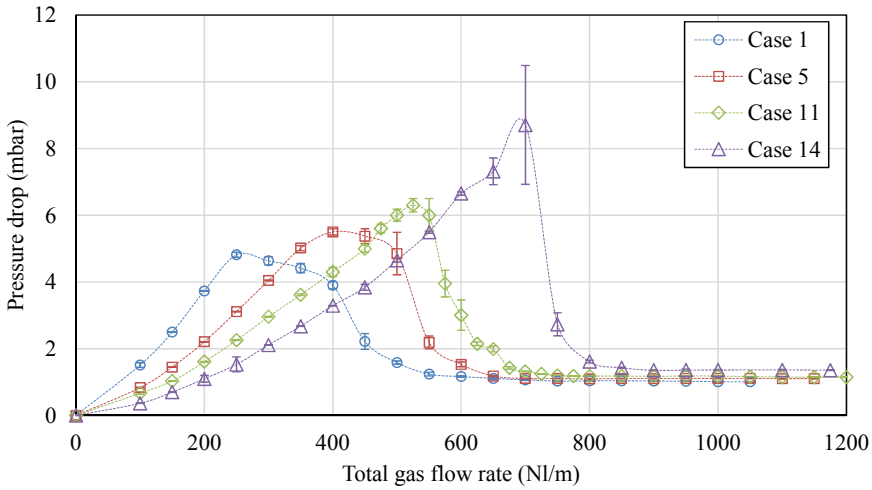

Figure 4.18: Pressure drop versus total gas flow rate on different particle types (H_{EZ}, H_{DT} and H_{Bed} are 27, 150, 170 mm)

The shift of the minimum stable spouting flow to the high values might be due to the high required gas velocity for large particles to the draft tube to reach the terminal velocity of the particles. When the test rig is operated at a flow below the minimum spouting condition, it behaves like a fixed bed. Thus, for the large particles, the pressure drop is low at the same gas velocity based on the Ergun's correlation (Equation (4.3)).

The results in regime (3) show that pressure drop for the velocities higher than the minimum stable spouting is independent of the particle size when the geometric parameters are kept constant.

Corresponding cases are studied for the condition where height of the entrianed zone is 37 mm which is presented in Figure 4.19. The results confirm the similar behavior of the pressure drop when the particle sizes are changed.

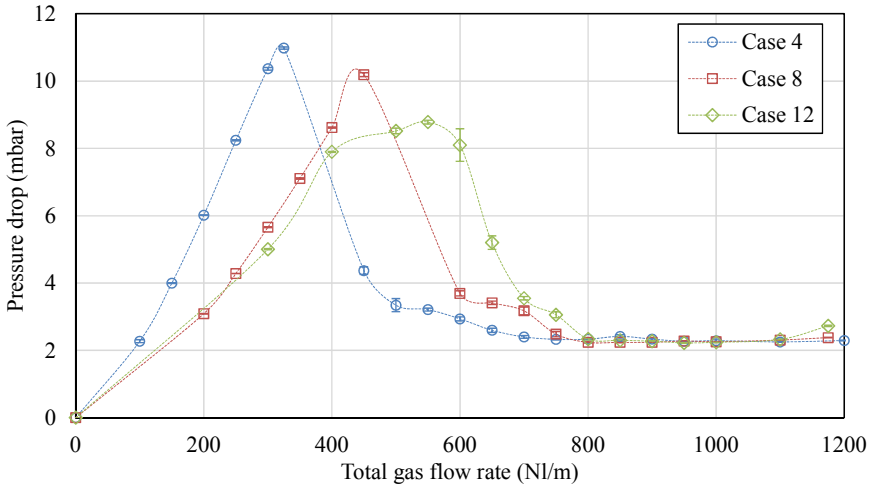

Figure 4.19: Pressure drop versus total gas flow rate on different particle types (H_{EZ}, H_{DT} and H_{Bed} are 37, 150, 170 mm)

4.2.1.4 Summary of the pressure drop of coarse particles

The overall trend of the operation of the 4-DTPT test rig with only coarse particles is summarized as follows:

- An increase of the height of the entrained zone leads to a high pressure drop.
- An increase of the size of the draft tube and the height of the dense bed results in a high pressure drop.
- Large particle shifts the operating regimes to the high gas flow rates.
- Approximately similar operating regime boundaries are observed for a single type of particle. It sounds the particles size is the most effective parameter of the Equation 4.4.

4-DTPT test rig behaves similar to the DTSB. In the following section, fine particles are inserted to the bed of coarse particles and influence of their presence on pressure drop and ISCR are studied.

4.2.2 Primary results from feeding of the fine particles

Cement raw meal was used as fine particles for these experiments. The size range of the particles utilized for performing the experiments of the 4-DTPT test rig was from 0.2 to 300 μm and d_{50} of 9 μm. This material is considered as one of the most severe cases containing more than 70% of the Group C particles. Accumulated distribution of the cement raw meal type II was measured by Laser scattering particle size distribution analyzer Partica LA-960, which is shown in Figure 4.20.

The 4-DTPT test rig was examined for transportation of fine particles at various conditions which were defined by case numbers listed in Table 4.6. It is observed that the moving bed in the annular section is fluctuated for the gas flow rates around the minimum spouting flow rates. In such situation, fluctuation of the bed surface leads to feeding of an unexpected amount of fine particles to the test rig which is hard to be handled. The presence of the large amount of the fine particles in the moving bed results in blockage of the moving bed and after a short while further feeding of fine particles is not possible. Thus, the conditions are chosen for the gas flow larger than the minimum spouting flow rate.

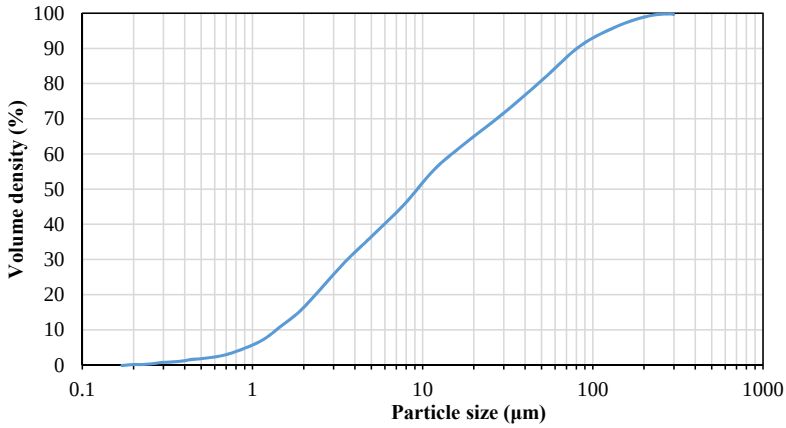

Figure 4.20: Accumulative distribution of the raw meal type II for operation of the 4-DTPT

During the experiments, the set-up runs at a flow rate higher than the minimum stable spouting condition. After reaching the steady state, the fine particles are fed to the set-up. By varying the solid feeding rate of the fine particles to have a constant height of the fine particles in the standpipe, a constant transportation rate of the fine particles is obtained.

4.2.2.1 Pressure drop

The pressure drop of the set-up after the feeding of the fine particles is compared with the pressure drop curves for the cases with only the coarse particles. Presumably, pressure drop of the case with fine particles through the dense bed in the annular section is higher than the case without fine particles due to presence of the fine particles and resulting in a low void. Low void results in a high pressure drop according to the Ergun's correlation (Equation 4.3).

Figures 4.21 and 4.22 present a comparison of the pressure drop of the cases with and without fine particles. Indeed, the pressure drop of the cases with fine particles is higher than the cases without out. With the presence of the fine particles, the influence of the geometric parameters shows the same trend as without fine particles.

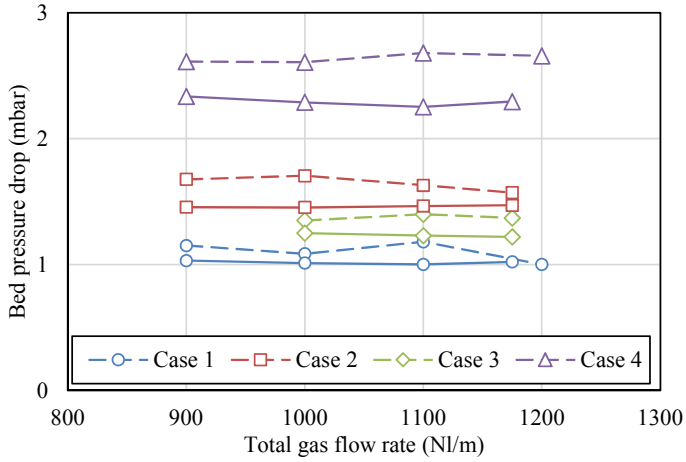

Figure 4.21: Pressure drop sand type SD-1014. (—) Cases without fine particles and (– –) Cases with fine particles

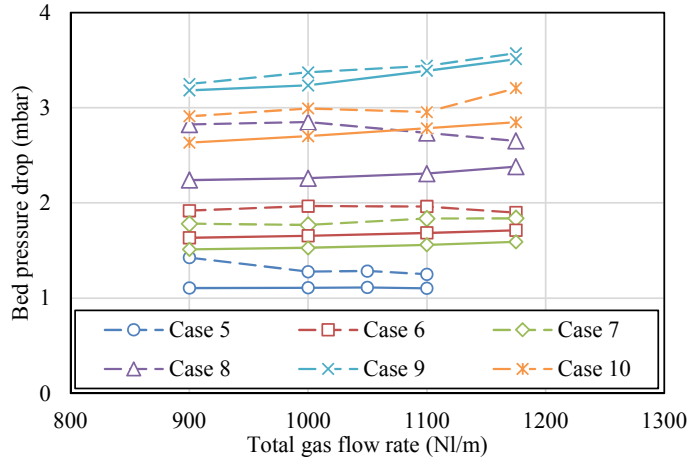

Figure 4.22: Pressure drop sand type SD-1417. (—) Cases without fine particles and (– –) Cases with fine particles

For both particle sizes groups (sand type SD-1014 and 1417), it shows that shorter height of the draft tube results in higher pressure drop difference between the cases with and without fine particles. Same trend is also observed for the height of the dense bed.

More results are shown in Figures A.1 and A.2 in Appendix.

4.2.2.2 Internal solid circulation rate (ISCR)

Coarse particles as the bed inventory for each set of the experiments are internally recirculated through the draft tube then depositing on the dense bed surface, moving down toward the entrained zone and again accelerating in the draft tube. Superficial gas velocity in the draft tubes is higher than the terminal velocity of the coarse particles which leads to the pneumatic transportation of the particles through the draft tube. After feeding the fine particles, those have reached the entrained zone are carried with the flow of the gas and the coarse particles through the draft tube.

ISCR of the coarse particles in the 4-DTPT is identified as the same procedure as the DTSB. In following the ISCR of the 4-DTPT in presence of fine particles is presented with a low limit for the gas flow rate. This limit is imposed by the fine particles where the 4-DTPT cannot transport the fine particles for the gas flow rates below that minimum value. For different geometric and operating parameters gas flow rates below 900 Nl/min was rarely succeeded to handle the fine particles. So, the results in this section are represented for the gas flow rates between 900 and 1200 Nl/min. Besides, the results are in presence of fine particles unless it has been indicated that only coarse particles are applied.

Figure 4.23 shows that generally increasing the total gas flow rate leads to higher ISCR. Similarly, this trend is observed for other cases but regarding the different operating conditions and the geometric parameters, various gradients are experienced.

For the sand type SD-1014, highest ISCR is observed for the case 2 and operates under high gas flow rates. Comparing the case 4 with the case 1 where height of the entrained zone has increased, it leads to the higher ISCR but not as much as the effect which height of the draft tube has on the ISCR. Longer draft tube and deeper dense bed are contributed to the higher ISCR due to the higher pressure drop through the deeper dense bed which may lead to the higher solid concentration in the draft tube and consequently higher ISCR.

But the ISCR results do not confirm this theory for all cases, it seems

other parameters should be taken into account to be able to conclude whether higher pressure drop is resulted in higher ISCR or not. Looking into the results of the case 4, see Figure 4.23, reveals that higher height of the entrained zone causes higher pressure drop but there might be a limit for the solid pass from the dense zone to the dilute entrained zone.

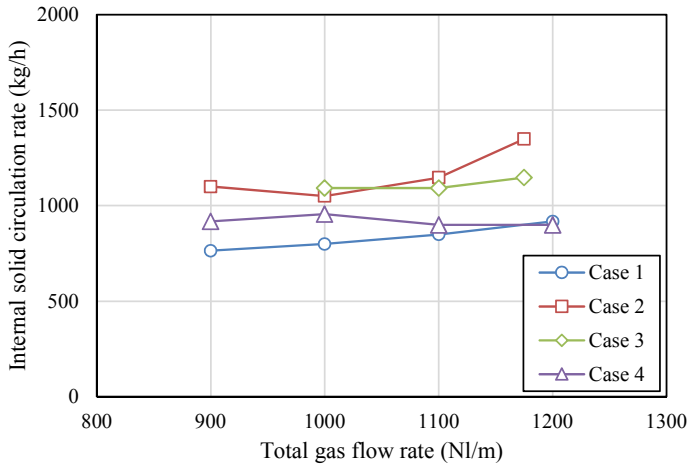

Figure 4.23: ISCR versus total gas flow rate for sand type SD-1014 with fine particles

The possible corresponding cases on Figures 4.23 and 4.24 are investigated and following statements are conducted:

- Higher height of the entrained zone results in the higher ISCR
- Longer draft tube results in the higher ISCR
- Deeper dense bed has a conditional effect on the ISCR
- Larger particle size leads to the higher ISCR

ISCR results for the other cases with the sand types SD-1720 and 2030 are shown in Figures A.3 and A.4 in Appendix. The results of ISCR in the 4-DTPT test rig with and without fine particles are shown in Figure 4.25.

Similar trend as was reported for ISCR of the DTSB, see Figure 4.7, is also observed for ISCR of the only coarse particles in the 4-DTPT device.

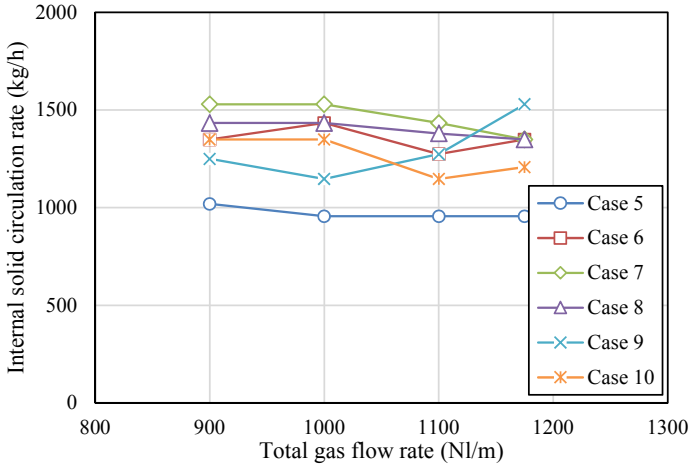

Figure 4.24: ISCR versus total gas flow rate for sand type SD-1417 with fine particles

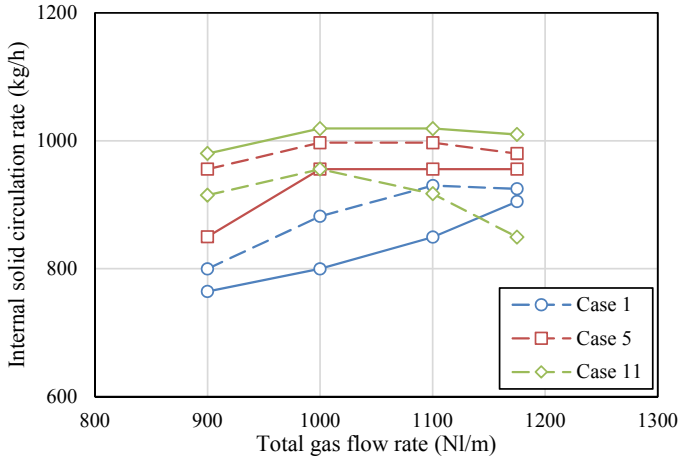

Figure 4.25: ISCR versus total gas flow rate. Operation (—) with fine and coarse particles and (– –) with coarse particles

ISCR increases to reach a maximum and then decreases again by further increase of the total gas flow rate. But in presence of fine particles, ISCR of the coarse particles reaches a maximum and for further increase of the gas flow rate stays constant.

4.2.2.3 Solid transportation rate (STR)

Fine particles transportation rate is one of the most crucial parameters for these studies. During the steady state condition by variation of the feeding rate of the feeder for fine particles and keeping the height of fine particles constant in the standpipe, the solid transportation rate (STR) of fine particles is identified.

STR investigation

The results of STR as a function of gas flow with sand type SD-1040 are shown in Figure 4.26. An increase in gas flow rate results in a increase in the STR of fine particles. The possible reasons might be:

- Higher superficial gas velocity in the freeboard which minimizes the residence time of fine particles in the 4-DTPT, by means of higher acceleration and elutriation of fine particles and also reducing the internal recirculation of fines particles.

- Higher ISCR of coarse particles which leads to higher transportation rate of the fine particles from the feeding port (bottom of the standpipe) to the entrained zone. When higher amount of fine particles reaches the entrance of the draft tube, higher STR may be expected.

Long draft tube (in case 2) and high height of the dense bed (in case 3) result in low STR of the fine particles. High height of the entrained zone (in case 4) leads to further decease of the STR.

Results of the solid transportation rate for the other cases are shown in Figures A.5 to A.7 in Appendix. The results show that bigger size coarse particles increases the STR of fine particles, but there is an upper limit for the size of the coarse particles regarding the geometric parameters.

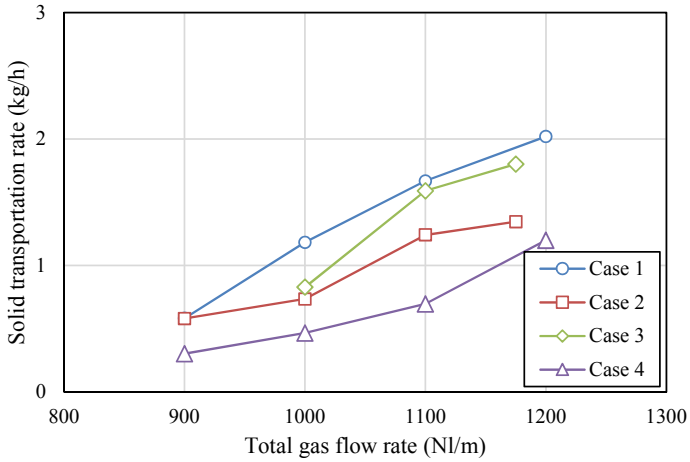

Figure 4.26: Solid transportation rate versus total gas flow rate for sand type SD-1014

Comparison of STR of two different samples

The solid transportaion rate of the fine particles samples are investigated. Particles size distribution of the cement raw meal type I and II are shown in Figures 3.8 and 4.20, respectively. Figures 4.27 and 4.28 show the comparison of the STR results of the Case 1 and 5 operated with raw meal type I and II.

These results shows that STR of the raw meal type II is lower the STR of the raw meal type I. In spite that the particle size distribution of two samples are quite in a same range. The reason can be sought by looking into the results from flowability of these samples. The flowability was investigated through the new idea of characterization, see Figure 3.9.

The sliding and resting angle of the raw meal type I are 62° and 32° degrees, respectively. And for raw meal type II, these angles are 85° and 38° degrees, respectively. The results show that the raw meal type II has lower flowability which likely results in lower transportation rate through the 4-DTPT.

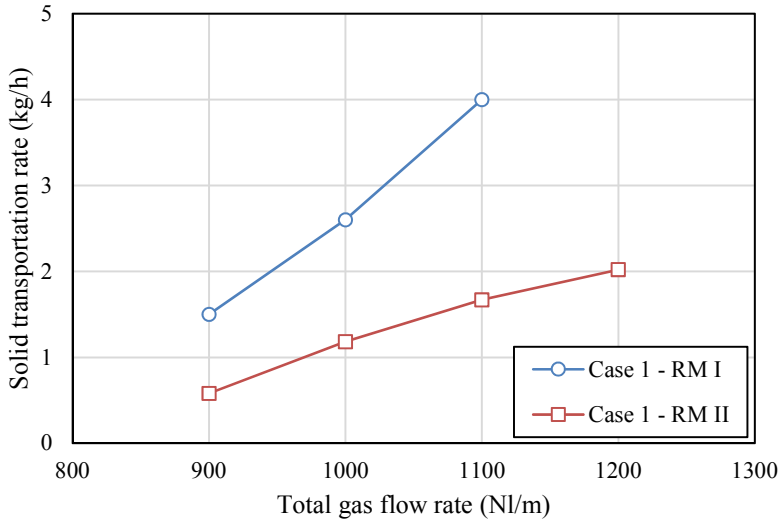

Figure 4.27: Solid transportation rate for Case 1 - Rawmeal type I and II

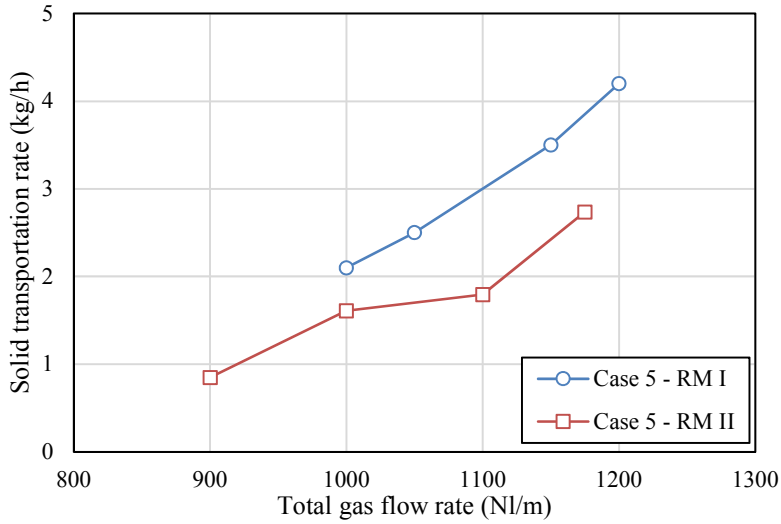

Figure 4.28: Solid transportation rate for Case 5 - Rawmeal type I and II

Table 4.8: Effect of geometric and operating parameters

Parameter	ΔP	ISCR	STR
d_P	↗	↗	↗
H_{DT}	↗	↗	↘
H_{EZ}	↗	↗	↘
H_{Bed}	↗	↗	↘
Q_{tot}	↗	↗	↗

4.2.3 Summary of the results of the 4-DTPT

Effects of the geometric parameters and the operating conditions are summarized in Table 4.8. Each arrow shows how greater values of the listed parameter influence the trend of the ΔP, the ISCR and the STR.

Main purpose of design and application of the 4-DTPT is for transportation of fine particles. Coarse particles are utilized to provide a mean for internal transportation of the fine particles (from the feeding port to the transportation zone). Additionally, the feeding port is submerged to the bed of coarse particles which makes the 4-DTPT test rig a sealing device. Thus, the 4-DTPT can be introduced as a non-mechanical valve which might be applied in circulating and interconnected fluidized beds.

Solid transportation rate (STR) of fine particles is considered as an optimization factor. The geometric and operating parameters are studied to find the conditions at which the STR is maximum. Big particle sizes and high gas flow rates result in high STR. Low length of the draft tube, low height of the bed in the annular section and low height of the entrained zone lead to higher STR of fine particles.

Regarding the lower and upper boundaries of each of these parameters, more investigation is needed to be able to precisely optemize the hydrodynamics and operational characteristics of the 4-DTPT for particular design conditions. Further studies may provided adequate knowledge to find the optimized geometric and operating conditions as well as the size of coarse particles.

Chapter 5

Simple models for DTSB and 4-DTPT

Gas-solid flow in DTSB and 4-DTPT is complicated, especially with presence of fine particles. For such systems, simple models might be useful to explain the inherent phenomenon. In order to describe the hydrodynamics of the DTSB and the 4-DTPT test rigs, the semi-empirical models are implemented. The model for the DTSB applies a correlation for gas flow distribution which is fitted to the experimental results. This correlation covers all the geometric parameters, particle size and gas flow rate. Pressure drop, internal solid circulation rate and the solid concentration in the drat tube are calculated and compared to the experimental results.

The model for the 4-DTPT applies the pressure drop from the experiments to calculated the gas flow rate to the annular section. ISCR of coarse particles and STR of fine particles are taken into account to estimate the fraction of fine and coarse particles in the moving bed. The mean particle size and voidage of the moving bed are recalculated in the Ergun's equation for estimation of the gas velocity through the annular section.

5.1 Draft tube spouted bed

5.1.1 Model assumptions

For the modeling of the DTSB, it is assumed that: (1) Particles in the annular section are in a condition below the minimum fluidization. (2) Transported particles from the annular section to the entrained zone do not remain in this zone and accelerated abruptly after reaching the gas stream. (3) Considering a dilute draft tube, particle-particle and particles-wall contacts are disregarded.

5.1.2 Model descriptions

Mean particle diameter of each particle group (d_P), the draft tube inner diameter (D_{DT}), the height of the entrained zone (H_{EZ}), the bottom cone inner angle (α) and the total gas flow rate (Q_T) are reassembled to provide the various geometric parameters and the operating conditions. Pressure drop of the draft tube and the annular section of the DTSB set-up is measured, and the internal solid circulation rate (ISCR) of the particles are calculated considering the particles velocity on the outer surface of the annular section.

The input parameters of the model are:

- Mean diameter of the particle group (d_P)
- Draft tube inner diameter (D_{DT})
- Height of the entrained zone (H_{EZ})
- Bottom cone inner angle (α)
- Total gas feeding rate (Q_T)

and unknown parameters are:

- Pressure drop (ΔP)
- Fraction of gas to the draft tube(X_{DT})
- Internal solid circulation rate ($ISCR$, $\dot{m}_s$)
- Solid concentration in the draft tube (ε_s) or the average solid velocity in the draft tube (V_s)

Ergun correlation [143] is applied to calculate the pressure drop of the annular section, but before that the fraction of the gas flow rate to the annular section ($1 - X_{DT}$) should be identified to be able to calculate the superficial gas velocity through the dense bed in annular section. Equation (5.1) represents the Erqun's correlation.

$$\Delta P_{AN} = \frac{150\mu_g(1-\varepsilon_{mf})^2 V_{g,AN} H_{AN}}{\varepsilon_{mf}^3(\psi_P d_P)^2} + \frac{1.75(1-\varepsilon_{mf})\rho_g V_{g,AN}^2 H_{AN}}{\varepsilon_{mf}^3(\psi_P d_P)} \tag{5.1}$$

where P, g and AN are the indices for particles, gas phase and annular section, and parameters μ, ρ, ε, V, H and ψ are viscosity, density, void fraction, velocity, height and sphericity, respectively.

Pressure drop of the draft tube [145] comprises of corresponding static head of solid and gas in the draft tube and kinetic energy of the solid particles which these terms are shown respectively in equation (5.2).

$$\begin{aligned} \Delta P_{DT} &= \varepsilon_{s,DT}\,\rho_P\,g\,h_{DT} \\ &+ \varepsilon_g\,\rho_g\,g\,h_{DT} \\ &+ \frac{1}{2}\,\varepsilon_{s,DT}\,\rho_P\,g\,{V_s}^2 \end{aligned} \tag{5.2}$$

where V_s is the average particle velocity within the draft tube and written by Equation (5.3).

$$V_s = \frac{\dot{m}_s}{\rho_P\,A_{DT}\,\varepsilon_{s,DT}} \tag{5.3}$$

Moreover, it is assumed that the draft tube is operated at fast fluidization regime. Then pressure drop of the draft tube can be conducted from the expression for pressure drop of a turbulent or fast fluidized bed which is shown by equation (5.4) [1].

$$\begin{aligned} \Delta P_{DT} &= (1.15)\,\frac{Solid\ weight}{Cross\ section\ area\ of\ the\ bed} \\ &= (1.15)\,\frac{\rho_P\, g\, (A_{DT}\, h_{DT})\, \varepsilon_{s,DT}}{A_{DT}} \\ &= (1.15)\,\rho_P\, g\, L_{DT}\, \varepsilon_{s,DT} \end{aligned} \tag{5.4}$$

Solid void fraction is calculated from equation (5.4), considering equal pressure drop of the annular section and the draft tube. So, the solid void fraction from equation (5.4) is located in equation (5.3) then solid circulation rate ($\dot{m}_s$) is given by locating the mean particle velocity in equation (5.2). After all substitutions Equation (5.5) is rewritten to conduct the ISCR.

$$\dot{m}_s = \sqrt{\frac{\Delta P - \varepsilon_{s,DT}\, \rho_P\, g\, h_{DT} - \varepsilon_g\, \rho_g\, g\, h_{DT}}{\frac{1}{2}\, \varepsilon_{s,DT}\, \rho_P\, g}}\ \rho_P\, A_{DT}\, \varepsilon_{s,DT} \tag{5.5}$$

The fraction of the gas which is distributed between the draft tube and the annular section is calculated based on the developed correlation from the experimental data. Initially, the feeding gas flow rate (Q_T) gets dimensionless by the minimum gas flow rate (see Equation (4.1)) which the set-up is operated at minimum spouting velocity ($Q_{min,T}$) which is expressed by equation (5.6).

$$Q_{min,T} = Re_{min} \left(\frac{\mu_g}{\rho_P\, d_P}\right) \left(\frac{\pi {D_{inlet}}^2}{4}\right) \tag{5.6}$$

where A, B, C, D and E parameters are given in Table 4.1.

The gas flow fraction correlation is developed considering the particle size (d_P), the draft tube inner diameter (D_{DT}), the bottom cone inner angle (α), height of the entrained zone (H_{EN}) and the dimensionless gas flow rate (Q_T^*), which shows by equation 5.7.

$$x_{AN} = A\,(Ar)^B \left(\frac{D_{DT}}{d_P}\right)^C \left(\frac{H_{EZ}}{d_P}\right)^D \left(\frac{H_{AN}}{d_P}\right)^E \left(tan\left(\frac{\alpha}{2}\right)\right)^F (Re_P)^G\, e^{(Re_P)^H} \quad (5.7)$$

where the parameters A, B, C, D, E, F, G and H are listed in Table 5.1.

Table 5.1: Coefficients of the Equation (5.7)

A	B	C	D	E	F	G	H
0.001534	1.1235	-0.4235	1.1756	-0.3952	0.1603	-1.4159	0.04886

5.1.3 Results

Comparison of the experimental and modeling cases (listed in Tabel 5.2) are shown in Figures 5.1 to 5.3. In the legends, SCR, dp, x_DT, and e_DT are solid circulation rate, pressure drop, gas flow fraction to the draft tube, void fraction of the draft tube, respectively.

Table 5.2: The cases to compare the experimental and modeling results

d_P (μm)	D_{DT} (mm)	H_{EZ} (mm)	α ($degree$)	Case Number
(1000-2000)	17	30	55	(I)
(707-1000)	17	30	55	(II)
(2000-2360)	17	30	55	(III)
(707-1000)	17	20	55	(IV)
(1000-2000)	17	20	80	(V)
(1000-2000)	14	20	80	(VI)

As it is observed from the Figures 5.1 to 5.3, the model does not follow the increasing-decreasing trend of the internal solid circulation rate and decreasing-increasing trend of the pressure drop. If an advanced model is developed, it probably may cover more hydrodynamics details. Thus, calculated results with better agreement with experiments can be expected.

For some cases, fraction of the gas flow to the annular section (x_{AN}) which is correlated by Equation (5.7), cannot predict properly for low total gas flow rates Q_T^*. Mostly the range at which the gas flow fraction to the draft tube (x_DT on the figures) has a larger deviation from experimental results. For instance, the draft tube gas flow fraction of the case (I) which is shown by Figure 5.1 represents this fact that the correlation (Equation (5.7)) cannot cover whole the data points while the gradient of changes is sharp at low gas flow rates.

The modeling of the DTSB shows that although the model was so simple to describe such sophisticated phenomena in a DTSB, trends of the results are fairly well approximated. Mentioning that, to find a better match between the calculated and experimental results a more advanced model is required. A computational fluid dynamic approach leads to higher resolution results which can be a topic for future studies of this topic.

Comparison of the rest cases are given in Figures B.1 to B.3 in Appendix.

5.2 Four draft tubes pneumatic transport

5.2.1 Model assumptions

Hydrodynamics of the 4-DTPT is modeled considering appropriate assumptions and applicable equations. The assumptions are as listed for modeling of the DTSB, relevant for this modeling. Regarding the below considerations, distribution of the gas flow to the annular section is the only parameter which is investigated: (1) Complexity in configuration of

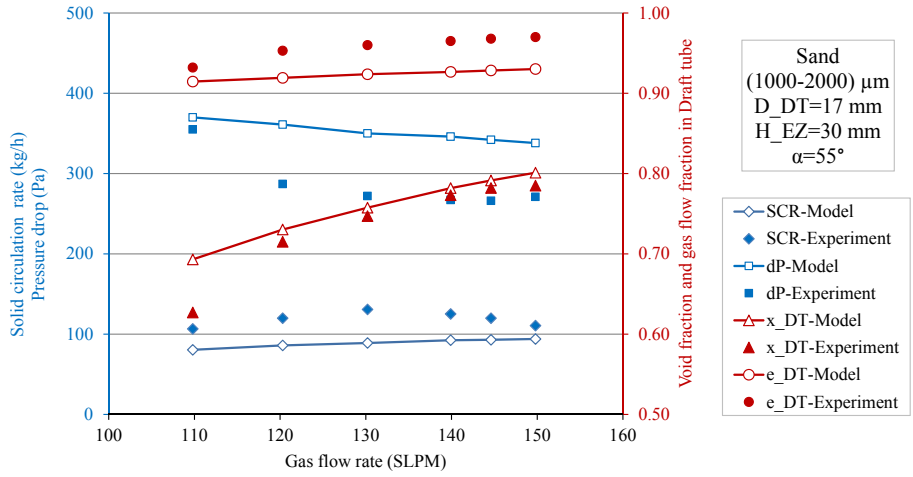

Figure 5.1: Comparison of experimental and modeling results of case (I)

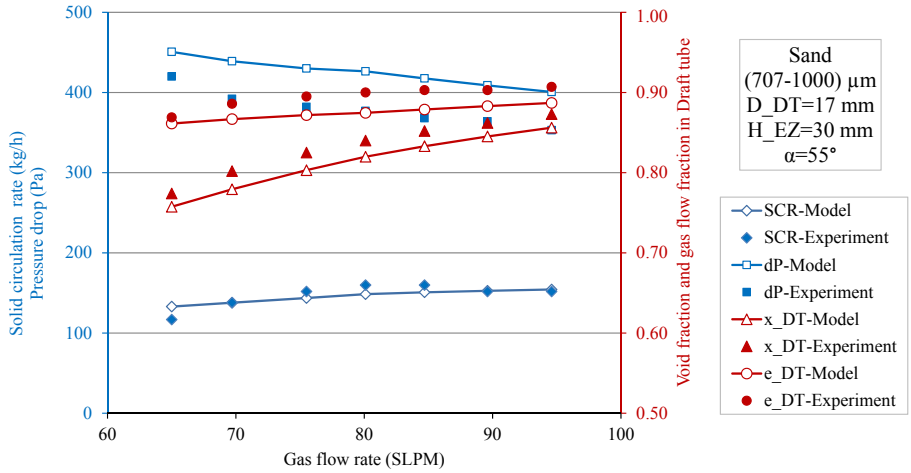

Figure 5.2: Comparison of experimental and modeling results of case (II)

the 4-DTPT to investigate the gas-solid system, (2) Especially in presence of the fine particles, the uncertainty about the fraction and distribution of the fine particles in the mixture increases, (3) On the other hand, more detailed modeling is needed to explain more of the hydrodynamics.

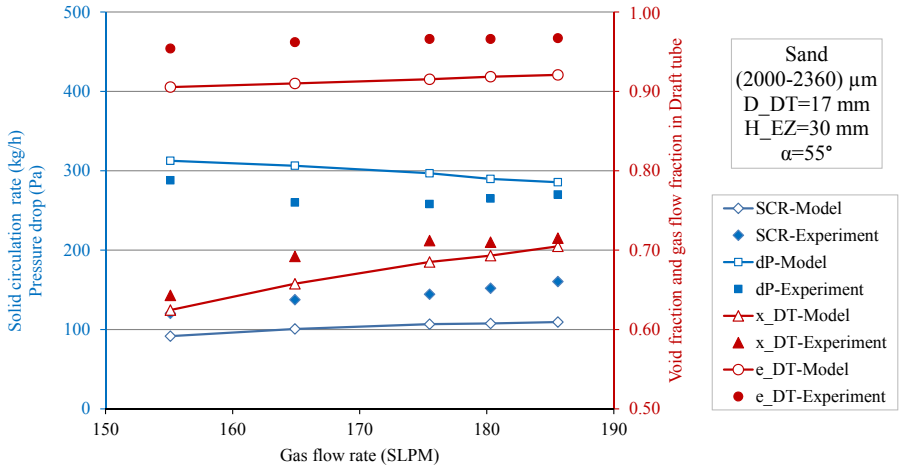

Figure 5.3: Comparison of experimental and modeling results of case (III)

5.2.2 Draft tube gas flow fraction

Gas flow fraction to the draft tube is investigated under two operating conditions where the system is operated solely with the coarse particles (Case C) and operated with the fine and the coarse particles for the purpose of the fine particles transportation (Case CF).

For both cases with and without presence of fine particles, pressure drop over the bed in the annular section are applied to predict fraction of the gas which passes through the annular section. It assumes that the particles in each type have a representative diameter equals to the average of the lower and upper boundary of the samples in each range.

Sphericity of the particles is assumed to be 0.85 for both fine and coarse particles [1]. Void fraction of the coarse particles in different types was measured and is about 0.4 ± 0.02 where assumed 0.4 for all cases. Void of the fine particles was measured and identified around 0.68 ± 0.01. Fluidization regime of the particles in the annular section is considered to be below minimum fluidization velocity. So Ergun's equation, see Equation (5.1), is applied to predict the gas velocity through the bed. The equation is rewritten for the cases without fine particles as:

$$
\begin{aligned}
&X\,{V_{AN}}^2 + Y\,V_{AN} + Z = 0 \qquad (5.8)\\
&X = 1.75\,\frac{1-\varepsilon_P}{{\varepsilon_P}^3}\,\frac{\rho_g\,H_{Bed}}{\psi_P\,d_P}\\
&Y = 150\,\frac{(1-\varepsilon_P)^2}{{\varepsilon_P}^3}\,\frac{\mu_g\,H_{Bed}}{(\psi_P\,d_P)^2}\\
&Z = -\Delta P
\end{aligned}
$$

Positive root of the Equation (5.8) is the average superficial gas velocity through the dense bed in the annular section.

After feeding the fine particles to the bed of particles in the annular section, void fraction (ε_P) and mean particles diameter (d_P) should bed recalculated considering fraction of the fine particles.

Following assumptions are taken into account to provide a practical calculate to update the void fraction and mean particles diameter:

- Fine particles are uniformly distributed in the dense bed of coarse particles. So, the fine particles fill specific fraction of the coarse particles void.

- Considering no accumulation of the fine particles in the annular dense bed, fine particles passes from the feeding port through the dense bed just once. In the other word, fine particles are not recirculated within the annular dense bed, and if there is fine particles recirculation it occurs just in the freeboard.

- Regarding the void of the fine particles and the fraction of the solid transportation rate to the internal solid circulation rate (STR/ISCR or SI), void of the mixture and the mean particles size are calculated.

$$\varepsilon_{P,CF} = (1 - X_{SI})\,\varepsilon_{P,C} - (1 - \varepsilon_{P,F})\,X_{SI} \tag{5.9}$$

$$d_{P,CF} = \frac{1}{\sum_i \frac{x_i}{d_{P,i}}} = \frac{1}{\frac{1 - X_{SI}}{d_{P,C}} + \frac{X_{SI}}{d_{P,F}}} \tag{5.10}$$

5.2.3 Results

Gas flow fraction to the annular section of the 4-DTPT device is calculated for the cases which are operated with and without fine particles. Results for the experiments on sand type SD-1014, referring section 4.2 as cases 1 to 4, are shown in Figure 5.4. And the calculated results for the experiments on sand type SD-1417, cases 5 to 10, are compared with the experimental results in Figure 5.5.

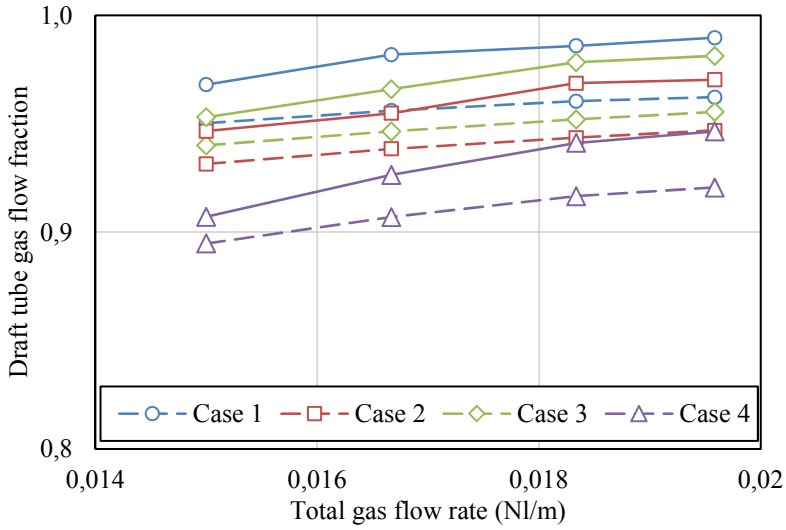

Figure 5.4: Fraction of the gas flow to the draft tube. Operation (—) with fine and coarse particles, and (– –) with coarse particles

Comparisons in Figures 5.4 and 5.5 reveal that the model can predict the trend of changes. But it under-predicts the gas flow fraction to the draft tube or in the other words, the model overpredicts the gas flow of the

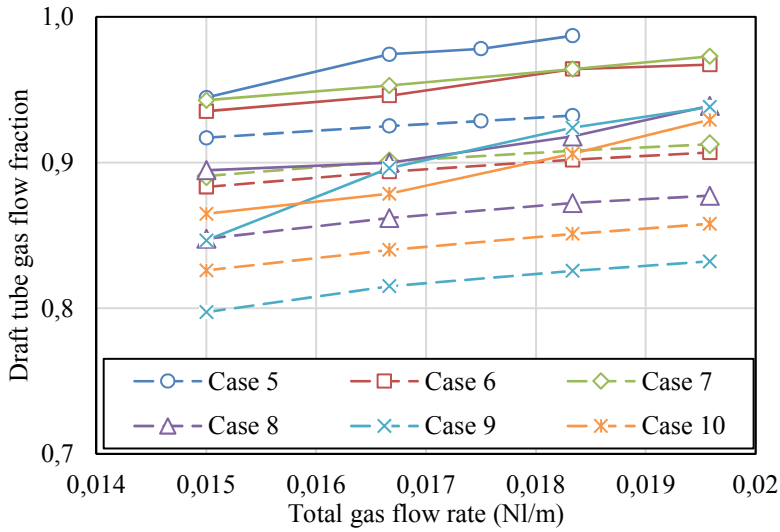

Figure 5.5: Fraction of the gas flow to the draft tube. Operation (—) with fine and coarse particles, and (– –) with coarse particles

annular section. By looking into the Ergun's equation, it may conclude that:

- Ergun pressure drop equation is so sensitive to the void fraction of the particles. Even a few percentage offset may result in remarkable deviations in pressure drop calculations.

- Mean diameter of the sample of coarse particles is roughly approximated. And, mean diameter of the mixture is predicted based on some assumptions which may not be so realistic

Mentioned items influence the calculation of the gas velocity through the bed and leads to the discrepancies between the predicted and experimental results.

5.3 Summary

Investigation of a DTSB is performed based on a simple model which even leads to the results in quite good agreement with experiments. Although, a more advanced model covering more fact and less general assumption may conclude to a model with the a better prediction. By having this consideration in mind, implementing the similar approach for the 4-DTPT does not result in more valuable data for modeling the 4-DTPT. Moreover, presence of fine particles and complexity in inserting the interparticle forces to the model is not a straight forward task, regarding the mentioned uncertainties about the fraction and distribution of the fine particles in the annular section. So, for modeling of the 4-DTPT, pressure drop was studied as a parameter which can be addressed to a semi-empirical correlation.

Presence of fine particles was taken into account based on the uniform distribution and the fine to the coarse particles fraction from STR to ISCR. The assumptions for measuring and calculating the ISCR import extra uncertainty to the model in addition to the bed void fraction and particles mean diameter. These uncertainties leads the modeling results to deviate from the experiments. Therefor, more realistic assumptions are required to expect better prediction, although these are the applicable present assumptions.

Chapter 6

Conclusion and future works

6.1 Conclusion

The main objective of this project is dealing with an industrial challenge which is the difficulty of fluidization and particularly recircualtion of fine particles. This is also a challenge for the non-mechanical valves of the circulating or the interconnected fluidized beds (CFB or IFB). The difficulty results from two reasons: (1) interparticle forces are the dominant force when the fine particles are operated under low fluidization regimes; (2) operating condition of the conventional non-mechanical valves are around minimum fluidization.

By reviewing literature, a new type of non-mechanical valve for recirculation of fine particles is proposed, based on the draft tube spouted bed (DTSB) with coarse particles for assisting the fluidization and transportation of fine particles. Several configurations of the DTSB have been designed and the hydrodynamic parameters of the DTSB were investigated. During the operation of the DTPT test rig, some challenges were experienced such as introducing the fine particles to the moving bed of

coarse particles and keeping the operation of the DTSB smooth after inserting the fines considering the asymmetry in feeding of fine particles.

Series of auxiliary tests were performed to figure out the solutions. Modification on the configuration and the location of the feeding tube were examined. The investigation was ended up to another concept which can deal with the transportation of the fine particles. To characterize the flowability of the sole and mixture of the coarse and fine particles, a device was developed and tested. The findings from the investigations and the hydrodynamics of the DTSB led to proposal of a new non-mechanical valve. For design of the new valve, following considerations were taken into account:

- Draft tube with large diameter
- Larger height of the entrained zone
- Smaller inner angle of the conical section
- Higher gas flow rates

are conducted to the higher internal solid circulation rates (ISCR) of the coarse particles. Presumably, higher ISCR of the coarse particles may result in higher internal transportation of the fine particles from the feeding port to the draft tube (as the transportation device).

Throughout one of the supportive experiments, vertical feeding of the fine particle to the middle of the moving dense bed of the coarse particles was examined and showed success. Thus, the new concept with a DTSB configuration and possibility of having a vertical tube to the annular section as well as keeping the symmetry of the device was concluded to a configuration including four draft tubes and the feeding tube at the central axis.

The 4-DTPT test rig is capable of transportation of fine particles while the issue with introducing the fine particles to the bed of coarse particles was solved. Preliminary experiments were performed to investigate the influence of the geometric parameters and the operating conditions on transportation of the fine particles.

Experimental studies on the 4-DTPT shows that:

- Larger particles size
- Shorter draft tube
- Lower height of the entrained zone
- Lower depth of the dense bed
- Higher gas flow rate

result in higher solid transportation rate (STR) of fine particles.

6.2 Future works

Commissioning, operation and characterization of the 4-DTPT device have been performed within this PhD project. The experimental results reveal that the 4-DTPT with this configuration is capable of acting as a pneumatic valve (transportation and sealing device) for handling the fine particles. The 4-DTPT device can be integrated to a circulating or an interconnected fluidized bed where the fine and ultrafine particles are dealt with.

Future investigations of the 4-DTPT are suggested as follows:

- Systematic investigation of the geometric and operating parameters of the 4-DTPT test rig for the purpose of characterization of the influential parameters.
- Results show that the STR of fine particles is fairly low. So, ideas for development of the present test rig may be introduced to investigate higher STR of fine particles..
- New configuration (revolved draft tube pneumatic transport comprises of infinite number of DTPT instead of four in a 4-DTPT configuration) may be studied and has the potential for scale-up.

Appendix A

Operation of the 4-DTPT

A.1 4-DTPT operation with Rawmeal type II

A.1.1 Pressure drop - with and without fine particles

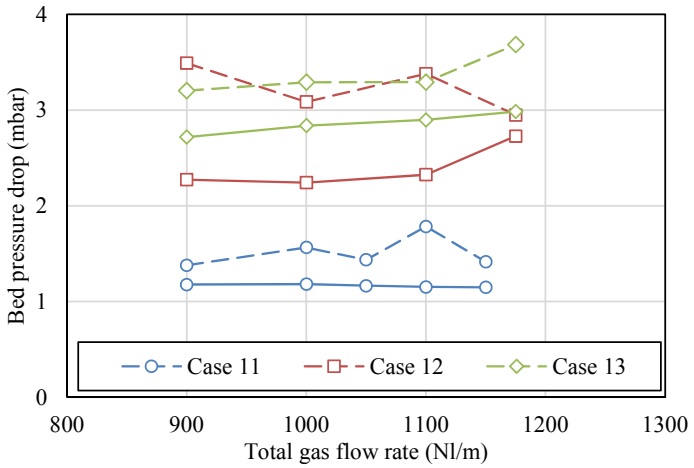

Figure A.1: Pressure drop of the 4-DTPT with sand type SD-1720. (—) with coarse particles and (– –) with coarse and fine particles

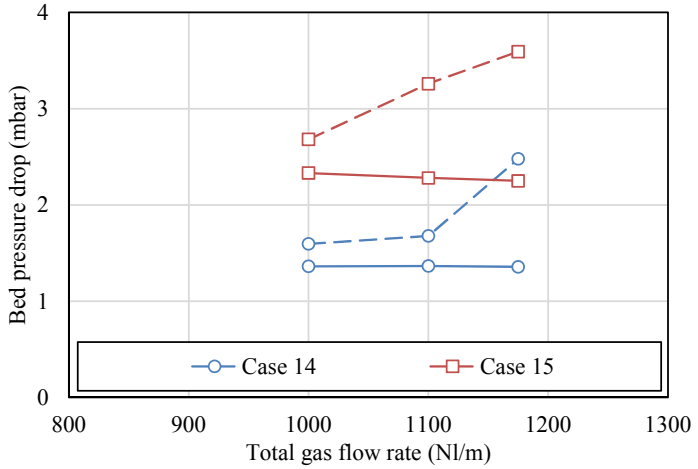

Figure A.2: Pressure drop of the 4-DTPT with sand type SD-2030. (—) with coarse particles and (– –) with coarse and fine particles

A.1.2 ISCR - with fine particles

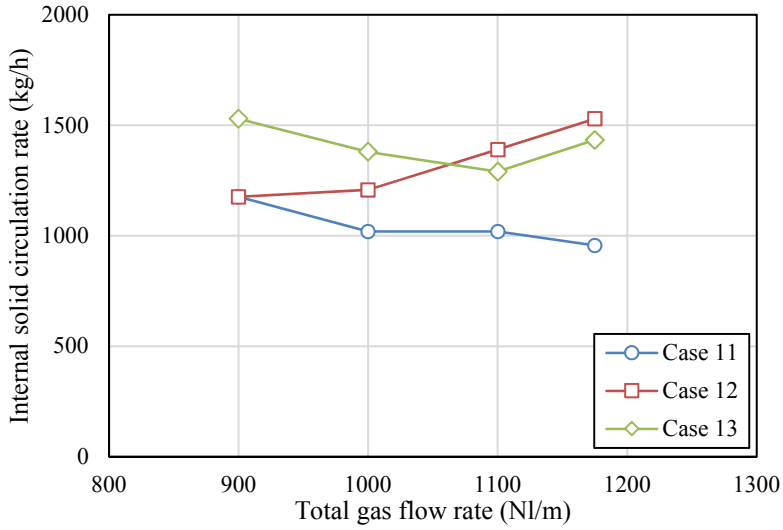

Figure A.3: ISCR versus total gas flow rate for sand type SD-1720

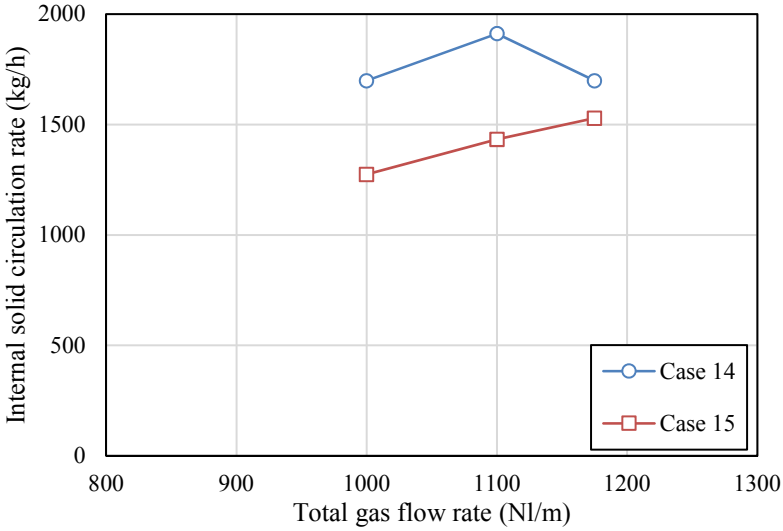

Figure A.4: ISCR versus total gas flow rate for sand type SD-2030

A.1.3 Solid transportation rate of fine particles

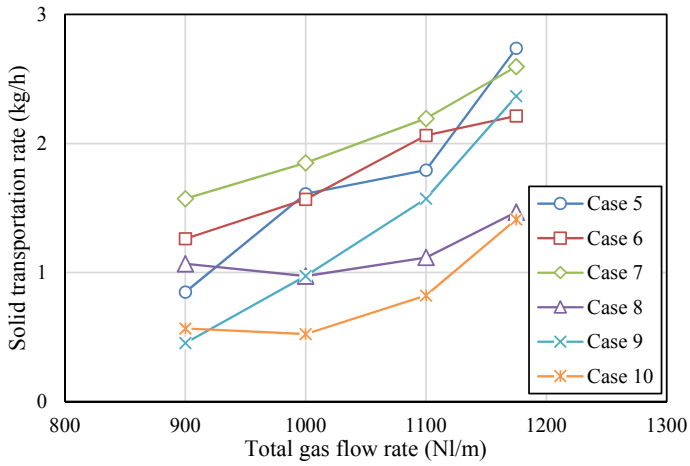

Figure A.5: Solid transportation rate versus total gas flow rate for sand type SD-1417

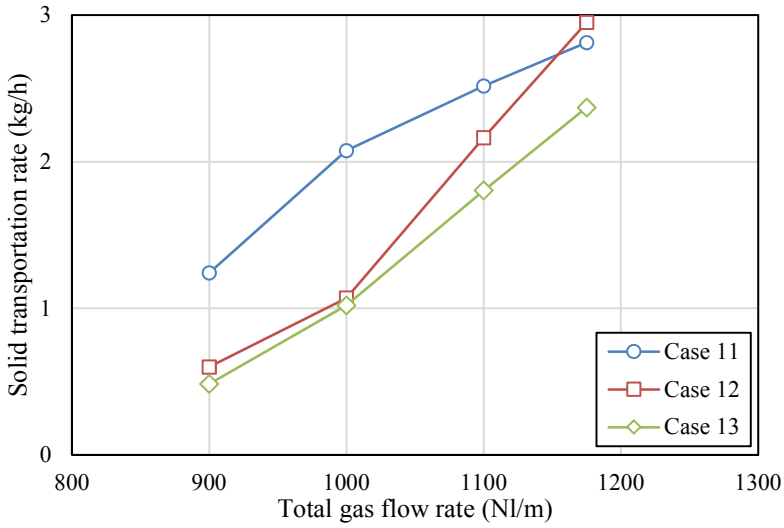

Figure A.6: Solid transportation rate versus total gas flow rate for sand type SD-1720

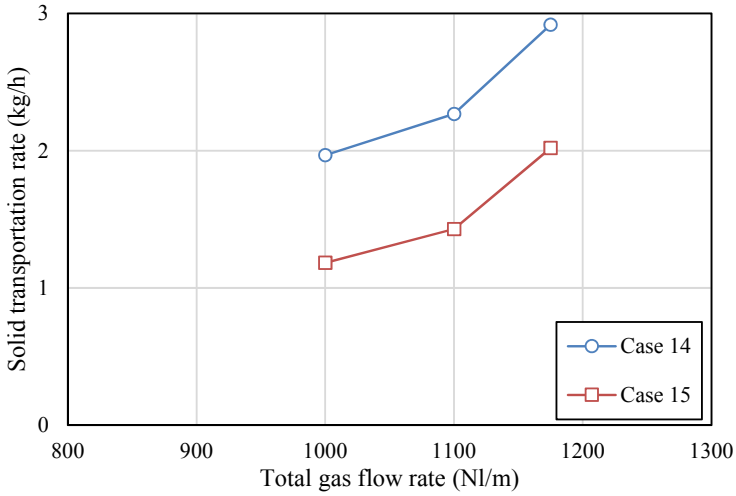

Figure A.7: Solid transportation rate versus total gas flow rate for sand type SD-2030

A.2 Particles size distribution of cement rawmeal type I

Particles size distribution of the cement raw meal type I is shown in Figure 3.8.

Appendix B

Modeling of the DTSB

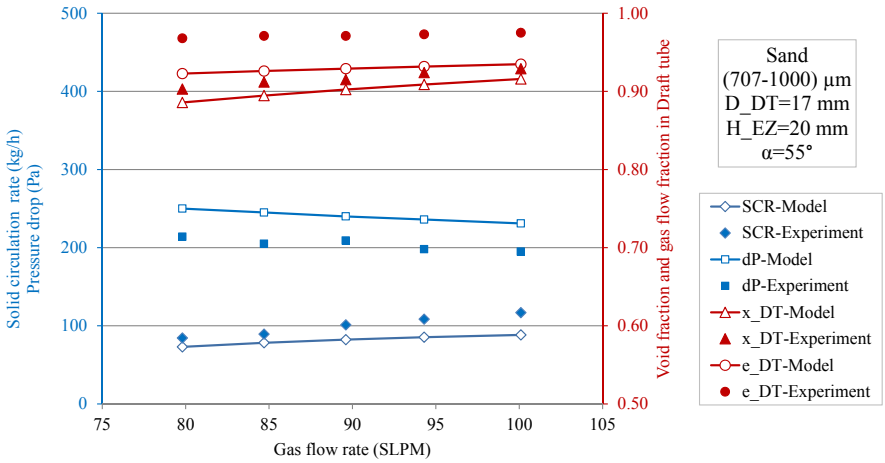

Figure B.1: Comparison of experimental and modeling results of case (IV)

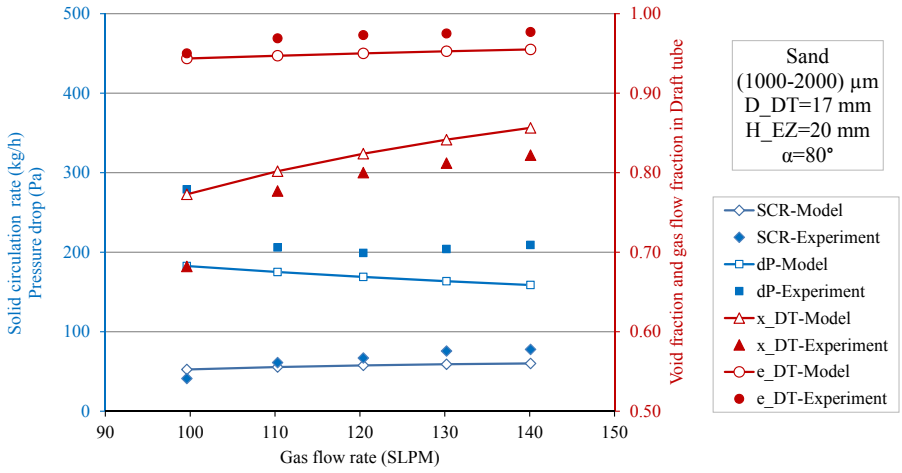

Figure B.2: Comparison of experimental and modeling results of case (V)

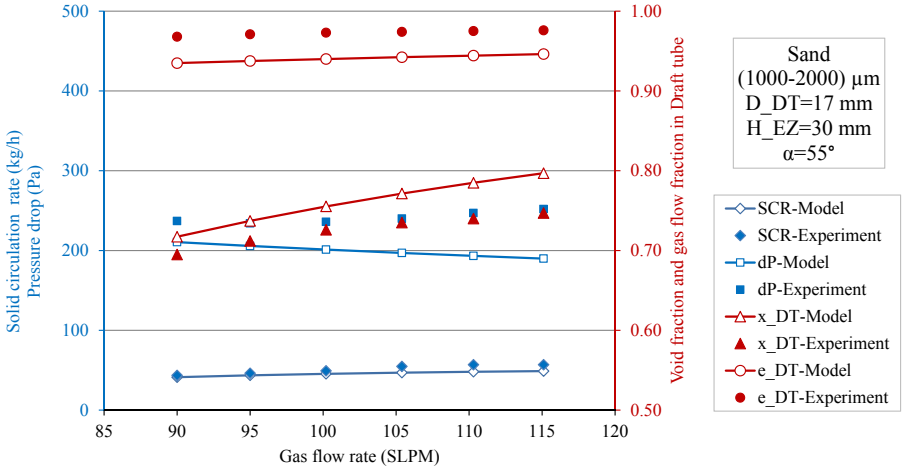

Figure B.3: Comparison of experimental and modeling results of case (VI)

Appendix C

Investigation of the 4-DTPT

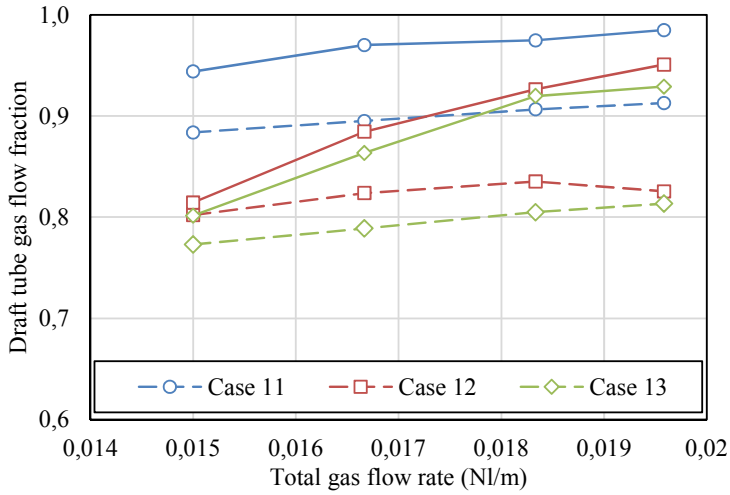

Figure C.1: Fraction of the gas flow to the draft tube. Operation (—) with fine and coarse particles, and (– –) with coarse particles

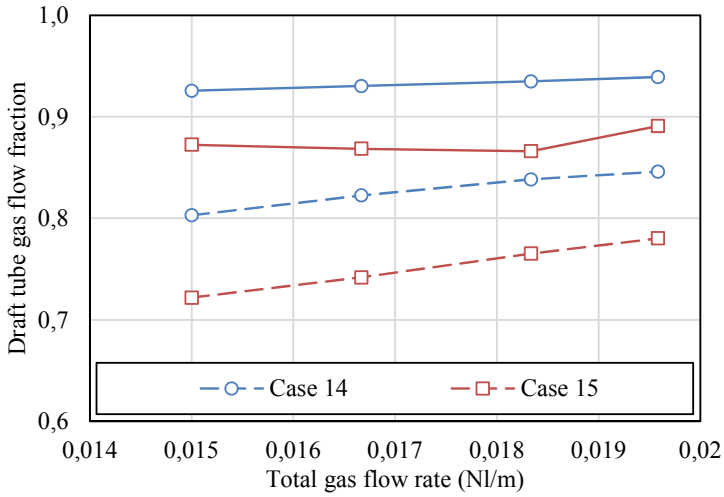

Figure C.2: Fraction of the gas flow to the draft tube. Operation (—) with fine and coarse particles, and (– –) with coarse particles

Appendix D

Nomenclature

Parameters

Ar	Archemides number $\left(Ar = \frac{{d_p}^3 \rho_g (\rho_s - \rho_g) g}{\mu^2}\right)$
BFB	Bubbling fluidized bed
CFB	Circulating fluidized bed
CLC	Chemical looping combustion
CSIC	The Spanish National Research Council
d	diameter
DOE	Department of energy
DT	Draft tube
DZ	Dense zone
EZ	Entrained zone
F	Force
FB	Fluidized bed
FCC	Fluid catalytic cracking
FFB	Fast fluidized bed
hr	Hardnes of softer body
hw	Liftshits-Var der Waals coefficient
IFB	Interconnected fluidized bed
IFK	Institute of combustion and power plant technology
ISCR	Internal solid circulation rate
k	Size ratio, Young modulus

Kc	Spring constant
LS	Loop-seal
P	Pressure, Particle
R	Radius
Re	Reynolds number $\left(Re = \frac{\rho U d}{\mu}\right)$
S	Solid
SCR	Solid circulation rate
STD	Solid transportation device
STR	Solid transportation rate
SZ	Splashing zone
TDH	Transport disengaging height
tot	total
TZ	Transport zone
U	velocity
u*	Dimensionless velocity
V	superficial velocity
VUT	Vienna technical university
Z	distance between bodies

Greek letters

γ	spring strain
δ	Bubble fraction
μ	Viscousity
ρ	Density
σ	tensile strength
ψ	Sphericity
ξ	interparticle attractive constant

Indeces

a	Annulus
ag	agglomerate
as	asperity
att	attainable
Bed	Bed of particles
b	bubble
c	Core
dw	disintegration per unit-weight
cpl	Capillary
esf	Electrostatic
g	gas
IPF	interparticle force
LSF	local shear force
mf	minimum fluidization

p	particle
s	solid
tf	throughflow
tr	terminal
vdw	Van der waals
vis	visibile
∞	Height above TDH

Bibliography

[1] D. Kunii and O. Levenspiel. *Fluidization Engineering*. Butterworth-Heinemann, Massachusetts, 1991.

[2] Thomas H. Hsiung and George Thodos. Expansion characteristics of gas-fluidized beds. *The Canadian Journal of Chemical Engineering*, 55(2):221–224, apr 1977.

[3] J. R. Grace. Contacting modes and behaviour classification of gas-solid and other two-phase suspensions. *The Canadian Journal of Chemical Engineering*, 64(3):353–363, June 1986.

[4] F. A. Zenz and D. F. Othmer. *Fluidization and Fluid-Particle Systems*. Reinhold Publishing Corporation, New York, 1960.

[5] A. A. Avidan and J. Yerushalmi. Bed Expansion in High Velocity Fluidization. *Powder Technology*, 32:223–232, 1982.

[6] W. C. Yang. *Handbook of Fluidization and Fluid-Particle Systems*. Marcel Dekker Incorporation, 2003.

[7] C. K. Stanley, J. Bridgwater, and J. S. M. Botterill. Solids Flow Between Interconnected Shallow Fluidized Beds. *Chemical Engineering Science*, 39(12):1797–1806, 1984.

[8] T. Shimizu, T. Hirama, H. Hosoda, K. Kitano, M. Inagaki, and K. Tejima. A Twin Fluid-Bed Reactor for Removal of CO_2 from

Combustion Processes. *Transactions of The Institution of Chemical Engineers*, 77(Part A):62–68, 1999.

[9] M. Mortensen, R. G. Minet, T. T. Tsotsis, and S. W. Benson. The development of a dual fluidized-bed reactor system for the conversion of hydrogen chloride to chlorine. *Chemical Engineering Science*, 54:2131–2139, 1999.

[10] A. Lyngfelt, B. Leckner, and T. Mattisson. A fuidized-bed combustion process with inherent CO_2 separation; application of chemical-looping combustion. *Chemical Engineering Science*, 56:3101–3113, 2001.

[11] J. Drake. *Hydrodynamic Characterization of 3D FluidizedBeds Using Noninvasive Techniques.* Phd thesis, Iowa State University, 2011.

[12] R. Korbee, O. C. Snip, J. C. Schouten, M. van den Bleek, and C. M. Van den Bleek. Rate of solids and gas transfer via an orifice between partially and completely fluidized beds. *Chemical Engineering Science*, 49(24):5819–5832, December 1994.

[13] C. S. Stellema, A. W. Gerritsen, Z. I. Kolarl, J. J. M. D. Goeijl, and C. M. van den Bleek. Flow of Solids in an Interconnected Fluidized Beds System Investigated Using Positron Emission Particle Tracking. *The Canadian Journal of Chemical Engineering*, 79:314–321, 2001.

[14] A. Reichhold and H. Hofbauer. Internally circulating fluidized bed for continuous adsorption and desorption. *Chemical Engineering and Processing: Process Intensification*, 34(6):521–527, December 1995.

[15] O. C. Snip, R. Korbee, J. C. Schouten, and C. M. van den Bleek. Regenerative Desulfurization in Coal Conversion Processes Applying the Interconnected Fluidized Bed System. *Coal Science*, 24:1847–1850, 1995.

[16] M. Mortensen, R. G. Minet, T. T. Tsotsis, and S. Benson. A two-stage cyclic fluidized bed process for converting hydrogen chloride to chlorine. *Chemical Engineering Science*, 51(10):2031–2039, May 1996.

[17] S. Kaiser, G. Löffler, K. Bosch, and H. Hofbauer. Hydrodynamics of a dual fluidized bed gasifier. Part II: simulation of solid circulation rate, pressure loop and stability. *Chemical Engineering Science*, 58(18):4215–4223, September 2003.

[18] T. Pröll and H. Hofbauer. H_2 rich syngas by selective CO_2 removal from biomass gasification in a dual fluidized bed system — Process modelling approach. *Fuel Processing Technology*, 89(11):1207–1217, November 2008.

[19] T. Pröll, P. Kolbitsch, J. Bolhàr-nordenkampf, and H. Hofbauer. A Dual Circulating Fluidized Bed (DCFB) System for Chemical Looping Processes. In *AIChE Annual Meeting*, pages 1–8, 2008.

[20] T. Pröll, K. Rupanovits, P. Kolbitsch, J. Bolhàr-Nordenkampf, and H. Hofbauer. Cold Flow Model Study on a Dual Circulating Fluidized Bed (DCFB) System for Chemical Looping Processes. *Chemical Engineering & Technology*, 32(3):418–424, March 2009.

[21] L. Mleczko, S. Malcus, and T. Wurzel. Catalytic Reformer-Combustor: A Novel Reactor Concept for Synthesis Gas Production. *Industrial & Engineering Chemistry Research*, 36(1993):4459–4465, 1997.

[22] F. Snieders, A. C. Hoffmann, J. G. Yates, and D. Cheesman. Experimental Investigation of the Behaviour of Coarse Particles in an Interconnected Fluidized Bed. In *World Congress on Particle Technology 3*, pages 1–8. IChemE, 1998.

[23] A. M. C. Janse, P. Maarten Biesheuvel, W. Prins, and W. P. M. van Swaaij. A novel interconnected fluidised bed for the combined flash pyrolysis of biomass and combustion of char. *Chemical Engineering Journal*, 75(2):121–130, October 1999.

[24] E. Johansson, A. Lyngfelt, T. Mattisson, and F. Johnsson. Gas leakage measurements in a cold model of an interconnected fluidized bed for chemical-looping combustion. *Powder Technology*, 134(3):210–217, September 2003.

[25] E. Johansson, T. Mattisson, A. Lyngfelt, and H. Thunman. A 300 W laboratory reactor system for chemical-looping combustion with particle circulation. *Fuel*, 85(10-11):1428–1438, July 2006.

[26] E. Johansson, T. Mattisson, A. Lyngfelt, and H. Thunman. Combustion of Syngas and Natural Gas in a 300 W Chemical-Looping Combustor. *Chemical Engineering Research and Design*, 84(9):819–827, September 2006.

[27] M. Ryden, A. Lyngfelt, and T. Mattisson. Synthesis gas generation by chemical-looping reforming in a continuously operating laboratory reactor. *Fuel*, 85(12-13):1631–1641, September 2006.

[28] O. Rubio, J. Herguido, M. Menéndez, G. Grasa, and J. C. Abanades. Oxidative dehydrogenation of butane in an interconnected fluidized-bed reactor. *AIChE Journal*, 50(7):1510–1522, July 2004.

[29] J. C. Abanades, M. Alonso, N. Rodríguez, B. González, G. Grasa, and R. Murillo. Capturing CO_2 from combustion flue gases with a carbonation calcination loop. Experimental results and process development. *Energy Procedia*, 1(1):1147–1154, February 2009.

[30] M. Alonso, N. Rodríguez, G. Grasa, and J. C. Abanades. Modelling of a fluidized bed carbonator reactor to capture CO_2 from a combustion flue gas. *Chemical Engineering Science*, 64(5):883–891, March 2009.

[31] M. Alonso, N. Rodríguez, B. González, G. Grasa, R. Murillo, and J. C. Abanades. Carbon dioxide capture from combustion flue gases with a calcium oxide chemical loop. Experimental results and process development. *International Journal of Greenhouse Gas Control*, 4(2):167–173, March 2010.

[32] Nuria Rodríguez, M. Alonso, and J. C. Abanades. Experimental Investigation of a Circulating Fluidized-Bed Reactor to Capture CO_2 with CaO. *AIChE Journal*, 57(5), 2011.

[33] J. C. Abanades, M. Alonso, and N. Rodriguez. Experimental validation of in-situ CO_2 capture with CaO during the low temperature combustion of biomass in a fluidized bed reactor. *International Journal of Greenhouse Gas Control*, 5(3):512–520, May 2011.

[34] J. Adánez, P. Gayán, J. Celaya, L. F. de Diego, F. García-Labiano, and A. Abad. Chemical Looping Combustion in a 10 kW_{th} Proto-

type Using a CuO/Al_2O_3 Oxygen Carrier: Effect of Operating Conditions on Methane Combustion. *Industrial & Engineering Chemistry Research*, 45(17):6075–6080, August 2006.

[35] A. Martínez, P. Lisbona, Y. Lara, and L. M. Romeo. Carbonate looping cycle for CO_2 capture: Hydrodynamic of complex CFB systems. *Energy Procedia*, 4:410–416, January 2011.

[36] A. Cuadrat, A. Abad, F. García-Labiano, P. Gayán, L. F. de Diego, J. Adánez, and L. F. D. Diego. The use of ilmenite as oxygen-carrier in a 500 W_{th} Chemical-Looping Coal Combustion unit. *International Journal of Greenhouse Gas Control*, 5(6):1630–1642, November 2011.

[37] A. Abad, I. Adánez-Rubio, P. Gayán, F. García-Labiano, L. F. de Diego, and J. Adánez. Demonstration of chemical-looping with oxygen uncoupling (CLOU) process in a 1.5 kW_{th} continuously operating unit using a Cu-based oxygen-carrier. *International Journal of Greenhouse Gas Control*, 6:189–200, January 2012.

[38] P. U. Foscolo, A. Germanà, N. Jand, and S. Rapagnà. A Novel Fluidized Bed Biomass Gasifier. In *Energy: Production, distribution and conservation*, pages 51–60, Milan, 2006.

[39] H. J. Ryu and G. T. Jin. Chemical-looping hydrogen generation system: Performance estimation and process selection. *Korean Journal of Chemical Engineering*, 24(3):527–531, December 2007.

[40] H. J. Ryu, S. Y. Lee, Y. C. Park, and M. H. Park. Solid Circulation Rate and Gas Leakage Measurements in an Interconnected Bubbling Fluidized Beds. *World Academy of Science, Engineering and Technology*, 28:169–174, 2007.

[41] M. Xu, N. Ellis, C. Jim Lim, and H. J. Ryu. Mapping of the Operating Conditions for an Interconnected Fluidized Bed Reactor for CO_2 Separation by Chemical Looping Combustion. *Chemical Engineering & Technology*, 32(3):404–409, March 2009.

[42] J. H. Goo, M. W. Seo, S. D. Kim, and B. H. Son. Effects of Temperature and Particle Size on Minimum Fluidization and Transport

Velocities in a Dual Fluidized bed. In *Proceedings of the 20th International Conference on Fluidized Bed Combustion*, pages 305–310, 2010.

[43] M. W. Seo, T. D. B. Nguyen, Y. I. Lim, S. D. Kim, S. Park, B. H. Song, and Y. J. Kim. Solid circulation and loop-seal characteristics of a dual circulating fluidized bed: Experiments and CFD simulation. *Chemical Engineering Journal*, 168(2):803–811, April 2011.

[44] J. Jung and I. K. Gamwo. Multiphase CFD-based models for chemical looping combustion process: Fuel reactor modeling. *Powder Technology*, 183(3):401–409, April 2008.

[45] B. Acharya, A. Dutta, and P. Basu. Chemical-Looping Gasification of Biomass for Hydrogen-Enriched Gas Production with In-Process Carbon Dioxide Capture. *Energy & Fuels*, 23(10):5077–5083, October 2009.

[46] R. T. Symonds, D. Y. Lu, R. W. Hughes, E. J. Anthony, and A. Macchi. CO_2 Capture from Simulated Syngas via Cyclic Carbonation / Calcination for a Naturally Occurring Limestone: Pilot-Plant Testing. *Industrial & Engineering Chemistry Research*, 48(18):8431–8440, September 2009.

[47] N. Rodríguez, M. Alonso, J. C. Abanades, A. Charitos, C. Hawthorne, G. Scheffknecht, D. Y. Lu, and E. J. Anthony. Comparison of experimental results from three dual fluidized bed test facilities capturing CO_2 with CaO. *Energy Procedia*, 4:393–401, January 2011.

[48] J. Li, C. Dong, J. Zhang, and Y. Yang. Experimental Research on Gas-solid Flow in a Dual Fluidized Bed. In *International Conference on Sustainable Power Generation and Supply*, pages 1–6, 2009.

[49] J. Zhang, J. Jiang, Q. Lu, C. Dong, T. Zhang, X. Liu, Z. Liang, and Y. Yang. The Design and Tests in a Three Interconnected Fluidized Bed. *2010 International Conference on Digital Manufacturing & Automation*, pages 648–652, December 2010.

[50] W. Shuai, L. Guodong, L. Huilin, C. Juhui, H. Yurong, and W. Jiaxing. Fluid dynamic simulation in a chemical looping combustion with two interconnected fluidized beds. *Fuel Processing Technology*, 92(3):385–393, March 2011.

[51] H. Y. Zhang, R. Xiao, Q. W. Pan, Q. L. Song, and H. Huang. Hydrodynamics of a Novel Biomass Autothermal Fast Pyrolysis Reactor: Flow Pattern and Pressure Drop. *Chemical Engineering & Technology*, 32(1):27–37, January 2009.

[52] Y. Zhang, J. Xiao, and L. Shen. Simulation of Methanol Production from Biomass Gasification in Interconnected Fluidized Beds. *Industrial & Engineering Chemistry Research*, 48(11):5351–5359, June 2009.

[53] H. Zhang, S. Shao, R. Xiao, Q. Pan, R. Chen, and J. Zhang. Numerical Study on the Hydrodynamics of a Self-Heating Biomass Fast Pyrolysis Reactor. *Energy & Fuels*, 25(9):4077–4084, September 2011.

[54] H. Zhang, R. Xiao, D. Wang, J. Cho, G. He, S. Shao, and J. Zhang. Hydrodynamics of a novel biomass autothermal fast pyrolysis reactor: Solid circulation rate and gas bypassing. *Chemical Engineering Journal*, 181-182:685–693, February 2012.

[55] H. An, T. Song, L. Shen, C.i Qin, J. Yin, and B. Feng. Coal gasification with in-situ CO_2 capture by the synthetic CaO sorbent in a 1 kW_{th} dual fluidised-bed reactor. *International Journal of Hydrogen Energy*, 37(19):14195–14204, 2012.

[56] T. Song, J. Wu, L. Shen, and J Xiao. Experimental investigation on hydrogen production from biomass gasification in interconnected fluidized beds. *Biomass and Bioenergy*, 36:258–267, January 2012.

[57] T. Song, J. Wu, H. Zhang, and L. Shen. Characterization of an Australia hematite oxygen carrier in chemical looping combustion with coal. *International Journal of Greenhouse Gas Control*, 11:326–336, November 2012.

[58] H. Kruggel-Emden, S. Rickelt, F. Stepanek, and A. Munjiza. Development and testing of an interconnected multiphase CFD-model

for chemical looping combustion. *Chemical Engineering Science*, 65(16):4732–4745, August 2010.

[59] A. Charitos, C. Hawthorne, A. R. Bidwe, S. Sivalingam, A. Schuster, H. Spliethoff, and G. Scheffknecht. Parametric investigation of the calcium looping process for CO_2 capture in a 10 kW_{th} dual fluidized bed. *International Journal of Greenhouse Gas Control*, 4(5):776–784, September 2010.

[60] S. Rifflart, A. Hoteit, M. M. Yazdanpanah, W. Pelletant, and K. Surla. Construction and operation of a 10 kW CLC unit with circulation configuration enabling independent solid flow control. *Energy Procedia*, 4:333–340, January 2011.

[61] M. M. Yazdanpanah, A. Hoteit, A. Forret, A. Delebarre, and T. Gauthier. Experimental Investigations on a Novel Chemical Looping Combustion Configuration. *Oil & Gas Science and Technology – Revue d'IFP Energies nouvelles*, 66(2):265–275, April 2011.

[62] M. M. Yazdanpanah, A. Forret, T. Gauthier, and A. Delebarre. An experimental investigation of L-valve operation in an interconnected circulating fluidized bed system. *Powder Technology*, 221:236–244, May 2012.

[63] W. R. Wang, N. Ding, Y. Zheng, C. Luo, P. F. Fu, and C. G. Zheng. Development and Testing of an Interconnected Fluidized-Bed System for Chemical Looping Combustion. *Chemical Engineering & Technology*, 35(3):532–538, March 2012.

[64] A. Bischi, Ø. Langørgen, and O. Bolland. Double loop circulating fluidized bed reactor system for two reaction processes, based on pneumatically controlled divided loop-seals and bottom extraction/lift. *Powder Technology*, 246:51–62, September 2013.

[65] P. Lisbona, A. Martínez, and L. M. Romeo. Hydrodynamical model and experimental results of a calcium looping cycle for CO_2 capture. *Applied Energy*, 101:317–322, January 2013.

[66] Yanjun Guan, Jian Chang, Kai Zhang, Baodong Wang, and Qi Sun. Three-dimensional CFD simulation of hydrodynamics in an inter-

connected fluidized bed for chemical looping combustion. *Powder Technology*, 268:316–328, dec 2014.

[67] Jinchen Ma, Haibo Zhao, Xin Tian, Yijie Wei, Yongliang Zhang, and Chuguang Zheng. Continuous Operation of Interconnected Fluidized Bed Reactor for Chemical Looping Combustion of CH 4 Using Hematite as Oxygen Carrier. *Energy & Fuels*, 29(5):3257–3267, may 2015.

[68] T. Clayton. Fluidized Bed. In *Multiphase Flow Handbook*, pages 1–5, 93. CRC Press, 2006.

[69] F. Winkler. German Patent, 1922.

[70] J. Yates and S. Simon. Experimental methods in fluidization research. *International Journal of Multiphase Flow*, 20:297–330, 1994.

[71] B. Rouge. The Fluid Bed Reactor. Technical report, American Chemical Society, Luisiana, The US, 1998.

[72] L. Massimilla. *Flow Properties of the Fluidized Dense Phase*. Academic Press, London, 1971.

[73] O. C. Snip, M. Woods, R. Korbee, J. C. Schouten, and C. M. van den Bleek. Regenerative removal of SO_2 and NOx for a 150 MWe power plant in an interconnected fluidized bed facility. *Chemical Engineering Science*, 51(10):2021–2029, May 1996.

[74] T. Mattisson, Q. Zafar, M. Johansson, and A. Lyngfelt. Chemical-looping combustion as a new CO_2 management technology. In *First Regional Symposium on Carbon Managemnet*, pages 1–19, Dhahran, Saudi-Arabia, 2006.

[75] A. Abad, T. Mattisson, A. Lyngfelt, and Magnus Rydén. Chemical-looping combustion in a 300 W continuously operating reactor system using a manganese-based oxygen carrier. *Fuel*, 85(9):1174–1185, June 2006.

[76] C. Linderholm, A. Cuadrat, and A. Lyngfelt. Chemical-looping combustion of solid fuels in a 10 kW_{th} pilot-batch tests with five fuels. *Energy Procedia*, 4:385–392, January 2011.

[77] C. Linderholm, A. Lyngfelt, A. Cuadrat, and E. Jerndal. Chemical-looping combustion of solid fuels- Operation in a 10kW unit with two fuels, above-bed and in-bed fuel feed and two oxygen carriers, manganese ore and ilmenite. *Fuel*, 102:808–822, December 2012.

[78] T. Mattisson, A. Lyngfelt, and P. Cho. The use of iron oxide as an oxygen carrier in chemical-looping combustion of methane with inherent separation of CO_2. *Fuel*, 80(13):1953–1962, October 2001.

[79] P. Cho, T. Mattisson, and A. Lyngfelt. Comparison of iron-, nickel-, copper- and manganese-based oxygen carriers for chemical-looping combustion. *Fuel*, 83(9):1215–1225, June 2004.

[80] A. Abad, T. Mattisson, A. Lyngfelt, and M. Johansson. The use of iron oxide as oxygen carrier in a chemical-looping reactor. *Fuel*, 86(7-8):1021–1035, May 2007.

[81] E. Jerndal, T. Mattisson, I. Thijs, F. Snijkers, and A. Lyngfelt. NiO particles with Ca and Mg based additives produced by spray-drying as oxygen carriers for chemical-looping combustion. *Energy Procedia*, 1(1):479–486, February 2009.

[82] P. Cho, T. Mattisson, and A. Lyngfelt. Carbon Formation on Nickel and Iron Oxide-Containing Oxygen Carriers for Chemical-Looping Combustion. *Industrial & Engineering Chemistry Research*, 44(4):668–676, February 2005.

[83] A. Lyngfelt. Oxygen Carriers for Chemical Looping Combustion - 4000h of Operational Experience. *Oil & Gas Science and Technology – Revue d'IFP Energies nouvelles*, 66(2):161–172, April 2011.

[84] P. Kolbitsch, T. Pröll, J. Bolhar-Nordenkampf, and H. Hofbauer. Design of a Chemical Looping Combustor using a Dual Circulating Fluidized Bed (DCFB) Reactor System. *Chemical Engineering & Technology*, 32(3):398–403, March 2009.

[85] N. Rodríguez, M. Alonso, G. Grasa, and J. C. Abanades. Capture of CO_2 from Combustion Gases in a Fluidized Bed of CaO. *AIChE Journal*, 50(7):1614–1622, 2004.

[86] M. Alonso, N. Rodriguez, B. Gonzalez, B. Arias, and J. C. Abanades. Capture of CO_2 during low temperature biomass combustion in a fluidized bed using CaO. Process description, experimental results and economics. *Energy Procedia*, 4:795–802, January 2011.

[87] A. Abad, J. Adánez, F. García-Labiano, L. F. de Diego, P. Gayán, and J. Celaya. Mapping of the range of operational conditions for Cu-, Fe-, and Ni-based oxygen carriers in chemical-looping combustion. *Chemical Engineering Science*, 62(1-2):533–549, January 2007.

[88] E. J. Gohr. *Fluidization*. Reinhold Publishing Corporation, New York, 1956.

[89] Y. Ikeda and S. Tashiro. *Fluidization Technology*. SCEJ Kanto Branch, Gakkai, 1981.

[90] A. Sánchez-Biezma, J. C. Ballesteros, L. Diaz, E. de Zárraga, F. J. Álvarez, J. López, B. Arias, G. Grasa, and J. C. Abanades. Post-combustion CO_2 capture with CaO. Status of the technology and next steps towards large scale demonstration. *Energy Procedia*, 4:852–859, January 2011.

[91] M. Kramp, A. Thon, E. U. Hartge, S. Heinrich, and J. Werther. The Role of Attrition and Solids Recovery in a Chemical Looping Combustion Process. *Oil & Gas Science and Technology – Revue d'IFP Energies nouvelles*, 66(2):277–290, May 2011.

[92] A. Cuadrat, A. Abad, J. Adánez, L. F. de Diego, F. García-Labiano, and P. Gayán. Behavior of ilmenite as oxygen carrier in chemical-looping combustion. *Fuel Processing Technology*, 94(1):101–112, February 2012.

[93] S. K. Jeong, T. S. Park, and S. C. Hong. Simultaneous SOx / NOx removal in a fluidized bed reactor using natural manganese ore. *Journal of Chemical Technology & Biotechnology*, 76(10):1080–1084, October 2001.

[94] S. M. Jeong and S. D. Kim. NOx removal by selective noncatalytic reduction with urea solution in a fluidized bed reactor. *Korean Journal of Chemical Engineering*, 16(5):614–617, September 1999.

[95] Q. Guo, Y. Liu, and H. Tian. Recent Advances on Preparation and Characteristics of Oxygen Carrier Particles. *International Review of Chemical Engineering*, 1(July):357–368, 2009.

[96] H. Richter and K. Knoche. Reversibility of Combustion Processes. *ACS Symposium Series*, 235:71–86, 1983.

[97] M. Ishida and H. Jin. A novel combustor based on chemical-looping reactions and its reaction kinetics. *Journal of Chemical Engineering of Japan*, 27(3):296–301, 1994.

[98] M. Anheden, A. S. Näsholm, and G. Svedberg. Chemical-looping Combustion - Efficient Conversion of Chemical Energy in Fuels into Work. In *Proceedings of Intersociety Enrgy Conversion Engineering Conference*, pages vol. 30 (75–81), 1995.

[99] Q. Zafar, T. Mattisson, and B. Gevert. Redox Investigation of Some Oxides of Transition-State Metals Ni, Cu, Fe, and Mn Supported on SiO_2 and $MgAl_2O_4$. *Energy & Fuels*, 20(1):34–44, January 2006.

[100] H. Fang, L. Haibin, and Z. Zengli. Advancements in Development of Chemical-Looping Combustion: A Review. *International Journal of Chemical Engineering*, 2009(ii):1–16, 2009.

[101] A. Lyngfelt and H. Thunman. Construction and 100h of operational experience of a 10 kW chemical looping combustor. In London Thomas, D. Elsevier Science, editor, *Carbon Dioxide Capture for Storage in Deep Geologic Formations-Results from the* CO_2 *Capture Project*, volume 1, chapter 36, pages 625–645. Elsevier Science, 2005.

[102] B. Kronberger, E. Johansson, G. Löffler, T. Mattisson, A. Lyngfelt, and H. Hofbauer. A Two-Compartment Fluidized Bed Reactor for CO_2 Capture by Chemical-Looping Combustion. *Chemical Engineering & Technology*, 27(12):1318–1326, December 2004.

[103] S. R. Son and S. D. Kim. Chemical-Looping Combustion with NiO and Fe_2O_3 in a Thermobalance and Circulating Fluidized Bed Reactor with Double Loops. *Industrial & Engineering Chemistry Research*, 45(8):2689–2696, April 2006.

[104] L. M. Romeo, J. C. Abanades, J. C. Ballesteros, A. Valero, J. M. Escosa, A. Giménez, C. Cortés, and J. Paño. Process Optimization in Postcombustion CO_2-Capture by means of Repowering and Reversible Carbonation/Calcination Cycle. In *8^{th} International Congress on Greenhouse Gas Control Technologies GHGT-8*, page Norway, 2006.

[105] Y. Lara, P. Lisbona, A. Martínez, and L. M. Romeo. Comparative study of optimized purge flow in a CO_2 capture system using different sorbents. *Energy Procedia*, 1(1):1359–1366, February 2009.

[106] J. C. Abanades, E. J. Anthony, J. J. S. Wang, and J. E. Oakey. Fluidized bed combustion systems integrating CO_2 capture with CaO. *Environmental Science and Technology*, 39(8):2861–2866, 2005.

[107] N. Rodriguez, M. Alonso, G. Grasa, and J. C. Abanades. Heat requirements in a calciner of $CaCO_3$ Integrated in a CO_2 Capture System Using CaO. *Chemical Engineering Journal*, 138:148–154, 2008.

[108] L. M. Romeo, J. C. Abanades, J. M. Escosa, J. Paño, A. Giménez, A. Sánchez-Biezma, and J. C. Ballesteros. Oxyfuel Carbonation/Calcination Cycle for Low Cost CO_2 Capture in Existing Power Plants. *Energy Conversion and Management*, 49:2809–2814, 2008.

[109] H. J. Ryu, Y. C. Park, S. H. Jo, and M. H. Park. Development of novel two-interconnected fluidized bed system. *Korean Journal of Chemical Engineering*, 25(5):1178–1183, January 2008.

[110] M. C. Romano. Modeling the carbonator of a Ca-looping process for CO_2 capture from power plant flue gas. *Chemical Engineering Science*, 69(1):257–269, February 2012.

[111] T. Pröll, P. Kolbitsch, J. Bolhàr-Nordenkampf, and H. Hofbauer. A novel dual circulating fluidized bed system for chemical looping processes. *AIChE Journal*, 55(12):3255–3266, December 2009.

[112] F. F. F. Snieders, A. C. C. Hoffmann, D. Cheesman, J. G. Yates, M. Stein, and J. P. K. Seville. The dynamics of large particles in a four-compartment interconnected fluidized bed. *Powder Technology*, 101(3):229–239, March 1999.

[113] M. Kuramoto, D. Kunii, and T. Furusawa. Flow of dense fluidized particles through an opening in a circulation system. *Powder Technology*, 47(2):141–149, July 1986.

[114] N. Rodríguez, B. Arias, and J. C. Abanades. Biomass Combustion with in-situ CO_2 Capture with CaO. I . Process Description and Economics. *Industrial & Engineering Chemistry Research*, 50:6972–6981, 2011.

[115] M. Alonso, N. Rodríguez, B. González, B. Arias, and J. C. Abanades. Biomass Combustion with in-situ CO_2 Capture by CaO. II. Experimental Results. *Industrial & Engineering Chemistry Research*, 50(11):6982–6989, June 2011.

[116] P. Stoholm, M. W. Fock, and U. B. Henriksen. Low Temperature CFB Gasifier. Conceptual Ideas and Applications. In *Proceedings of the 15^{th} International Conference on Fluidized Bed Combustion*, Savannah, USA, 1999.

[117] P. Stoholm, R. G. Nielsen, H. Nygaard, L. Tobiasen, M. W. Fock, K. Richardt, and U. B. Henriksen. Low temperature CFB gasifier conceptual ideas, applications and first test results. *Biomass for Energy and Industry*, 2000.

[118] R. G. Nielsen, P. Stoholm, M. B. Nielsen, J. Krogh, N. Nørholm, S. Antonsen, B. Sander, U. B. Henriksen, and E. B. Qvale. The LT-CFB Gasifier - First Test Results from the 500 kW Test Plant. In *14^{th} European Biomass Conference*, Paris - France, 2005.

[119] N. H. Florin and Andrew T. Harris. Enhanced hydrogen production from biomass with in-situ carbon dioxide capture using calcium oxide sorbents. *Chemical Engineering Science*, 63(2):287–316, January 2008.

[120] M. Rydén and P. Ramos. H_2 production with CO_2 capture by sorption enhanced chemical-looping reforming using NiO as oxygen carrier and CaO as CO_2 sorbent. *Fuel Processing Technology*, 96:27–36, April 2012.

[121] G. T. Jin, H. Ryu, S. H. Jo, S. Y. Lee, S. R. Son, and S. D. Kim. Hydrogen Production in Fluidized Bed by Chemical-looping Cycle. *Korean Journal of Chemical Engineering*, 24(3):542–546, 2007.

[122] S. R. Son, K. S. Go, and S. D. Kim. Thermogravimetric Analysis of Copper Oxide for Chemical-Looping Hydrogen Generation. *Industrial & Engineering Chemistry Research*, 48(1):380–387, January 2009.

[123] F. X. Chiron and G. S. Patience. Kinetics of mixed copper–iron based oxygen carriers for hydrogen production by chemical looping water splitting. *International Journal of Hydrogen Energy*, 37(14):10526–10538, July 2012.

[124] A. Murugan, A. Thursfield, and I. S. Metcalfe. A chemical looping process for hydrogen production using iron-containing perovskites. *Energy & Environmental Science*, 4(11):4639, 2011.

[125] C. Zhu, Q. Yu, R. N. Dave, and R. Pfeffer. Gas fluidization characteristics of nanoparticle agglomerates. *AIChE Journal*, 51(2):426–439, February 2005.

[126] J. Shabanian, R. Jafari, and J. Chaouki. Fluidization of Ultrafine Powders. *International Review of Chemical Engineering*, 4(January):16–50, 2012.

[127] H. Krupp. Particle adhesion theory and experiment. *Advances in Colloid and Interface Science*, 1(2):111–239, May 1967.

[128] J. R. van Ommen, J. M. Valverde, and R. Pfeffer. Fluidization of nanopowders: A review. *Journal of nanoparticle research: an interdisciplinary forum for nanoscale science and technology*, 14(3):737, March 2012.

[129] S. W. Kim, W. Namkung, and S. D. Kim. Solids flow characteristics in loop-seal of a circulating fluidized bed. *Korean Journal of Chemical Engineering*, 16(1):82–88, January 1999.

[130] P. Basu. *Combustion and Gasification in Fluidized Beds*. Taylor & Francis, 2006.

[131] T. M. Knowlton. Circulating Fluidized Beds. In J. R. Grace, A. A. Avidan, and T. M. Knowlton, editors, *Circulating fluidized bed*, pages 214–260. Springer Netherlands, Dordrecht, 1997.

[132] E. Botsio and P. Basu. Experimental Investigation into the Hydrodynamics of Flow of Solids through a Loop Seal Recycle Chamber. *The Canadian Journal of Chemical Engineering*, 83(3):554–558, May 2008.

[133] H. Nagashima, T. Ishikura, and M. Ide. Hydrodynamics of a spouted bed with an impermeable draft tube for binary particle systems. *Korean Journal of Chemical Engineering*, 16(5):688–693, September 1999.

[134] H. Nagashima, K. Suzukawa, and T. Ishikura. Hydrodynamic performance of spouted beds with different types of draft tubes. *Particuology*, 11(5):475–482, October 2013.

[135] X. L. Zhao, Q. Yao, and S. Q. Li. Effects of Draft Tubes on Particle Velocity Profiles in Spouted Beds. *Chemical Engineering & Technology*, 29(7):875–881, July 2006.

[136] J. G. Wang, S. F. Zhang, and L. He. Hydrodynamics Characteristics of Spouted Bed with Porous Draft Tube. *Advanced Materials Research*, 550-553:3045–3048, July 2012.

[137] W. Thielicke and E. J. Stamhuis. PIVlab – Towards User-friendly, Affordable and Accurate Digital Particle Image Velocimetry in MATLAB. *Journal of Open Research Software*, 2, oct 2014.

[138] H. Altzibar, S. Alvarez, M. J. San José, R. Aguado, J. Bilbao, and M. Olazar. Hydrodynamic Aspects and Correlations for the Design of Draft-Tube Conical Spouted Beds. In *The 12th International Conference on Fluidization - New Horizons in Fluidization Engineering*, pages 561–568, 2007.

[139] O. Gryczka, S. Heinrich, V. Miteva, N.G. Deen, J.A.M. Kuipers, M. Jacob, and L. Mörl. Characterization of the pneumatic behavior of a novel spouted bed apparatus with two adjustable gas inlets. *Chemical Engineering Science*, 63(3):791–814, February 2008.

[140] M. C. Matthew, M. H. Morgan, and H. Littman. Study of the hydrodynamics within a draft tube spouted bed system. *The Canadian Journal of Chemical Engineering*, 66(6):908–918, December 1988.

[141] H. Altzibar, G. Lopezy, M. Olazarz, and J. Bilbao. Study of The Minimum Spouting Velocity in A Draft Tube Conical Spouted Bed. In *The 13th International Conference on Fluidization - New Paradigm in Fluidization Engineering*, pages 1–8, 2010.

[142] E. Piskova and L. Mörl. Fluidization regimes in different spouted bed apparatus constructions. *Chemical Engineering and Processing: Process Intensification*, 46(8):695–702, August 2007.

[143] S. Ergun. Flow through Packed Bed Columns. *Chemical Engineering Progress*, 48 (2):89, 1952.

[144] S. Azizaddini, W. Lin, and K. Dam-Johansen. Experimental investigation of a Draft Tube Spouted Bed for Effects of Geometric Parameters on Operation. In *Proceeding of 1st International Symposium on Theoretical, Experimental and Computational Mechanics*, Rhodes, Greece, September 2015. American Institute of Physics.

[145] M. Rhodes. *Introduction to Particle Technology*. John Wiley & Sons, Ltd, Chichester, UK, March 2008.